AFWL-TR-87-94

AFWL-TR-
87-94

SHIELDING ANALYSIS OF A SMALL COMPACT SPACE NUCLEAR REACTOR

L. W. Lee, Jr.

August 1987

Final Report

Approved for public release; distribution unlimited.

AIR FORCE WEAPONS LABORATORY
Air Force Systems Command
Kirtland Air Force Base, NM 87117-6008

This final report was prepared by the Air Force Weapons Laboratory, Kirtland Air Force Base, New Mexico, under Job Order 57972301. First Lieutenant Lennard W. Lee, Jr. (AWYS) was the Laboratory Project Officer-in-Charge.

When Government drawings, specifications, or other data are used for any purpose other than in connection with a definitely Government-related procurement, the United States Government incurs no responsibility or any obligation whatsoever. The fact that the Government may have formulated or in any way supplied the said drawings, specifications, or other data, is not to be regarded by implication, or otherwise in any manner construed, as licensing the holder, or any other person or corporation; or as conveying any rights or permission to manufacture, use, or sell any patented invention that may in any way be related thereto.

This report has been authored by an employee of the United States Government. Accordingly, the United States Government retains a nonexclusive, royalty-free license to publish or reproduce the material contained herein, or allow others to do so, for the United States Government purposes.

This report has been reviewed by the Public Affairs Office and is releasable to the National Technical Information Service (NTIS). At NTIS, it will be available to the general public, including foreign nationals.

If your address has changed, if you wish to be removed from our mailing list, or if your organization no longer employs the addressee, please notify AFWL/AWYS, Kirtland AFB, NM 87117-6008 to help us maintain a current mailing list.

This report has been reviewed and is approved for publication.

Lennard W Lee Jr.

LENNARD W. LEE, JR.
1st Lt, USAF
Project Officer

FOR THE COMMANDER

David R Boyle

DAVID R. BOYLE
Maj, USAF
Chief, Space Applications Branch

Wayne T Graybeal

WAYNE T. GRAYBEAL
Lt Col, USAF
Acting Chief, Applied Technical Division

DO NOT RETURN COPIES OF THIS REPORT UNLESS CONTRACTUAL OBLIGATIONS OR NOTICE ON A SPECIFIC DOCUMENT REQUIRES THAT IT BE RETURNED.

REPORT DOCUMENTATION PAGE

1a. REPORT SECURITY CLASSIFICATION Unclassified	1b. RESTRICTIVE MARKINGS
2a. SECURITY CLASSIFICATION AUTHORITY	3. DISTRIBUTION/AVAILABILITY OF REPORT Approved for public release; distribution unlimited.
2b. DECLASSIFICATION/DOWNGRADING SCHEDULE	
4. PERFORMING ORGANIZATION REPORT NUMBER(S) AFWL-TR-87-94	5. MONITORING ORGANIZATION REPORT NUMBER(S)
6a. NAME OF PERFORMING ORGANIZATION Air Force Weapons Laboratory 6b. OFFICE SYMBOL (If applicable)	7a. NAME OF MONITORING ORGANIZATION
6c. ADDRESS (City, State, and ZIP Code) Kirtland Air Force Base, NM 87117-6008	7b. ADDRESS (City, State, and ZIP Code)
8a. NAME OF FUNDING/SPONSORING ORGANIZATION 8b. OFFICE SYMBOL (If applicable)	9. PROCUREMENT INSTRUMENT IDENTIFICATION NUMBER
8c. ADDRESS (City, State, and ZIP Code)	10. SOURCE OF FUNDING NUMBERS PROGRAM ELEMENT NO. 62601F; PROJECT NO. 5797; TASK NO. 23; WORK UNIT ACCESSION NO. 01

11. TITLE (Include Security Classification)
SHIELDING ANALYSIS OF A SMALL COMPACT SPACE NUCLEAR REACTOR

12. PERSONAL AUTHOR(S)
Lee, Lennard Woodrow, Jr.

13a. TYPE OF REPORT	13b. TIME COVERED	14. DATE OF REPORT (Year, Month, Day)	15. PAGE COUNT
Final	FROM _____ TO _____	1987, August	214

16. SUPPLEMENTARY NOTATION
Thesis

17. COSATI CODES			18. SUBJECT TERMS (Continue on reverse if necessary and identify by block number)	
FIELD	GROUP	SUB-GROUP	Shield	Lithium Hydride Shield
18	05		Space Nuclear Reactor	Tungsten Shield
09	07		Space Nuclear Reactor Shield	Boron Carbide Shield

19. ABSTRACT (Continue on reverse if necessary and identify by block number)

Early space nuclear reactor concepts have used lithium hydride as the primary neutron attenuator. Lithium hydride is desirable because of its low density, its hydrogen content, and its historical data base from use during the SNAP program. However, lithium hydride has a low melting point, hydrogen dissociation, a volume exp[illegible]ion of 25% during a phase change, and a tendency to react with other materials. Also, l[illegible]ium 6 has an exothermic (n, α) reaction that produces tritium, an alpha particle, and about 4.8 MeV of energy producing internal heating in the shield. For future, higher power nuclear reactors, studies indicate that a neutron shielding material other than lithium hydride will need to be developed. The SP-100 reactor concept, currently in its developmental stage, has a layered tungsten--lithium hydride shield. Studies indicate that this shield configuration is the lightest weight shield.

(over)

20. DISTRIBUTION/AVAILABILITY OF ABSTRACT ☒ UNCLASSIFIED/UNLIMITED ☐ SAME AS RPT. ☐ DTIC USERS	21. ABSTRACT SECURITY CLASSIFICATION Unclassified
22a. NAME OF RESPONSIBLE INDIVIDUAL L. W. Lee, Jr.	22b. TELEPHONE (Include Area Code) (505) 844-0252 22c. OFFICE SYMBOL AWYS

DD FORM 1473, 84 MAR 83 APR edition may be used until exhausted. All other editions are obsolete.

18. SUBJECT TERMS

Beryllium Shield	Lithium Hydride and Tungsten Shield	K-effective
Shield Volume	Boron Carbide and Tungsten Shield	Criticality
Shield Mass	Analyze	Radiation Dose

19. ABSTRACT (Continued)

This configuration and three other shielding concepts were analyzed to determine the lightest shield and to determine the shield configuration with the smallest volume. The other three concepts were a boron carbide--beryllium layered shield, and a lithium hydride--beryllium shield.

FEMP2D and FEMP1D codes were used in this analysis. These codes were developed at Sandia National Laboratory (SNL), using the input from another code, RFCC, which produced energy-dependent dose conversion factors, and determined the shields' ability to attenuate the neutron and gamma radiation to permissible dose limits.

The results of this analysis show that the lithium hydride--tungsten layered shield was indeed the lightest weight shield. However, a boron carbide--tungsten shield was calculated to have the least volume. This is important since launch vehicles may have a cargo bay volume constraint. Therefore volume, not weight, may be the driving factor in determining the shield configuration.

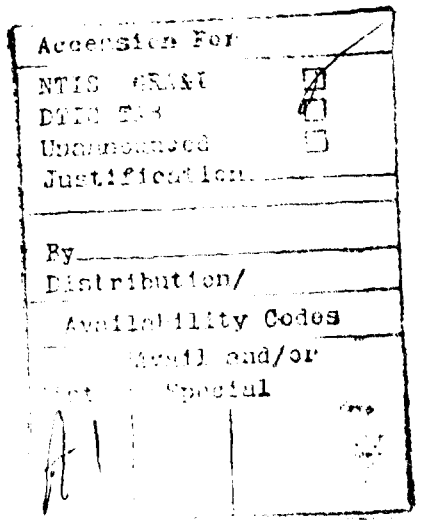

ACKNOWLEDGEMENTS

I would like to express my sincere thanks to the following individuals whose help was invaluable in this research project. First, thanks goes to the committee members, Dr. Norman Roderick, my committee chairperson, Dr. Mohamed El-Genk, Dr. Patrick McDaniel, and Dr. Charles Sparrow. The help and guidance from each of these gentlemen will always be cherished by myself and my family. I could not have written this thesis without the superlative guidance from Dr. McDaniel and Dr. Charles Sparrow.

My appreciation goes to the Air Force Weapons Laboratory for the support I've received while writing this thesis. A special thanks goes to retired Lt Col James Lee for his insight in requiring all of his lieutenants to enroll in a graduate program at UNM. My career will definitely be enhanced because of his farsightedness.

I would like to give a special thanks to my wife, Sabrina, who suffered gracefully while I researched and wrote this thesis. To my children, Matthew, Michael, and Mark, goes another special thanks; its because of them that I continue my education.

Finally, my thanks goes to God for giving me the opportunity, strength, and willpower to complete this work. Truly, without Him, nothing is possible; with Him everything is possible.

Shielding Analysis of a Small Compact Space Nuclear Reactor

Lennard W. Lee Jr.

B.S. Nuclear Engineering, Mississippi State University, 1983

M.S. Nuclear Engineering, University of New Mexico, 1987

Early space nuclear reactor concepts have used lithium hydride as the primary neutron attenuator. Lithium hydride is desirable because of its low density, its hydrogen content, and its historical data base from use during the SNAP program. However, lithium hydride has a low melting point, hydrogen dissociation, a volume expansion of 25% during a phase change, and a tendency to react with other materials. Also, lithium 6 has an exothermic (n, α) reaction that produces tritium, an alpha particle, and about 4.8 MeV of energy producing internal heating in the shield. Studies have indicated that for future, higher power nuclear reactors, that a neutron shielding material other than lithium hydride will need to be developed. The SP-100 reactor concept, currently in its developmental stage, has a layered tungsten - lithium hydride shield. Studies indicate that this shield configuration is the lightest weight shield.

This configuration and three other shielding concepts were analyzed to determine the lightest shield and to determine the shield configuration with the smallest

volume. The other three concepts were a boron carbide - tungsten layered shield, a boron carbide - beryllium layered shield, and a lithium hydride - beryllium shield. FEMP2D and FEMP1D codes were used in this analysis.

These codes were developed at Sandia National Laboratory. They used the input from another code, RFCC, which produced energy dependent dose conversion factors, and determined the shields' ability to attenuate the neutron and gamma radiation to permissible dose limits.

The results of this analysis show that the lithium hydride - tungsten layered shield was indeed the lightest weight shield. However, a boron carbide - tungsten shield was calculated to have the least volume. This is important since launch vehicles may have a cargo bay volume constraint. Therefore volume, not weight, may be the driving factor in determining the shield configuration.

I. Table of Contents

I. Table of Contents (Continued)

II. List of Figures

II. List of Figures (Continued)

III. List of Tables

1.0 INTRODUCTION

Apollo 11 climaxed with Neil Armstrong becoming the first human to walk on the moon on 20 July 1969. Six manned lunar landings followed with the last being Apollo 17 in April 1972. There is little doubt that man will return to the moon to mine its resources and use it as a base for planetary explorations in the next century. As space exploration resumes, there will be a need for a power source that's reliable, has a high power density, and, in some cases, portable. These reasons, and many more, make space nuclear reactors an attractive power source for future space missions.

The idea of using space nuclear reactors in space is not new. The United States has one nuclear reactor in orbit, the SNAP-10A, and the Soviet has more than twenty operational at the present time. (The United States' reactor, the SNAP-10A, has been shut down permanently.) Recently, the idea of space nuclear reactors has been rejuvenated with the projected power demands for future civilian and military space missions. Research on the Strategic Defense Initiative (SDI) projects power levels in the multimegawatt regime. Conventional power sources are not able to reasonably obtain these higher power levels. The Space Power 100 kWe (SP-100) space nuclear reactor is the first step in providing power levels beyond conventional levels.

Using a space nuclear reactor introduces several technological problems to be solved. For a reactor coupled to a satellite, the payload must be protected from radiation introduced to the environment by the nuclear reactor. While the physics of radiation is well known, the problem of shielding a space nuclear reactor is complicated by the need to use the strongest lightweight material to minimize the launching cost to the spacecraft.

Early space nuclear reactor concepts used lithium hydride (LiH) as the neutron shield. The SP-100 follows this lead. However, there is a need to investigate other neutron shielding materials because LiH has some properties degrading its integrity, especially at higher power levels. LiH has a melting point of about 960 K [Weast, et al., 1975]. At high temperatures, LiH has hydrogen dissociation. Hydrogen dissociation is most undesirable because hydrogen is the ultimate neutron attenuator. However, LiH is now the leading candidate as a neutron shield primarily because of its low weight density of about 0.775 grams/cc. But it is compulsory that, as space nuclear reactors evolve into higher power, there be a concentrated effort to develop other shielding materials other than LiH.

One possible alternate neutron shielding material is boron carbide (B_4C). B_4C has a low density, 2.52 gms/cc. Boron has a high probability or cross section for neutron absorption. This probability is increased when the neutrons are at lower energies, referred to as thermal energies.

Carbon adds strength; it also scatters neutrons which causes them to lose energy and, in effect, this slows the neutrons down to the thermal energy range increasing the B_4C's absorbing ability. This is an important interaction in B_4C's constituent atoms. B_4C has a melting point of 2623.15 K. This implies that it could survive a much higher power level than LiH. B_4C is very hard and brittle but has a very high compressive strength [Akerhielm, 1975].

However, since B_4C has a much higher density than LiH (and B_4C has no hydrogen in it), LiH is still currently the most desirable of the two materials, providing the temperature in the shield is at an acceptable range. A B_4C/W shield will be analyzed in this thesis.

Along with neutron attenuation, gamma ray shielding will also be looked at. Tungsten (W) is the leading candidate for photon shielding. Initial studies from many sources, including Oak Ridge National Laboratory, indicate that a LiH/W shield is the ultimate low mass radiation shield for a space nuclear reactor. This thesis will support this for missions in which the mass of the shield is the ultimate driver. However, some postulated Air Force missions may necessitate that volume, not mass, be the driving constraint for a shield.

2.0 BACKGROUND REVIEW

Space Nuclear Power is not new. In fact, it can trace its beginning back to 1948. In 1948, the Air Force initiated a program called Project Feedback. This was a study to develop reconnaissance satellites. The need for a reliable power source was a paramount issue [Voss, 1984]. This was a prelude to the Space Nuclear Auxiliary Power (SNAP) program which was initiated in 1955. The SNAP program was divided into two distinct parts; odd numbered SNAP projects referred to radioisotope generators while even numbered SNAP projects referred to space nuclear reactors. These projects, along with America's whole space program got a tremendous shot in the arm when an event took place in 1957.

On 4 October 1957, the Union of Soviet Socialist Republics launched Sputnik 1, the first man-made object put into a long duration orbit [Simons, et al., 1973]. It only weighed 184 pounds, transmitted data to Earth for only 21 days and was in orbit only 90 days, but it caused a near panic in the scientific and military communities. It was feared that now the Soviet Union had, or was close to having, the capability of delivering weapons to the North American continent from their own soil. This fear was not realistic, however; America's space program was accelerated because of it.

The United States preceded the Soviet Union in launching the first space nuclear reactor. The reactor was

called the SNAP-10A. SNAP-10A was launched on 3 April 1965 from Vandenberg Air Force Base, California. The reactor operated successfully for 43 days. A voltage regulator failure caused its permanent shutdown; it orbits in this mode today.

Another space reactor program was initiated in 1955. It was named Project ROVER. This program was to develop a nuclear rocket engine. These engines were at first developed to be a potential backup for intercontinental ballistic missile propulsion. However, it was later considered a candidate for boosters for manned Mars flights. The program terminated in January 1973, but by all accounts, the reactors developed are considered a technological success. In fact, the most powerful nuclear reactor ever built, the Phoebus-2A, reached a peak thermal output of 4080 megawatts when tested [Koenig, 1986].

While these two programs were terminated because of changing national priorities, they certainly left behind an enormous technology base for future development of space nuclear reactors. The ROVER program will serve as a stepping stone to the multimegawatt space nuclear program, and the SNAP program furnishes a technology base for the SP-100 program.

Future military and civilian space programs necessitated the SP-100 program. This program was born in 1982 by the Department of Energy (DOE) and the National Aeronautics and Space Agency (NASA) [Dix, et al., 1984]. A

tri-agency agreement between NASA, DOE, and the Defense Advanced Research Projects Agency (DARPA) signed in February 1983 established the SP-100 program [Wright, 1984]. This program will eventually lead to the development of higher power reactors. A major challenge facing the use of small compact core reactors is protecting the payload, whether it's human or electronic, from radiation induced by the nuclear reactor. The SP-100 uses LiH neutron shield (as did the SNAP program), and a W shield for gamma rays.

2.1 Past Shield Designs For Small Space Reactors. There have been many designs for space nuclear reactor shields. All of the ones fabricated have one thing in common; they use LiH as the neutron attenuator. (Except the shields used in the ROVER program.) The SNAP program is the technology base for LiH shield development. It seems prudent to examine the SNAP shields to get a good foundation for future shield development.

SNAP-2 was a small developmental reactor. The core diameter was 22.86 cm and produced a 3.5 kWe [Voss, 1984]. Two shields were developed for SNAP-2. The shields contained about 136 kg of LiH which allowed a large shadow of protection. SNAP-8 was a higher power reactor than SNAP-2. It was to provide 30-60 kWe. There were seven shields developed for SNAP-8. The shields consisted of W for gamma ray attenuation and LiH for neutron attenuation [Barattino, 1985]. The shields contained more LiH than the SNAP-2 shields, but they had a smaller void fraction.

The SNAP-10A shield development has some significance since this reactor was actually flown in space. The reactor was designed for low power; it only produced 500 We. This power level made LiH a most viable shielding material, and it also made the use of a gamma shield nonexistent. The shield contained about 91 kg of LiH in a stainless steel honeycomb [Anderson, et al., 1983]. A summary of the SNAP shield development is given in Table 2.1.

In the nuclear rocket program, ROVER, the hydrogen propellant was used as the shielding. This was most convenient since as the hydrogen was used up, the reactor shut down leaving only the fission products to shield. For an open cycle reactor system, this might be acceptable. However, for closed cycle high power reactor which probably will not use hydrogen coolant, this is not feasible and another concept must be explored.

Table 2.1 LiH Shields From The SNAP Program.

Reactor Type	Shield Mass	Shield Volume
SNAP-10A test casting	91 kg LiH	1.19×10^5 cc
SNAP-10A cast shield	91 kg LiH	1.22×10^5 cc
SNAP-10A developmental shield	91 kg LiH	1.22×10^5 cc
SNAP-2 developmental shield	136 kg LiH	1.78×10^5 cc
SNAP-2 DRM-1 shield	136 kg LiH	1.78×10^5 cc
SNAP-8 thermal shield	109 kg LiH	1.46×10^5 cc
SNAP-8 two-region test casting	205 kg LiH	2.66×10^5 cc
SNAP-8 two-region DRM-1 shield	327 kg LiH	4.23×10^5 cc
SNAP-8 experimental shield 1	91 kg LiH	1.22×10^5 cc
SNAP-8 experimental shield 2	91 kg LiH 91 kg W	1.20×10^5 cc
SNAP-8 DR shield	327 kg LiH	4.23×10^5 cc
SNAP-8 experimental shield 3	55 kg LiH	7.20×10^4 cc

[Anderson, et al., 1983]

2.2 Conclusions From Past Designs. LiH had some cracking problems in the SNAP shields. This is a potential problem since it could create streaming paths for the radiation to penetrate the shield. However, studies have shown that the cracks were random and did not create a straight streaming path, a problem referred to as "shine through". Ramping the reactor power up and down, thus changing the temperature of the LiH, will invoke creep stress in the shield and aggravate the cracking problem. Also, higher power levels will lead to hydrogen dissociation. Aiding in this reaction is an oxygen impurity found in LiH. This impurity combines with LiH to form lithium hydroxide [Welch, 1975]. The results is an outgassing of H_2. The governing reaction for this is:

$$LiH + LiOH \longrightarrow Li_2O + H_2.$$

This reaction becomes prevalent at temperatures above 680 degrees K. When coupled with meteoroid punctures in the shield H_2 can be released from the shield. If LiH melts, it changes volume drastically. It expands about 25%; this could pose major problems for the container of LiH and negate the neutron shield if the container is ruptured during expansion. This same thing could happen if the container holding liquid LiH was punctured by micro-meteorites. The ^{6}Li isotope in natural lithium can also cause problems. It will absorb neutrons and the resulting in the exothermic reaction:

$$^6Li_3 + ^1n_0 \rightarrow ^3H_1 + ^4\alpha_2 + 4.8\ MeV.$$

This causes the temperature in the shield to rise. Depleted

LiH (LiH with little or no ^{6}Li) could be a solution to this problem.

A minimum temperature of about 600 K will minimize radiological induced hydrogen dissociation. Thus, a temperature range for use of LiH is recommended to be between 600 and 680 K [Barattino, 1985].

LiH has other precarious physical properties. It is easy to burn, it has moderate strength, and it reacts with almost anything. To sensibly use LiH, the reactor power needs to be less than one megawatt thermal [Anderson, et al., 1983]. Also, the temperature in the shield must not exceed its melting point (960 K) and, as stated, its optimum operating temperature range should be between 600 and 680 K. To add strength and stability to LiH, a honeycomb matrix can be used as with the stainless steel matrix in the SNAP shields. However, for higher power reactors, LiH cannot be used unless an active cooling system is used to maintain the shield temperature at an acceptable level.

Tungsten appears to be the leading candidate for gamma shielding. It is expensive, but since the weight of the shield may be the initial ultimate driver in material selection, W is a solid choice. Gamma rays interact with electrons of atoms. W has a high electron density. Because of this, it takes less W than other conventional gamma shields to attenuate the gamma flux to the same level.

3.0 Radiation Attenuation

Charged particles are usually massive making it somewhat easy to stop them. Of the forms of radiation of concern, alpha, beta, gamma, and neutrons, the most penetrating are gamma rays and neutrons. If these are stopped, then the other forms of radiation pose no threat. The following sections are an explanation of the radiation interactions without going into detailed quantum mechanics.

3.1 Gamma Ray Attenuation. Gamma ray sources are fission gammas, fission-product-decay gammas, capture gammas, products of inelastic scattering, and reaction products [Schaeffer, 1973]. Gamma rays have no charge, therefore, they are very penetrating. Gamma rays interact with an atom's orbital electrons. Basically, there are three ways in which they do this. These are photoelectric absorption, Compton scattering, and pair production.

Photoelectric absorption, or photoelectric effect, occurs when a tightly bound electron is subjected to an incident gamma ray. The atom absorbs the photon which disappears; this results in an electron being ejected if the electron absorbs more energy than its binding energy. The ejected electron will have all the energy of the gamma minus its binding energy. At low energies, $E \leq 0.5$ MeV, this is the dominant gamma ray interaction.

When the photon energy is increased, $0.5 \leq E \leq 1.2$ MeV, Compton scattering becomes dominant. This process occurs

when a photon scatters with an orbital electron, and it loses some of its initial energy, and the electron is ejected from the atom. This can be thought of as scattering of electromagnetic waves by charged particles [Weidner et al., 1973]. It is obvious that this process is proportional to the electron density of the attenuating medium.

When the gamma ray is of high energy, then pair production threshold is dominant. This occurs when E $\geq$ 1.022 MeV which is equal to the combined rest energies of an electron and a positron [Hubbell et al., 1968]. The photoelectric effect and Compton effect are examples of electromagnetic energy of photons being converted to kinetic energy and potential energy of material particles [Weidner et al., 1973]. In pair production the photon produces two particles which have opposite charge, an electron and a positron. In this case, the incident photon disappears.

The absorption coefficient for each of these interactions accounts for the total absorption coefficient for gamma ray attenuation. The total absorption coefficient is expressed as

$$\mu_{tot} = \mu_{pe} + \mu_c + \mu_{pp}.$$

Since materials with a higher density usually have more electrons orbiting their atom's nucleus, there is a definite relationship between the absorption coefficient and the material's density. This introduces the idea of a mass attenuation coefficient, μ/ρ , where μ is the attenuation coefficient and has dimensions of cm^{-1}, and ρ is the density

of the material. The mass attenuation coefficient has units of cm^2/gm. This coefficient is proportional to the total gamma interaction probability or cross section.

3.2 Neutron Attenuation. There are three basic ways in which neutrons interact with matter: elastic scattering, inelastic scattering, and absorption. Elastic scattering is an event where kinetic energy is conserved and the internal energy of the nucleus is not changed. The final energy of the neutron can be related to the initial energy of the neutron by the formula:

$$E_f = \left[\frac{(1+\alpha)+(1-\alpha)\cos(\theta_c)}{2}\right] E_i.$$

Where: E_f =Final Energy
E_i =Initial Energy
$\alpha = \left(\frac{A-1}{A+1}\right)^2$
A =the Atomic number.
θ_c =the Center of Mass Scattering Angle.

Hydrogen with an atomic number of 1 can take all of the neutron's energy, and the maximum energy the neutron can lose corresponds to a backscattering event of 180 degrees in the center of mass system [Duderstadt, et al., 1976]. A neutron can survive enough scattering events until its kinetic energy is sufficiently degraded so that it can have its energy increased by hitting a thermal vibrating nucleus. The thermal neutron is eventually absorbed by a nucleus.

Another form of elastic scattering is resonance scattering. In this case the incident neutron is absorbed

by the nucleus. To return to its ground energy state, the nucleus will expel another neutron that has the same energy as the incident neutron [Selph, 1968].

In inelastic scattering the incident neutron is captured by the nucleus. This produces a compound nucleus in an energetically excited state; the nucleus then ejects a neutron, but this does not return the nucleus to its ground state, i.e., the expelled neutron has a lower energy than the incident neutron. In an attempt to return to ground state, the excited nucleus will giv off one or more gammas. Usually, this kind of scattering event occurs at high neutron energies, and a great deal of the incident neutron's energy can be given to the nucleus [Duderstadt et al., 1976]. This makes this an important reaction for shielding, but it generates secondary gammas which have to be attenuated.

Finally, absorption is an important interaction. This usually happens when the neutron is in the low or intermediate energy range as with the thermal neutrons mentioned above. The incident neutron is captured by the nucleus which excites it. The excited nucleus then attempts to go to its ground state by emitting one or more gammas. These gammas are usually highly energetic and they too must be attenu ted since they can contribute substantially to the radiation dose. As the neutron penetrates the shield, it undergoes scattering events which reduces its energy; if it survives long enough, it will eventually become an

intermediate or thermal neutron and most likely be absorbed. Therefore, this may be most important interaction in shielding.

Individual shielding materials have a higher probability for one of these events than another. Since fission neutrons are born with very high energies, and since high energy gammas also are produced, layered shields become important to maximize radiation attenuation and minimize the mass of the shielding concept. Besides having the ability to maintain its integrity under severe radiation, the shielding material must also be able to maintain its integrity when placed under severe thermal and mechanical stress. Minimizing mass, and maintaining structural integrity for the reactor's lifetime are the goals for a space nuclear reactor shield.

4.0 Radiation Damage to the Payload

It may be quite some time until humans are subjected to a close proximity to a space nuclear reactor. This is the reason early space nuclear reactors were concerned with shielding the electronics in the payload. However, in the not too far distant future, astronauts may have to perform maintenance on reactors or systems powered by reactors. The shield must be able to perform its protective function whether protecting humans or an electronic payload.

4.1 Human Exposure. The ultimate responsibility for setting guidelines for radiation safety is the International Commission on Radiological Protection (ICRP). In individual countries, national committees are set up to follow ICRP recommendations. This country has the National Committee on Radiation Protection and Measurements (NCRP) [Cember, 1969]. The criteria for human terrestrial occupational exposure set by the NCRP is well established and strictly adhered to by industries. However, for space nuclear reactors, this criteria would result in such massive shields that the concept of a space nuclear reactor might not be realistic (except for reactors used on the moon, etc.). Shield design for nearby human existence is beyond the scope of this thesis.

4.2 Radiation Exposure to Electronic Payloads. Protection of the electronic payload is the major function of early space reactor shields. Protecting the payload

electronics must include protection from space reactor induced radiation and natural radiation in space. Since many of our current spacecraft utilize radioactive elements, there is an experienced technology base for radiation protection of electronics from low energy gammas. However, radiation produced by a nuclear reactor introduces high energy neutrons and gamma rays which will take a more elaborate shielding scheme than what is presently used in spacecraft. Various research centers such as Sandia National Laboratory are engaged in extensive research to harden electronics to enable them to withstand a higher radiation flux. This will be most advantageous because it will take less shielding mass to protect the electronics, thus saving substantially on launch cost.

The basic radiation interactions were discussed in Sections 3.1 and 3.2. The different photon interactions, pair production, Compton scattering, and photoelectric effect are dominant in distinct energy regions. The particular energy ranges differ somewhat for different materials. Figure 4.1 shows the three gamma interactions as a function of the atomic number, Z, and gamma ray energy. Silicon (Si) is the primary material of concern in shielding electronics. Its atomic number, Z, is equal to 14. Photoelectric effect dominates photon interaction up to about 50 keV. Compton scattering dominates from 50 keV to about 19 MeV. Pair production dominates at photon energies greater than 19 MeV.

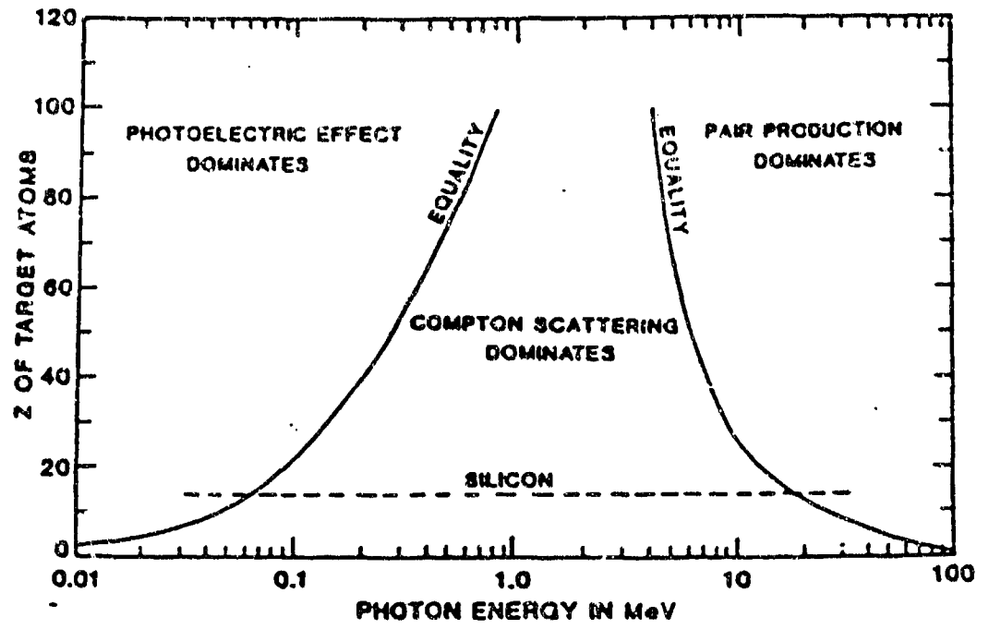

Figure 4.1 Photon Interactions.

Neutrons interact by elastic scattering, inelastic scattering, and absorption. Neutrons that collide with a nucleus in an elastic scattering event can knock that atom out of its lattice position. The energy necessary for this is about 25 eV in most materials. Knocking an atom out of the lattice position can cause it to dislodge other atoms as well. This process can alter the material's ability to conduct current or other desirable electronic properties. Inelastic scattering can also cause displacement of atoms in their lattice positions. Absorption sometimes leads to a transmutation, i.e., converting one element to another. Obviously, the properties of the target atom are lost. The dominant processes in silicon are the displacement of an atom from its lattice position and ionization. Ionization is

any process by which an atom, molecule, or ion gains or loses electrons resulting in a species having a net charge. This can be caused by energetic neutrons or gamma rays.

Any space nuclear reactor shield system must be able to protect the mixture of electronic devices contained in integrated circuits. Neutrons, gammas, and charged particles can permanently damage the electronics. Although redundancy will be used in the electronic circuits, a shield will still be essential to protect the payload for the lifetime of the reactor. But the most important aspect of the shield is that it provides the means to extend the lifetime of the electronic circuits insuring that the mission can be accomplished.

5.0 Analyzing the Reactor

The nuclear reactor design taken for this thesis is similar to the SP-100 reactor. The SP-100 is not in its final design state. Therefore, although the reactor design in this thesis is based on some of the features of the SP-100 as of 9 August 1985, it will not be the same as the final SP-100 configuration which may be built and deployed near future.

This reactor is a small compact reactor with highly enriched ^{235}U. It is designed to produced 2 MWt, and it serves as the baseline design for the FEMP1D shielding calculations with a few modifications.

FEMP2D was not used for the actual shielding analysis. However, it was run to determine some important features to be used in FEMP1D. Primarily, it aided in the selection of the proper energy structure for the cross sections. Collapsing the cross sections will allow the codes to run using less computer CPU time. The cross sections in the collapsed group structure are defined so as to preserve the interaction balance in each region. FEMP2D was used in an attempt to verify the interaction definition for each region since there were existing bench marks to verify FEMP2D's results. The same group structure could then be used with FEMP1D with more confidence. This Section will describe the reactor model use with FEMP2D and some of the code setup procedures.

5.1 Reactor Description. A cross sectional view of the core modeled is shown in Figure 5.1. Table 5.1 gives some reactor data. It has a radius of 27.5 cm and a height of approximately 62.25 cm (including the core structure). There are 696 fuel pins consisting of highly enriched Uranium Nitride (UN), 7 hexagonal in-core control and safety rods, a flow baffle on the outside boundary of the fuel pins consisting of a neutron absorbing material (B_4C) and structural container, and 16 external control drums placed in beryllium carbide (Be_2C) reflecting material.

The sixteen control drums are mostly Be_2C, but they also contain a 120 degree, 1 cm segment of B_4C which acts as a neutron absorber and is turned toward the core as in Figure 5.1 when the reactor is in a shutdown mode. However, for this analysis, the reactor is in its most critical configuration which would be represented with the B_4C turned to the outside. (This is the reactor's operational configuration.) In fact to simplify the configuration, the B_4C segment is ignored completely. (A neutron getting into the neutron absorber has a very small probability of scattering back into the core contributing to the reactor criticality.)

The center of the core consists of a hexagonal safety plug shown in Figure 5.2. The innermost rod consists of B_4C followed by Be_2C. When the reactor is shutdown, the B_4C is inserted into the core for neutron absorption, and when the reactor is operational, the Be_2C is inserted for neutron

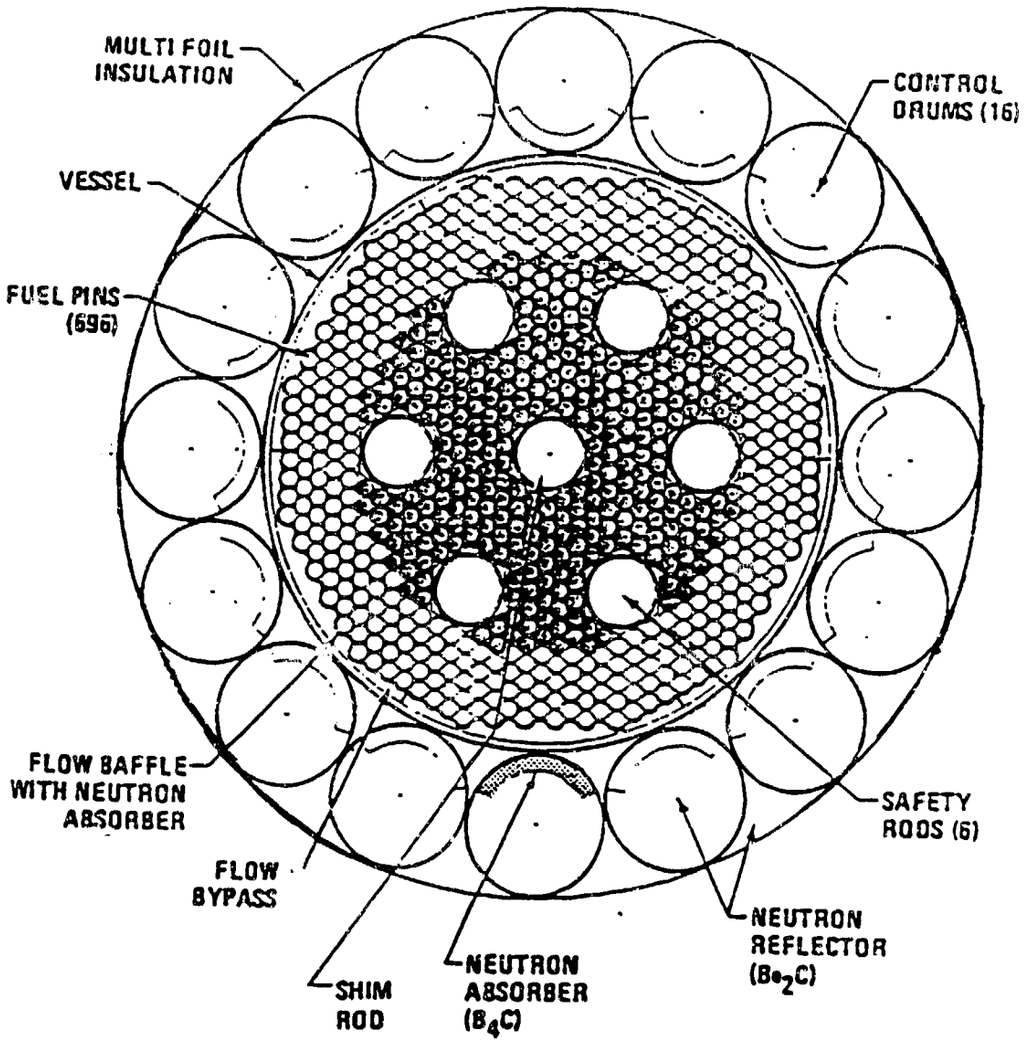

Figure 5.1. Reactor Core Cross Section.

Table 5.1 Reactor Characteristics.

Core Radius	27.5 cm
Core Height (Including Core Structure)	62.25 cm
Active Core Height	32.00 cm
Fuel Pins:	
Pin Diameter	1.05 cm
Pitch/Diameter	1.07
Fuel Pellet Material	Uranium Nitride
Density	14.32 g/cc
Melting Point	2740 K
Pellet Column Height	32 cm
Cladding Material:	99% Niobium 1% Zirconium
Cladding Thickness	0.074 cm
Density	8.4 g/cc
Melting Point	2640 K
Tungsten Liner	0.013 cm thick
Number of Fuel Pins	696
Enrichment:	
300 pins with 72% enrichment in the middle 20 cm section; 96% enrichment in top and bottom 12 cm.	
396 pins 96% enriched	
Coolant	Lithium

reflection. In the analysis, the reactor will be in the operational mode. The cladding material for the Be_2C rod consists of an niobium-zirconium alloy (Nb-1Zr) which is 1% zirconium. A gap separates the cladding and the outer region of the hexagonal element. The outer region also consists of Nb-1Zr. All of the remaining 6 internal control rods consist of these same materials.

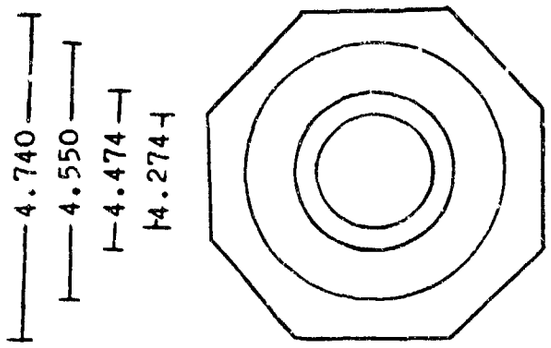

Figure 5.2 Hexagonal Control Rod.

The fuel rods consist of two different enrichments of UN, 96% enriched in uranium-235 (^{235}U) isotope and 72% enriched ^{235}U to flatten the flux in the core. Figure 5.3 shows a cross sectional view of the fuel rods. The fuel pellet in the center of the fuel pin is the UN. The pellets

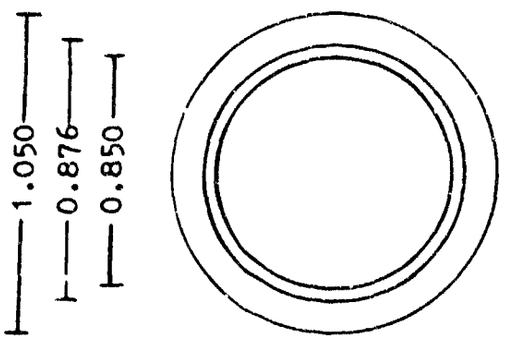

Figure 5.3 Cross Section of the Fuel Rods.

are 0.85 cm in diameter. The density of the UN is 96% of its theoretical density. The theoretical density of UN is 14.32 g/cc. The length of the fuel pellet column is 32 cm. A 0.013 cm thick W liner is placed between the fuel pellets and the cladding material. The cladding consists of Nb-1Zr 0.074 cm thick. The total diameter of the fuel pin is 1.05 cm and its pitch/diameter ratio is 1.07.

There are 300 fuel pins that have two axial enrichment zones. These pins concentrate themselves in the area from the center of the core joining the center safety plug with their outer boundary approximately along the outer edge of the 6 control rods shown in Figure 5.1. The remaining 396 fuel rods are uniformly 96% enriched.

A W wire spacer 0.0735 cm is wrapped helically around each fuel pin. The fuel rods are arranged in a triangular pitch with the outer boundary of the fuel area bounded by a coolant flow baffle.

The baffle consist of two walls of Nb-1Zr 0.125 cm thick. There is an inner neutron absorbing material, B_4C, which is 0.025 cm thick against each wall. The coolant flow region is approximately 0.15 cm thick.

The coolant is lithium (Li), which consist of 7.5 atom percent of the ^6Li isotope and 92.50 atom percent of the ^7Li isotope. The reactor core vessel is made of Nb-1Zr and the surrounding reflector material is Be_2C.

5.2 Finite Element Code. The codes used in the analyses were the Finite Element Multigroup P_n 1-Dimensional (FEMP1D) and the Finite Element Multigroup P_n 2-Dimensional (FEMP2D) codes. These radiation transport codes are based on a spatial discretization using finite element methods and an angle representation using spherical harmonic methods. They are able to treat eigenvalue problems, upscattering in the different energy groups, and coupled neutron and gamma problems. They will run on vector machines and are written in FORTRAN 77 [McDaniel, 1984]. The results reported this thesis were calculated using the VAX 11/750 version of FEMP1D.

5.3 Setting up the FEMP2D Input. The core design modeled for FEMP2D shown in Figure 5.1 was divided up into concentric cylinders two different ways as shown in Figures 5.4a and 5.4b. This was to determine the sensitivity of K-effective with FEMP2D to core division. The answers were essentially the same which indicates, for this reactor, that core division is not very critical. Therefore, the concentric division shown in Figure 5.4a was selected.

The material composition is modeled by creating a homogeneous mixture for each zone. Atom densities are calculated in such a way as to preserve the number of atoms of each nuclear species within each zone. This procedure is commonly termed "smearing." Effective radii must be calculated for these zones since the geometric

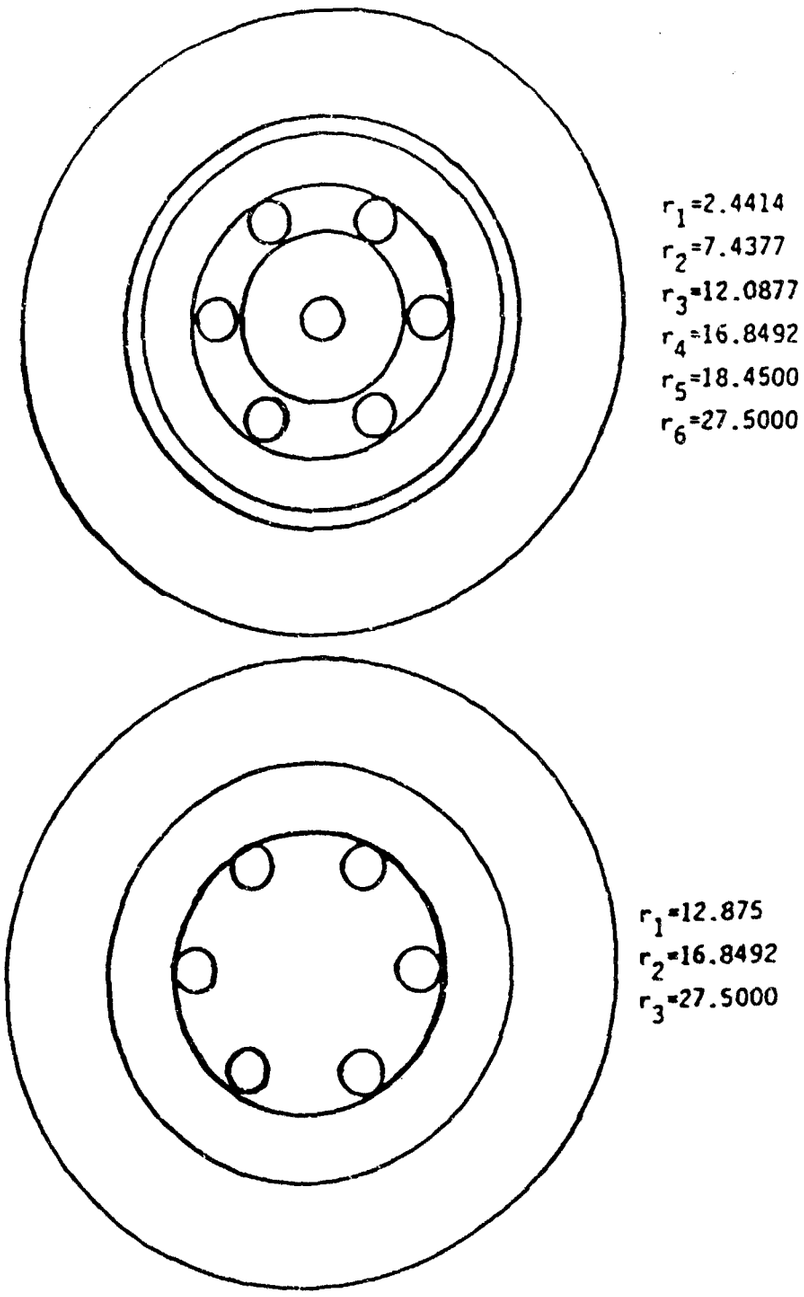

Figure 5.4a and Figure 5.4b. Smeared Zones for FEMP2D.

configurations of the materials at the zone boundaries are not circular. Radial zone 1 is bounded by an hexagonal element.

First, the area of the hexagonal element is calculated using the formula:

$$Area = n*r^2*\tan(PI/n).$$

Where:

n = the number of sides, 6.

r = the distance from the center of the hexagonal element to the center of one of the hexagonal edges.

PI = 3.14159.

Since the area of a circle is $PI*r^2$ the equivalent radius can be calculated as:

$$R_{req} = (Area/PI)^{0.5}.$$

This value is used as the effective radius of the first radial zone.

The next step is to calculate an effective radius to set the outer boundary of radial zone 3. There are 300 fuel pins and seven hexagonal control rods in this section. Also, there are coolant and wire spacers between the fuel rods and fuel rod/control rod boundaries. Since the fuel pins are in a triangular pitch, it will be necessary to analyze the area ratios for one triangular cell to determine the zone boundary. Figure 5.5 shows the triangular cell.

The diameter of the fuel pins is 1.05 cm. The pitch to diameter ratio is 1.07. Therefore, the pitch between the

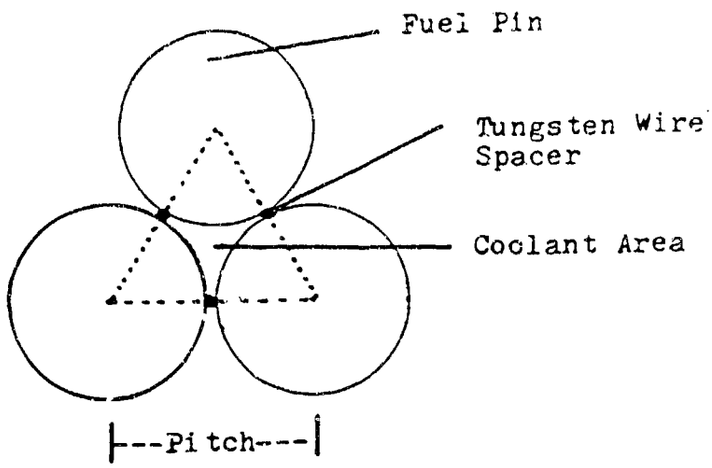

Figure 5.5 Triangular Cell.

the fuel pins is calculated by:

$$Pitch = (P/D) * D.$$

Where: P/D = the pitch to diameter ratio.

D = diameter of the fuel pins, 1.05 cm.

Next the total area of the triangle is calculated by using the formula:

$$Area = 0.5 * a^2 * \sin(theta).$$

Where:

a = pitch

theta = 60 degrees or PI/3 radians for an equilateral triangle.

Using the following formula to calculate the area of the fuel pins in the triangular zone,

$$Area = (1/6 + 1/6 + 1/6) * PI * (1.05/2)^2 ,$$

the ratio of the area of the fuel pins to the area of the total triangle can be obtained. The area of the 300 fuel

pins is 300 * PI * r^2. Taking this total and multiplying it by the inverse of the ratio of the fuel pins to the area of the total triangle calculated above gives the total area of the 300 fuel pins, the coolant channels and the wire spacers. The area of one hexagonal element has been calculated. Taking that value and multiplying it by seven gives the total area for the center safety plug and the six control rods. Adding the total area of the seven hexagonal elements to the total area of the 300 fuel rods, coolant channels, and wire spacer gives the total area bounded by this effective radius. Calculating this effective radius is done as above for the first effective radius. Appendix A shows these calculations.

Since r_1 and r_3, the effective radii calculated above, are now known, r_2 is obtained by subtracting twice r_1 (the diameter of the hexagonal elements) from r_3. r_4 is calculated by realizing that it is the boundary of all 696 fuel pins, coolant between the pins, the wire spacer, and the seven hexagonal elements. As before calculate the area of all 696 fuel pins, multiply by the inverse of the fuel pin to total area in the triangle. The value defined in this manner is total area of the 696 fuel pins, coolant and wire spacer. This total is added to the area of the seven hexagonal elements giving the total area of the fuel region. r_4 can now be calculated in the same way as r_1 and r_3 were using the same formula.

The other radii are given in Table 5.2. r_5 is the

radius from the center of the core to the reactor vessel. r_6 is the radius to the outer boundary of the reflector.

Table 5.2 Effective Radii for Radial Zones.

r_1 = 2.4414 cm
r_2 = 7.4377 cm
r_3 = 12.0877 cm
r_4 = 16.8492 cm
r_5 = 18.4500 cm
r_6 = 27.5000 cm

The core is then divided into axial zones. Figure 5.6 shows the homogeneous material zones used for determining the axial division. Going from left to right and bottom to top, the first zone is made up of Nb-1Zr which is the fuel pin cladding of the fuel pin plenum protruding out of the top of the core, B_4C, which is the follower in the seven hexagonal elements, and Li coolant. The second zone consists of structural material, primarily Nb-1Zr. The third zone is the core. The fourth is the Be_2C reflector. The fifth is a thin strip of fuel pin support structure or grid supporting the fuel pins. It is composed of Nb-1Zr. Finally, the top is a pool or reservoir of Li coolant. These physical boundaries, together with the different axial enrichment zones in the fuel, determine the axial zone divisions to be used in this analysis. The first 300 fuel

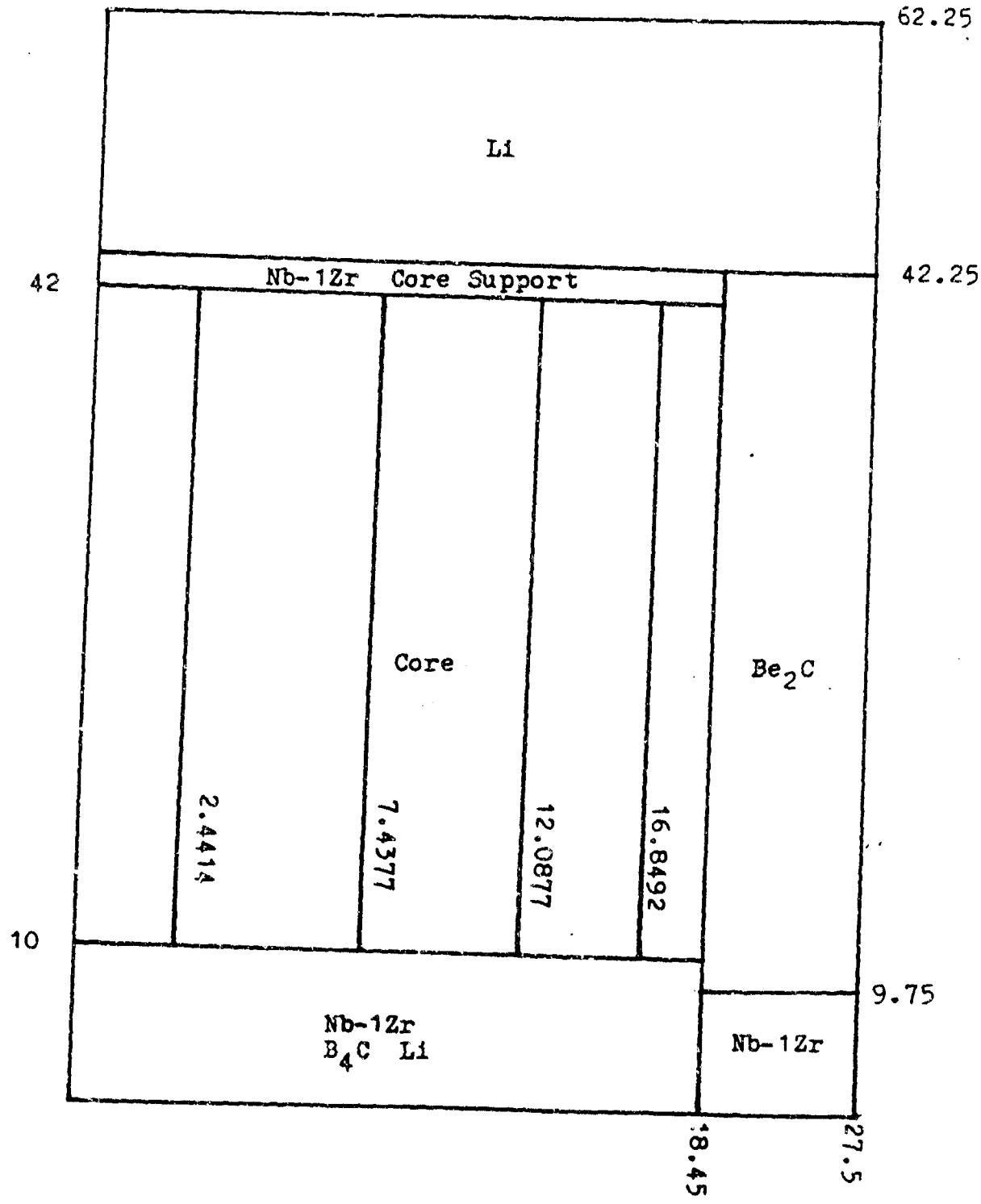

Figure 5.6. Axial Core Model.

pins in the center of the core have two enrichments of 72 and 96%. The top and bottom 12 cm of these pins are 96% enriched while the middle section is 72% enriched. Since there is a change in enrichment zones, there is a change in the atom densities also. Thus two axial boundaries are created; one 12 cm from the bottom of the fuel pins and one 12 cm from the top. Figure 5.7 shows the radial and axial zones created by the above scheme. The 42 material zones created by the core division shown in Figure 5.7 have nuclides whose atom densities will be smeared to constitute homogeneous mixtures. These homogeneous mixtures are considered by the code as constituting specific materials. This means that the homogeneous mixture in zone 1 is considered one material, the homogeneous mixture in zone 2 is another material, etc. Zones 1 and 2 could conceivably have the same nuclides in them, but not the same smeared atom density. Thus, the code considers the nuclides to be different materials.

Of course, different zones may be composed of the same homogenized material. This usually happens when a radially bounded zone is separated by an axial zone of different nuclides. Setting up the material zones is called setting up a mixing table.

5.4 Atom Density Calculations. The different nuclides used to model this reactor are listed in Table 5.3. The atom densities of each of these nuclides must first be calculated before they are smeared in their respective zones. To

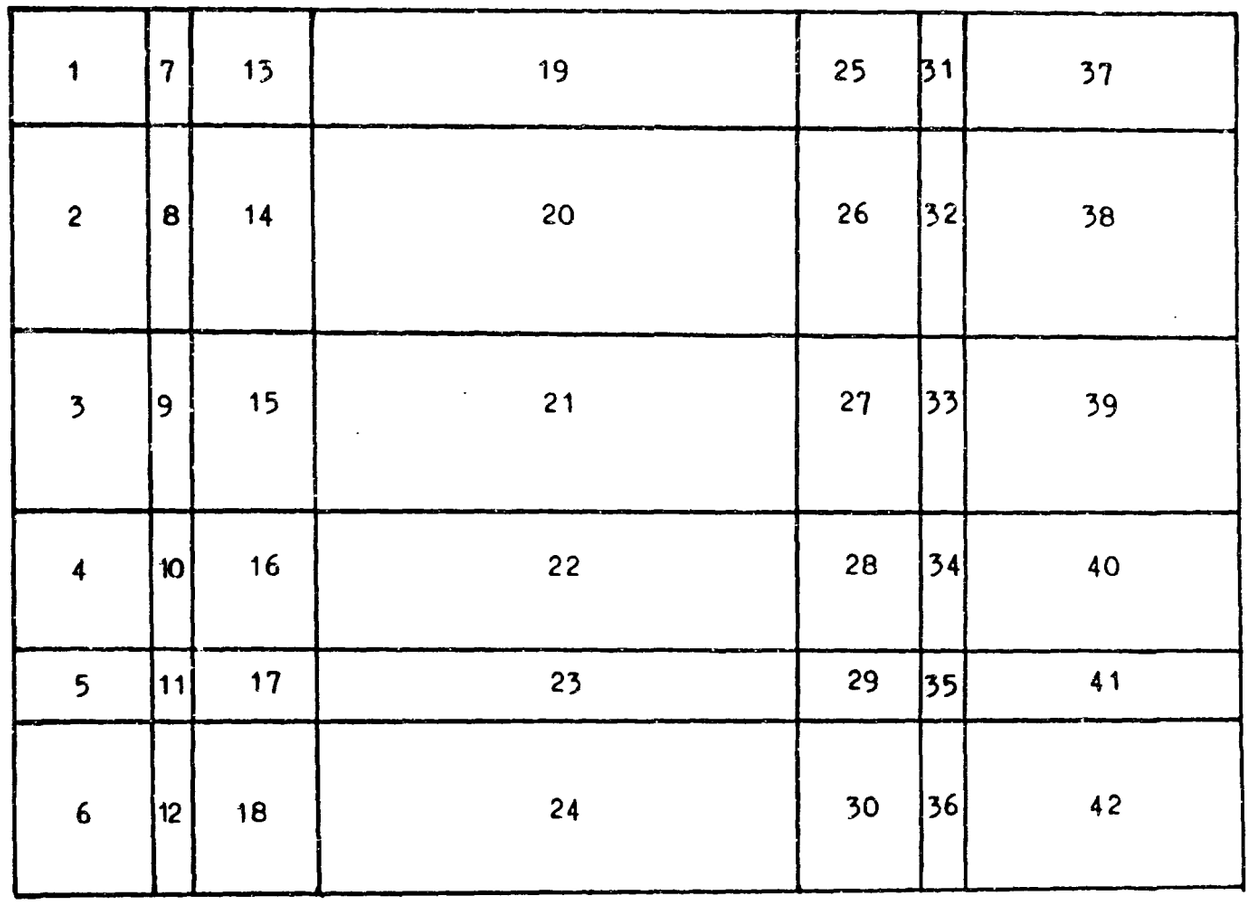

Figure 5.7. Core Zone Division.

Table 5.3 Nuclide Atom Densities. (Atoms/(Barn cm))

Nuclide	Atom Density
96% Enriched Fuel:	
Nitrogen	3.3226 E-2
^{235}U	3.1913 E-2
^{238}U	1.3129 E-3
72% Enriched Fuel:	
Nitrogen	3.3131 E-2
^{235}U	2.3939 E-2
^{238}U	9.1920 E-3
^{182}W	1.6627 E-2
^{183}W	9.0403 E-3
^{184}W	1.9389 E-2
^{186}W	1.8081 E-2
Niobium	5.5046 E-2
Zirconium	5.5602 E-4
^{6}Li	3.4748 E-3
^{7}Li	4.2856 E-2
Beryllium	7.6179 E-2
Carbon (In Be_2C)	3.8090 E-2
^{10}B	2.1970 E-2
^{11}B	8.7881 E-2
Carbon (In B_4C)	2.7463 E-2

calculate the atom densities of the materials for this model the following formula may be used:

$$N(\text{atoms/cc}) = \frac{\rho * Na}{Ma}$$

Where: Na = Avogadro's Number, 6.022045×10^{23} atoms/(gm atom) or molecules/(gm mole).

Ma = Molecular weight gm/(gm atom) or gm/(gm mole).

ρ = Nuclide density (gm/cc).

Consider Be_2C:

$$\rho = 1.9 \text{ g/cc}$$

$$Ma = 30.04 \text{ g/cc}$$

$$N = \frac{(1.9) * (6.022045 \times 10^{23})}{30.04}$$

$$= 3.8090 \times 10^{22} \text{ molecules/cc}$$

$$N(Be) = (2) * (3.8090 \times 10^{22})$$

$$= 7.6179 \times 10^{22} \text{ atoms/cc}$$

$$N(C) = 3.8090 \times 10^{22} \text{ atoms/cc}$$

The first calculation for N of Be_2C did not yield the atom density of any of the constituent atoms, Be or C. The value obtained has units if molecules/cc. In one molecule of Be_2C, there are 2 atoms of Be ard one atom of carbon. Therefore, the next two calculations yield the desired results, N_{Be}(atoms/cc) for Be and N_C(atoms/cc) for carbon. Since the FEMP codes require the atom densities in units of atoms/(barn cm), it is necessary to multiply the atom densities calculated by the above by 10^{-24} cm^2/barn.

Another way to calculate atom densities requires a

knowledge of the crystal structure. Consider the crystal structure of Nb-1Zr shown in Figure 5.8. The atoms form a cubic structure of 2 atoms per cell. For Nb-1Zr, in 50 cells, there are 100 atoms. 99 of these atoms are Nb while the other one is Zr. Since the sides of the crystal are 3.301 A, and 1 A equals 10^{-8} cm, the volume can be calculated:

$$\text{Volume of 50 cells} = (50) * (3.301 \times 10^{-8})^3$$
$$= 1.7985 \times 10^{-21} \text{ cc.}$$

To get the atom density of Zr:

$$1 \text{ Zr atom}/(1.7985 \times 10^{-21}) = 5.5602 \times 10^{22} \text{ atoms/cc.}$$

The atom density of Nb is:

$$99 \text{ Nb atoms}/(1.7985 \times 10^{-21}) = 5.5046 \times 10^{22} \text{ atoms/cc.}$$

Again, the values need to be multiplied by 10^{-24} to yield the correct units in atoms/(barn cm) for the FEMP inputs [Stein, 1986].

This technique works well for the simple crystal structure of Nb-1Zr. However, for complicated crystal structures, it may not be a very feasible way to calculate atom densities although it will always give the correct theoretical atom density.

After calculating the atom densities for each material, these atom densities are homogenized or smeared throughout the zone which they are in. Zones 1, 2, and 3 all contain Nb-1Zr. However, they also contain other materials and the Nb-1Zr comprises a different volume fraction of the total

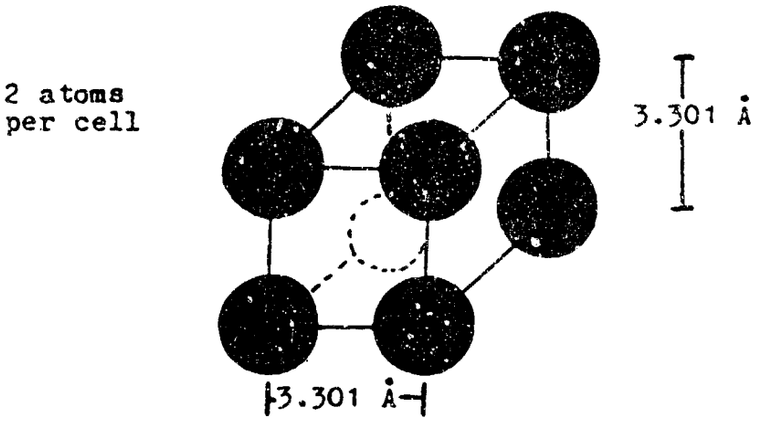

Figure 5.8. Crystal Structure of Nb-1Zr.

volume of the zones. This yields a different smeared atom density for Nb-1Zr for each of these zones when smeared in each one. Table 5.3 gives the nuclides in this reactor model with their respective atom densities.

To calculate the smeared atom densities for each zone, the following formula:

$$N(\text{smeared}) = N(\text{atoms/(barn cm)}) * (Vm/Vz)$$

Where: N(smeared) = the smeared atom density in the particular zone.

N(atoms/(barn cm)) = the atom density calculated above.

Vm/Vz = the ratio of the volume of the material in the zone to the total volume of the zone.

Consider the Nb-1Zr in zone 2 in Figure 5.7. That zone has four nuclides: Nb, Zr, ^{6}Li, and ^{7}Li. From Figure 5.7 it is obvious that it is bounded radially by r_1 and r_2 and axially by 9.75 cm. The volume for the whole zone is then:

$$Vz = 3.1416 * (7.4377^2 - 2.4414^2) * 9.75$$

$$= 1,511.8906 \text{ cc.}$$

The Nb-1Zr in this zone is the cladding of the fuel pins in the plenum section of the fuel pin. From the triangular cell analysis already done, the area of the fuel pins to the total area of the zone may be calculated. First, calculate the area of the zone:

$$\text{Area of the zone} = 3.1416 * (7.4377^2 - 2.4414^2)$$

$$= 155.0657 \text{ cm}^2.$$

From the triangular cell analysis discussed in Section 5.3, the ratio of the area of the fuel pins to the area of the triangular cell is:

$$A_{fp}/A_c = 0.4330/0.5466$$

$$= 0.7921.$$

Therefore, the area of fuel pins can now be calculated by multiplying this ratio by the area of the whole zone:

$$\text{Area of the fuel pins} = (0.7921) * (155.0657)$$

$$= 122.8275 \text{ cm}^2$$

Since Nb-1Zr is the cladding of the fuel pins, the ratio of the cladding area to the area of the fuel pins needs to be calculated. The cladding for these fuel pins is 0.074 cm thick. The area of the cladding for one fuel rod is:

$$A_c = 3.1416 * ((1.05/2)^2 - ((1.05 - (2 * 0.074))/2)^2)$$

And the area of one fuel pin:

$$A = 3.1416 * (1.05/2)^2$$

$$= 0.8659 \text{ cm}^2.$$

The ratio of the area of the cladding to the area of the fuel pin is:

$$Ac/A = 0.2269/0.8659$$
$$= 0.2620.$$

The total area of the Nb-1Zr is then obtained by multiplying the ratio calculated above and the area of the fuel pins calculated already:

$$A(Nb\text{-}1Zr) = (0.2620) * (122.8275)$$
$$= 32.1801 \text{ cm}^2.$$

And the volume of Nb-1Zr is: (32.1801)*9.75 = 313.7628 cc. There is now enough information to calculate the smeared atom density for Nb-1Zr for this cell.

$$N_{Zr} \text{ (smeared)} = (313.7628/1,511.8906) * 5.5602 \text{ X } 10^{-4}$$
$$= 1.1541 \text{ X } 10^{-4} \text{ atoms/(barn cm)}$$

$$N_{Nb} \text{ (smeared)} = (313.7628/1,511.8906) * 5.5046 \text{ X } 10^{-2}$$
$$= 1.1425 \text{ X } 10^{-2} \text{ atoms/(barn cm)}.$$

All the smeared atom densities in each zone can be calculated likewise. However, for some zones it is not necessary. For example, zone 25 is made up totally of Be_2C. In this case, the volume ratio is 1 and smearing in unnecessary. Also, when calculating the smeared densities in zones where the material has the same height as the zone (as was the case for the Nb-1Zr above), the smeared densities can be obtained by using the area ratios since the heights divide out in the volume ratios. The smeared atom densities in Appendix B are calculated using the area ratios for each zone.

5.5 Dividing the Core into a Fine Mesh. FEMP2D and FEMP1D permit the core to be divided into a fine mesh grid which is smaller than the zone division shown in Figure 5.7. Core division can cause problems when the divisions do not define flux alterations between the zone boundaries. For example, the flux profile in the fuel region and the flux profile in the control rods will be different. Therefore, caution should be taken as to where the homogenized zone boundaries are in the core. A consequence could be an erroneous criticality calculation. Using a fine mesh spacing allows for better numerical stability and could avoid this problem. The core modeled in this thesis did not show this sensitivity. Other core models may. The user should be aware of this potential problem because other core models may exhibit poor flux definition across zone boundaries.

Consider the radial zones, r_1 and r_2. There are 7 zones bounded by these radii: zones 2, 8, 14, 20, 26, 32, and 38. These zones have different materials in them. If the mesh spacing was left with no fine mesh between the two radii, then there is a good possibility that some of the neutron and gamma interactions with these materials would occur without the finite element scheme tracking it. Therefore, for all the zones bounded by these radii, there must be a fine mesh space defined radially such that the fine mesh will not be longer than the mean free path of a neutron in the materials for all the above zones. This means that the material with the smallest mean free path

should determine the fine mesh structure, and the mesh spacing should be no longer this value. This implies a difficult task to calculate all the mean free paths. However, the FEMP codes do this and they print these values out. The radial spacing can be picked arbitrary, the code run, then the mean free paths checked with the output file under a column called PLEN. This technique also applies for defining the mesh spacing in the axial direction.

Appendix C has an input file used for the FEMP2D analysis for this core. Determining the sensitivity of the input data is a major concern when running the code.

5.6 Sensitivity of Solution to Material Atom Densities. Since k-effective (K_{eff}) is sensitive to the core composition defined by the atom densities, the calculation of atom densities can make a big difference in the K_{eff} FEMP converges on. It is obvious that the higher the ^{235}U atom density, the less volume it takes to have a critical assembly. Also for higher neutron energies, there is some fission in the ^{238}U atoms. Other materials can also have an impact on the value of K_{eff}.

For certain energy groups, there is a higher probability for absorption. Although inelastic scattering is the dominant interaction for both Nb and Zr, they have a slightly higher absorption probability in two energy groups, the first and last. The last group is the lowest energy, and since this is a fast reactor, these probabilities are most likely not consequential. Since this material is 99%

Nb, the absorption cross section for Zr is not likely to have an effect on K_{eff}. The K_{eff} is sensitive to the W content.

All the W isotopes have a higher absorption probability in the lower energy groups. Couple this with the importance of W's scattering probability, the W liner and wire spacer could have an important contribution to the multiplication factor.

5.7 Group Cross Section Structure Selection. Group collapsing is when group constants are generated for a few-group calculation using the energy spectrum generated by a many-group calculation. The calculation group structure was composed of 25 neutron groups and 12 gamma groups shown in Appendix D. The groups finally used in the FEMP1D shielding calculations consisted of 16 neutron groups and 8 gamma groups. Cross section sets may be obtained with many more groups, but traditionally they are collapsed to smaller ones to save computation time. With the advent of the CRAY and other super fast computers, this may not be as big a factor in the future as it has been in the past. But it still is important to keep the computations within reasonable limits to avoid computation overkill.

In collapsing, the broad group assumption is made that, for the group selected, the energy spectrum will be the same as it is for the initial group. To demonstrate the collapsing process, consider only the absorption interaction

for only two groups.

The following equation is used for absorption:

$$\Sigma_a = \frac{\int_{E_2}^{E_0} dE\Sigma_a(E)\phi(E)}{\int_{E_2}^{E_0} dE\phi(E)} = \frac{\int_{E_1}^{E_0} dE\Sigma_a(E)\phi(E) + \int_{E_2}^{E_1} dE\Sigma_a(E)\phi(E)}{\int_{E_1}^{E_0} dE\phi(E) + \int_{E_2}^{E_1} dE\phi(E)}$$

$$= \frac{\Sigma_{r1}\phi_1 + \Sigma_{a2}\phi_2 - \Sigma_a\phi_1}{\phi_1 + \phi_2}$$

$$= \frac{\Sigma_{a1}\phi_1 + \Sigma_{a2}\phi_2}{\phi_1 + \phi_2}$$

The K_{eff} for both the 25 neutron and 12 gamma group structure and the 16 neutron and 8 gamma group structure was 0.995. This verified the use of the coarser group structure for the FEMP1D shielding analysis. For shielding analysis, the K_{eff} is not as important as generating the radiation flux profile.

6.0 FEMP1D Analysis

FEMP1D is the code used in the actual shielding analysis. Because the code is one dimensional and has no bounds in the Z direction, the core modeled for FEMP2D was modified with different material mixtures for each radial zone. There is a correction factor that takes into account the infinite cylinder model.

6.1 Buckling Height Correction Factor. For a nuclear reactor to be critical, the ratio of the neutron of a given generation to the neutrons of the previous generation must be equal to 1. This value is represented as K-infinity, the infinite medium multiplication factor, and it is used when there is no leakage of neutrons out of the reactor in a model of an infinite reactor with no physical bounds. Since a nuclear reactor has physical boundaries, another multiplication factor which includes neutron leakage, K_{eff}, is used to describe reactor criticality. It is referred to as the effective multiplication factor. If K_{eff} is less than 1, the reactor is said to be subcritical, and it will not sustain a chain reaction. If K_{eff} equals 1, the reactor is said to be critical, and if K_{eff} is greater than one, the reactor is supercritical. For a power reactor, the reactor should operate at a K_{eff} of 1.

FEMP2D can account for the flux distribution in both the R and the Z direction and thus the corresponding neutron leakage. FEMP1D models the reactor as an infinite cylinder.

Therefore, there is a correction factor to compensate for the neutron leakage in the Z direction. FEMP1D calls this the transverse dimensions for buckling correction by material, and it is the "equivalent height" for the transverse direction.

Table 6.1 shows these buckling correction factors as they are input into the code and their corresponding geometric buckling. $\tilde{R}$ and $\tilde{H}$ in Table 6.1 represent the

Table 6.1 Height Correction Factors.

Geometry	Geometric Buckling B^2_g	Equivalent Height
Rectangular Parallelepiped	$\left(\frac{\pi}{\tilde{a}}\right)^2+\left(\frac{\pi}{\tilde{b}}\right)^2+\left(\frac{\pi}{\tilde{c}}\right)^2$	$H=\frac{ab}{\sqrt{a^2+b^2}}$
Cylinder	$\left(\frac{\nu_0}{\tilde{R}}\right)^2+\left(\frac{\pi}{\tilde{H}}\right)^2$	H = R
Layered Cake Cylinder	$\left(\frac{\nu_0}{\tilde{R}}\right)^2+\left(\frac{\pi}{\tilde{H}}\right)^2$	$H=\frac{\pi\cdot R}{\nu_0}$
		$\nu_0 = 2.405$

extrapolated radii and heights for each geometric configuration. Each material must have a correction factor. The word material here actually means the mixture of nuclides in each zone. If zone 1 has four nuclides, Nb, Zr, B, and C, then the code would consider each of these nuclides as constituting one material. In other words, if the nuclides are homogeneously mixed in each zone, then the correction factor must be applied to each zone. In some zones, such as the shield, the factor may be zero since the shield is far enough away from the core that it contributes little to core criticality.

Some geometries do not have a correction factor. For example, a sphere, which has the most efficient geometry in terms of neutron leakage, does not have a transverse direction. Therefore, it has no correction factor.

The height correction factor adjusts the height somewhat so as to model the neutron leakage in the axial direction. Without it, the calculated K_{eff} would be too high since there would be no way to account for the neutron leakage in the axial or Z direction; these neutrons would then be assumed to be in the reactor contributing to fission.

6.2 LPN Determination. Many mathematical functions can be expressed as series expansions or by a set of polynomials. For example, a Taylor series can represent functions such as sin(x) or exp(x). When a series expansion is used, there comes a point when an appropriate number of terms are carried in the expansion such that the answer is affected negligibly by continuing with more terms. If a function describing the neutron flux can be expanded, then there needs to be a determination as to the order of the expansion to minimize computation time and cost.

Using spherical harmonics method, the flux can be expressed by Legendre polynomials [Henry, 1975]. Legendre polynomials can be derived (see Appendix E) by solving the following differential equation:

$$(1 - x^2)d^2y/dx^2 - 2x\ dy/dx + p(p + 1)y = 0.$$

The general solution to this equation is:

$$y = C_1 Up(X) + C_2 Vp(X).$$

Where:

$$Up(X) = 1 - (p(p+1)/2!)\,X2 + (p(p-2)(p+1)(p+3)/4!)X^4 - (p(p-2)(p-4)(p+1)(p+3)(p+5)/6!)X^6 + \ldots$$

And:

$$Vp(X) = X - ((p-1)(p+2)/3!)X^3 + ((p-1)(p-3)(p+2)(p+4)/5!)X^5 - ((p-1)(p-3)(p-5)(p+2)(p+4)(p+6)/7!)X^7 + \ldots$$

If p is zero or an even positive integer, then Up(X) will terminate with the X^n term. Therefore, it is a polynomial of degree n. If p is an odd positive integer, then Vp(X) can be expanded to a polynomial of degree n. Otherwise, these series diverge. If the series are convergence, they converge in the interval [-1, 1] [Hildebrand, 1976]. The neutron transport equation can be discretized in its angular dependence so that Legendre polynomials can be used.

The neutron transport equation can be written in the form:

$$\nabla\Omega\Psi(\mathbf{r},E,\Omega) + \Sigma_t(\mathbf{r},E)\Psi(\mathbf{r},E,\Omega) =$$

$$\int_{\Omega'}\int_{E'} \Sigma_s(\mathbf{r},E',\Omega' \rightarrow E,\Omega)\Psi(\mathbf{r},E',\Omega')dE'd\Omega'$$

$$+\int_{\Omega'}\int_{E'} \frac{\chi(E)}{4\pi}\nu\Sigma_f(E')\Psi(\mathbf{r},E,\Omega')dE'd\Omega'$$

$$+S(\mathbf{r},E,\Omega)$$

To simplify the geometry, consider a one dimensional slab defined in only one finite direction, Z. By problem selection,

$$\Omega \cdot \nabla \Psi = \Omega \cdot \frac{\partial \Psi}{\partial z} \cdot \mathrm{i}$$

$$= \Omega \cdot \mathrm{i} \frac{\partial \Psi}{\partial z}$$

$$= \mu \frac{\partial \Psi}{\partial z}; \quad \text{where } \mu = \cos(\theta).$$

Since the range of values of cos(θ) is the interval [-1, 1], it is auspicious that a spherical harmonics expansion leading to an expression in Legendre polynomials may be used. These polynomials are orthogonal:

$$\int_{-1}^{1} P_l(\mu') P_n(\mu') d\mu' = \frac{2}{2l+1} \text{ for } l = n$$

$$\int_{-1}^{1} P_l(\mu') P_n(\mu') d\mu' = 0 \text{ when } l \neq n.$$

They can be computed from the following three relations:

$$P_0(\mu) = 1$$

$$P_1(\mu) = \mu$$

$$(2l+1)\mu P_l(\mu) = (l+1)P_{l+1}(\mu) + P_{l-1}(\mu).$$

The angular flux density can be expanded:

$$\Psi(z, E, \mu) = \sum_{n=0}^{\infty} (2n+1)\Psi(z, E) P_n(\mu).$$

The FEMP codes have an input parameter in the 1$$ array which sets the spherical harmonic order called LPN. There needs to be a determination of order of expansion necessary to define the flux without computation overkill. This was done by making several FEMP1D runs setting LPN = 1, 3, 5, 7,

and 9 for both the LiH/W and the B_4C/W shield models. Figure 6.1 - Figure 6.14 show the results of this effort.

Consider Figures 6.1 and 6.5 to determine the effect spherical harmonic order had on reactor criticality for both the LiH/W and B_4C shield models. Between LPN = 1 and 3, there was a big relative change in K_{eff}. K_{eff} between LPN = 3 and 5, exhibits a smaller change. Then there is little or no change at all in K_{eff} between LPN = 5 and 9. This means that LPN = 5 is sufficient for reactor criticality calculations.

For the shielding analysis, there needs to be an examination of the flux definition in the shield itself to determine the spherical harmonic expansion effects for both shields. Figures 6.2 -6.4 and Figures 6.6 - 6.8 show the neutron fluence at 77, 100.2, and 130 cm from the end of the reactor. These points are all in the shield and the neutron fluence in plotted as a function of the spherical harmonic order, LPN. Again, there is a big relative change in the fluence between LPN = 1 and 3. Also, there is a smaller change between 3 and 5. When LPN = 5, the fluence stabilizes with very little or no change between 5, 7, and 9. This indicates that LPN = 5 is a sufficiently refined to define the neutron flux in the shield.

This same analysis was done for gammas. Figures 6.9 - 6.14 show these results. The same conclusion can be made about gamma profile as above for K_{eff} and the neutron flux. But consider the seemingly erratic behavior between LPN = 1

and LPN = 3 in Figure 6.9. This region of the shield is in W. It is expected that there are numerous secondary gammas being produced as a result of inelastic and capture in W isotope. Since this interaction rate is dependent upon group energy, it appears that energy dependent flux defined by LPN = 1 had a higher probability for secondary production than the the other spherical harmonic expansions did when it reached the W slab. The reason this doesn't happen in the B_4C shield is that the neutron energy is different at this point than in the LiH shield.

The importance of determining the spherical harmonic order is that it saves a substantial amount of CPU time which ultimately saves computation cost. For this reactor model, a spherical harmonic order of 5 was found to produce as accurate an answer in K_{eff}, the neutron flux, and the gamma flux as did the higher order expansions. Therefore, an order of 5 was selected for the shielding analysis.

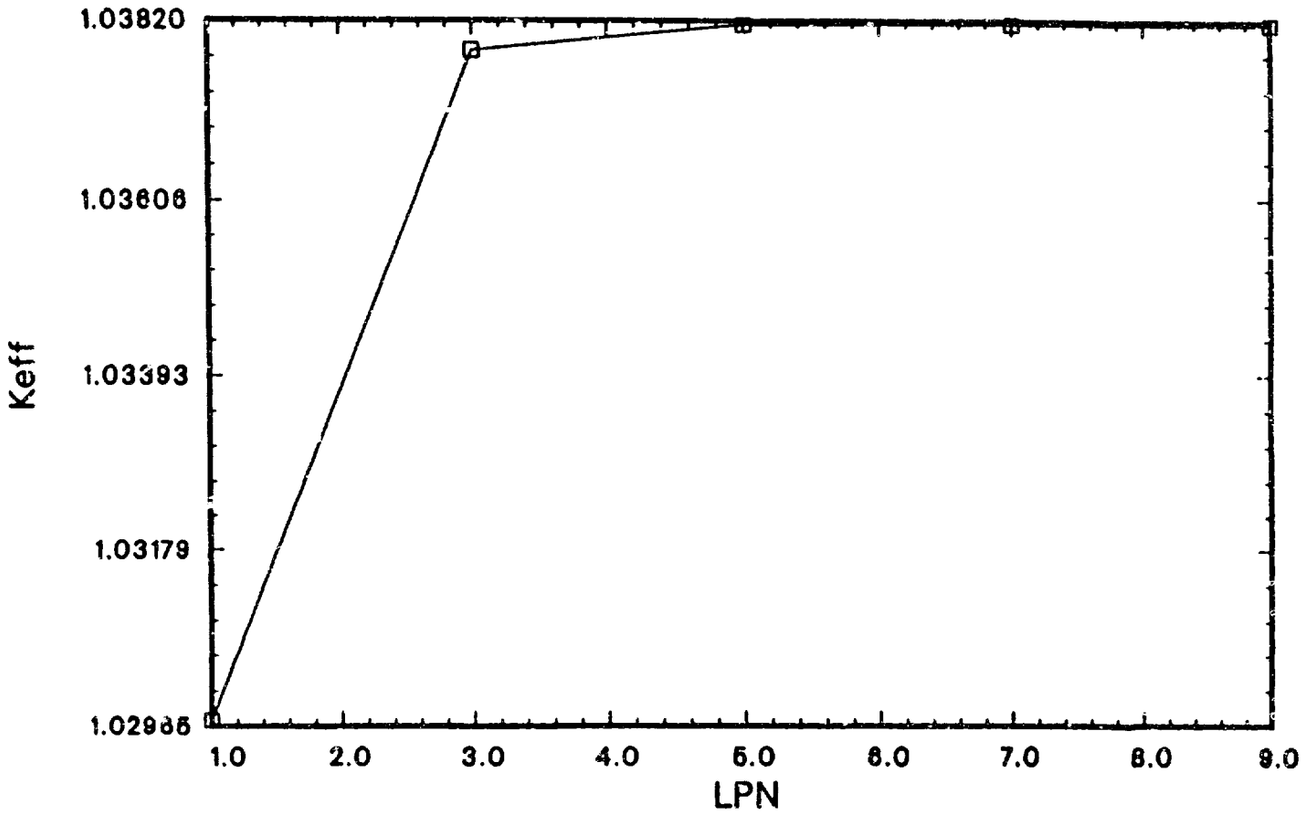

Figure 6.1. Keff vs Spherical Harmonic Order, LPN.
Tungsten - Lithium Hydride Shield.

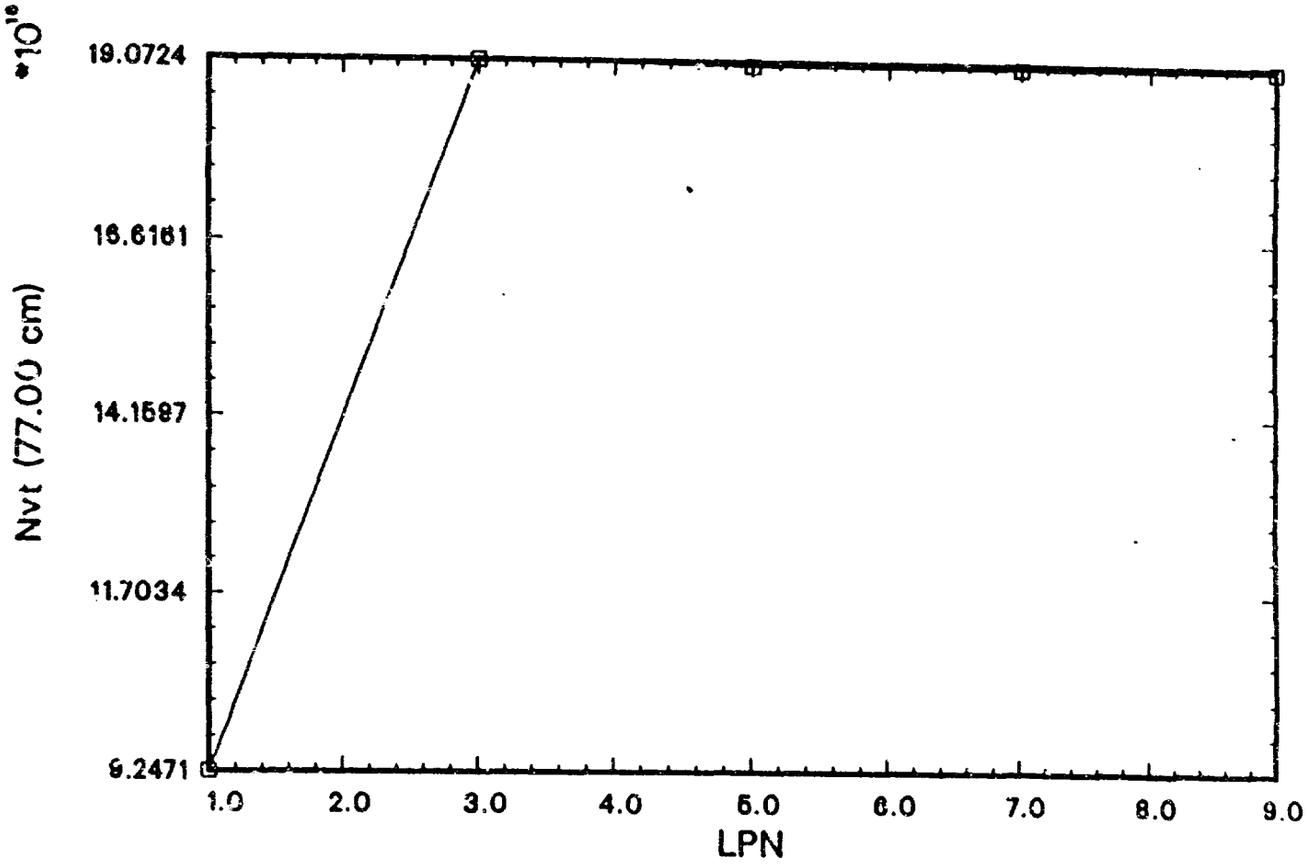

Figure 6.2. Nvt At 77.00 CM vs LPN.
Tungsten - Lithium Hydride Shield.

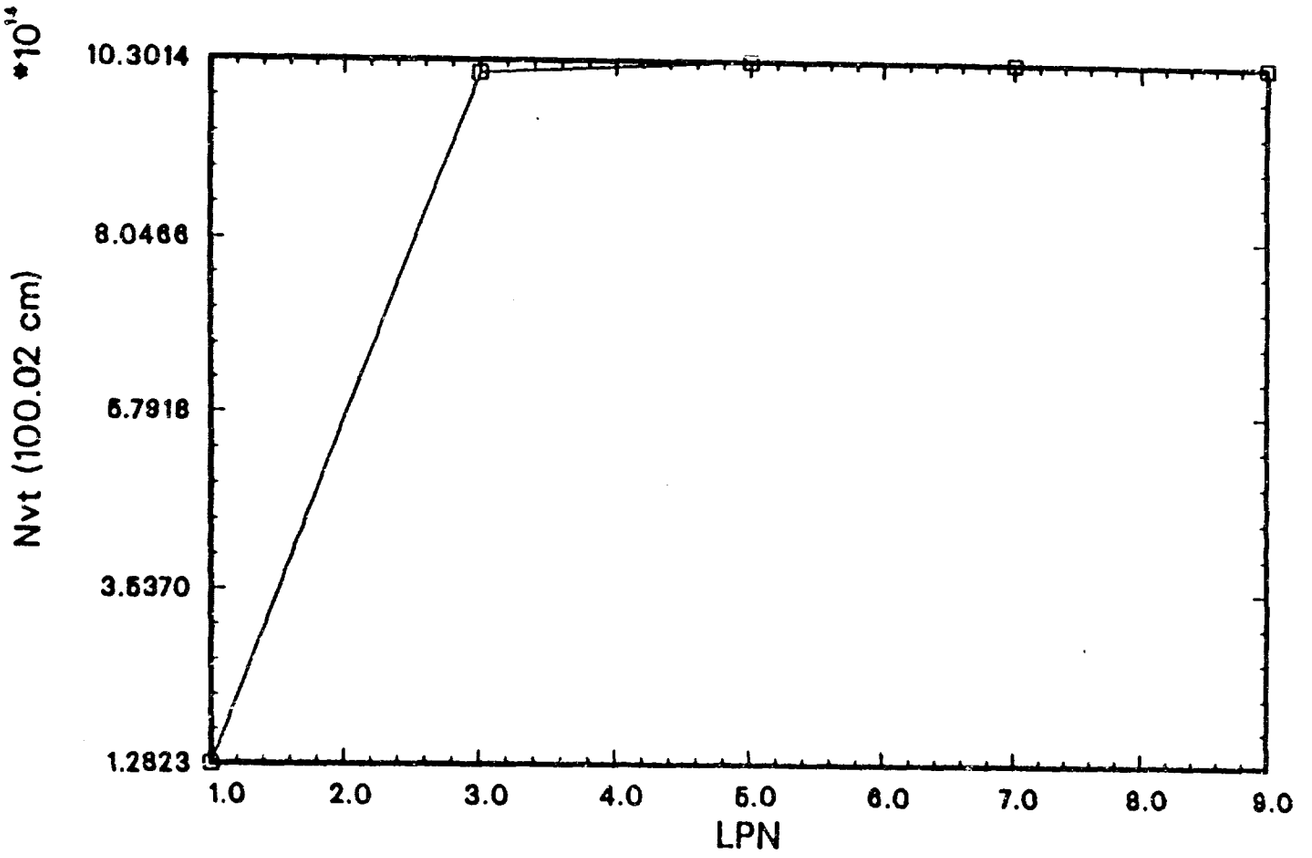

Figure 6.3. Nvt At 100.02 CM vs LPN.
Tungsten - Lithium Hydride Shield.

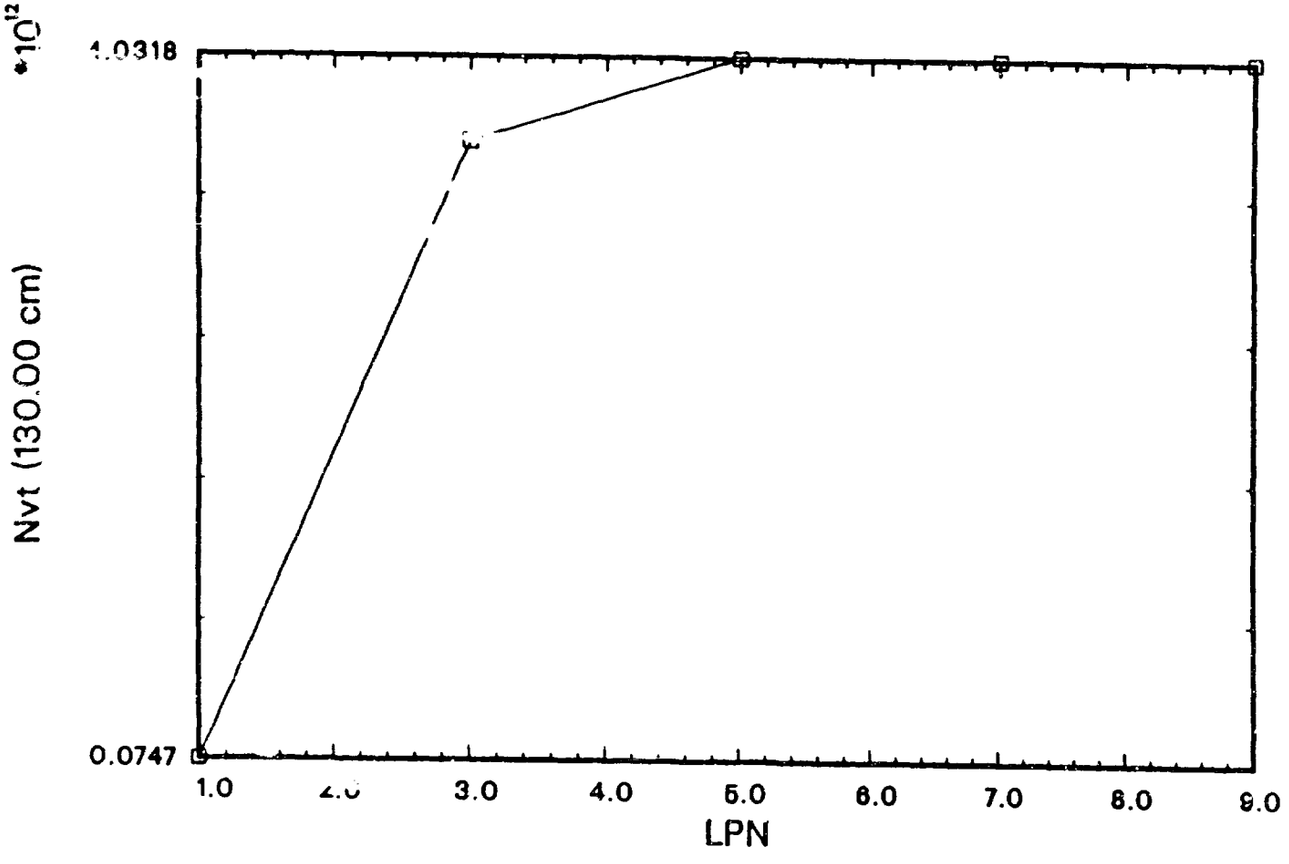

Figure 6.4. Nvt At 130.00 CM vs LPN.
Tungsten - Lithium Shield.

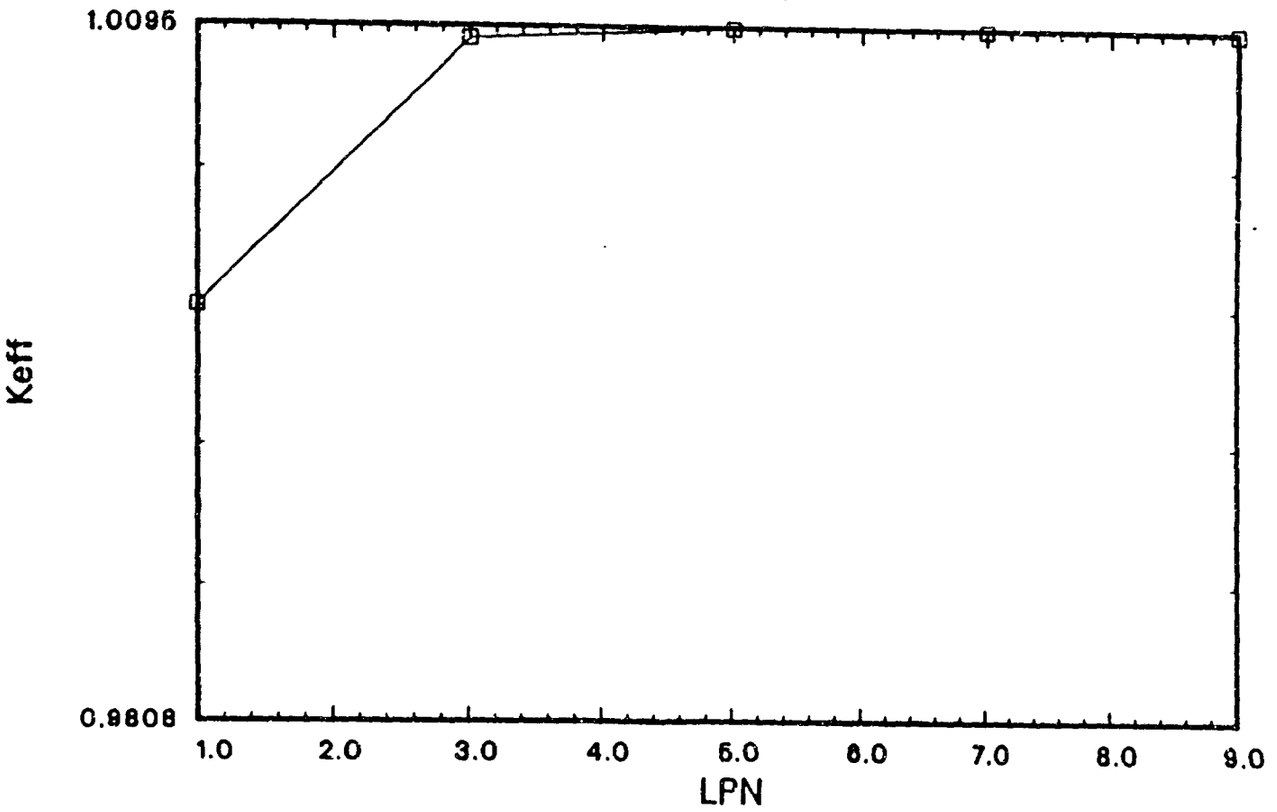

Figure 6.5. Keff vs Spherical Harmonic Order, LPN.
Tungsten - Boron Carbide Shield.

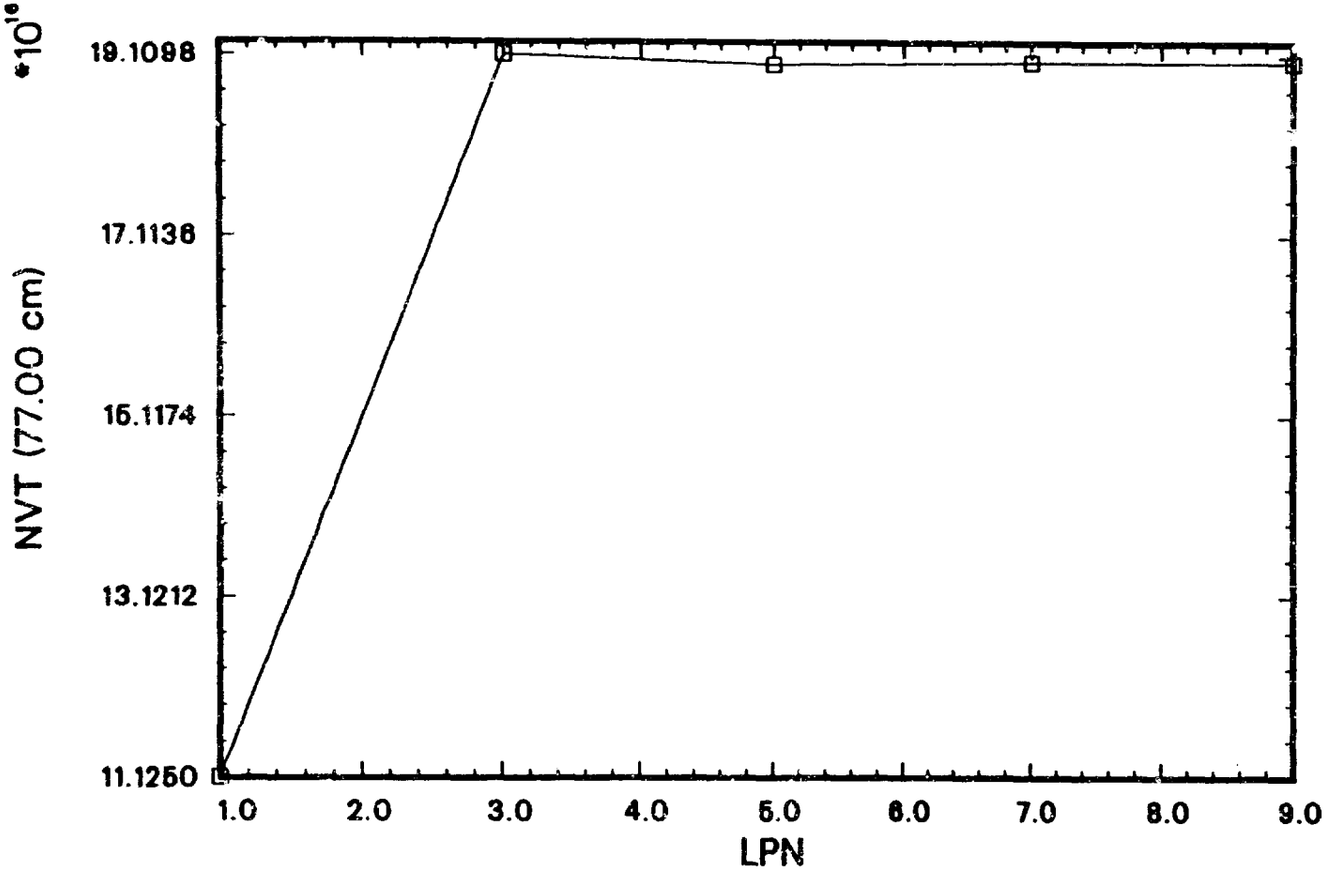

Figure 6.6. Nvt At 77.00 CM vs LPN.
Tungsten - Boron Carbide Shield.

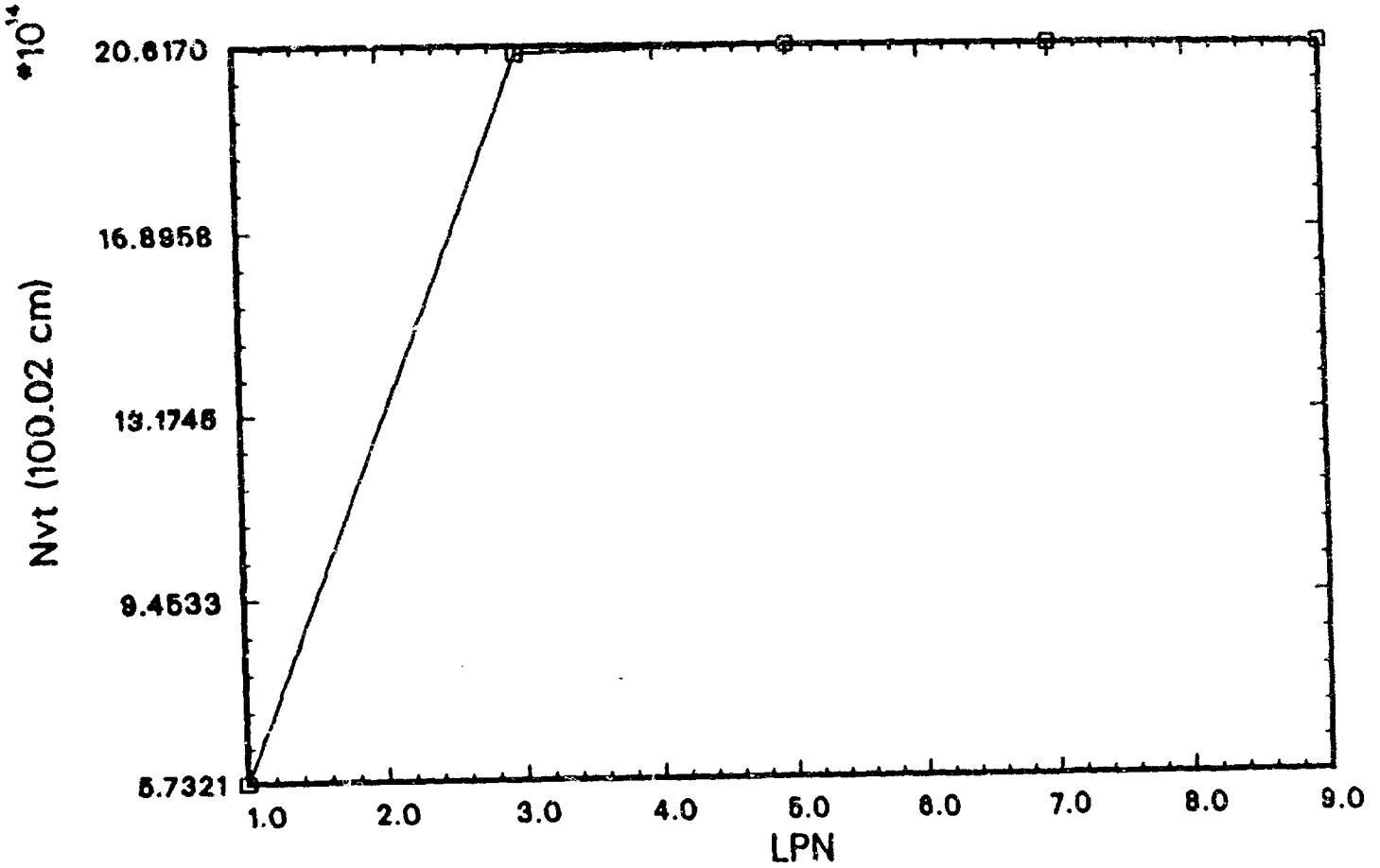

Figure 6.7. Nvt At 100.02 CM vs LPN.
Tungsten - Boron Carbide Shield.

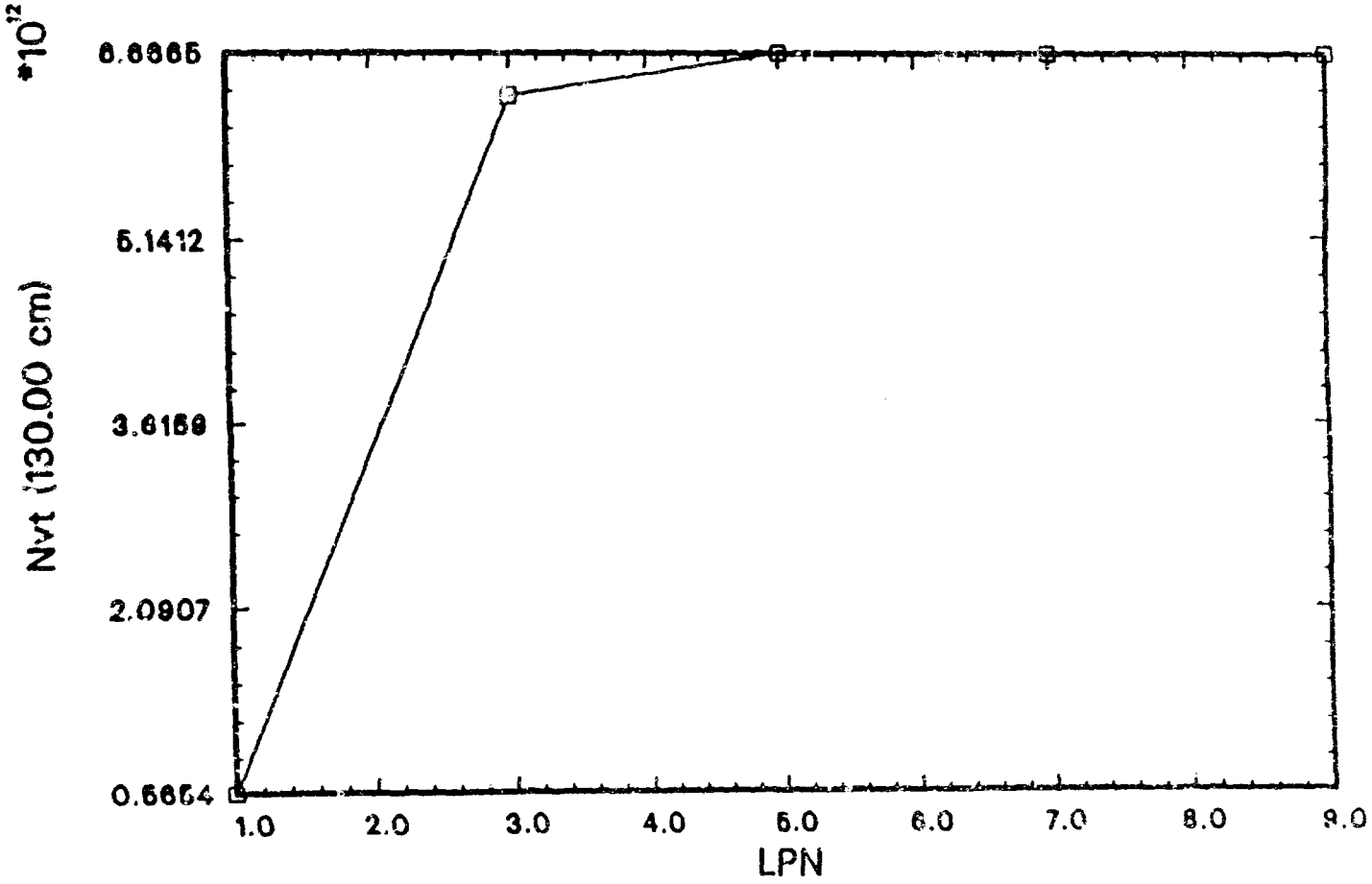

Figure 6.8. Nvt At 130.00 CM vs LPN.
Tungsten - Boron Carbide Shield.

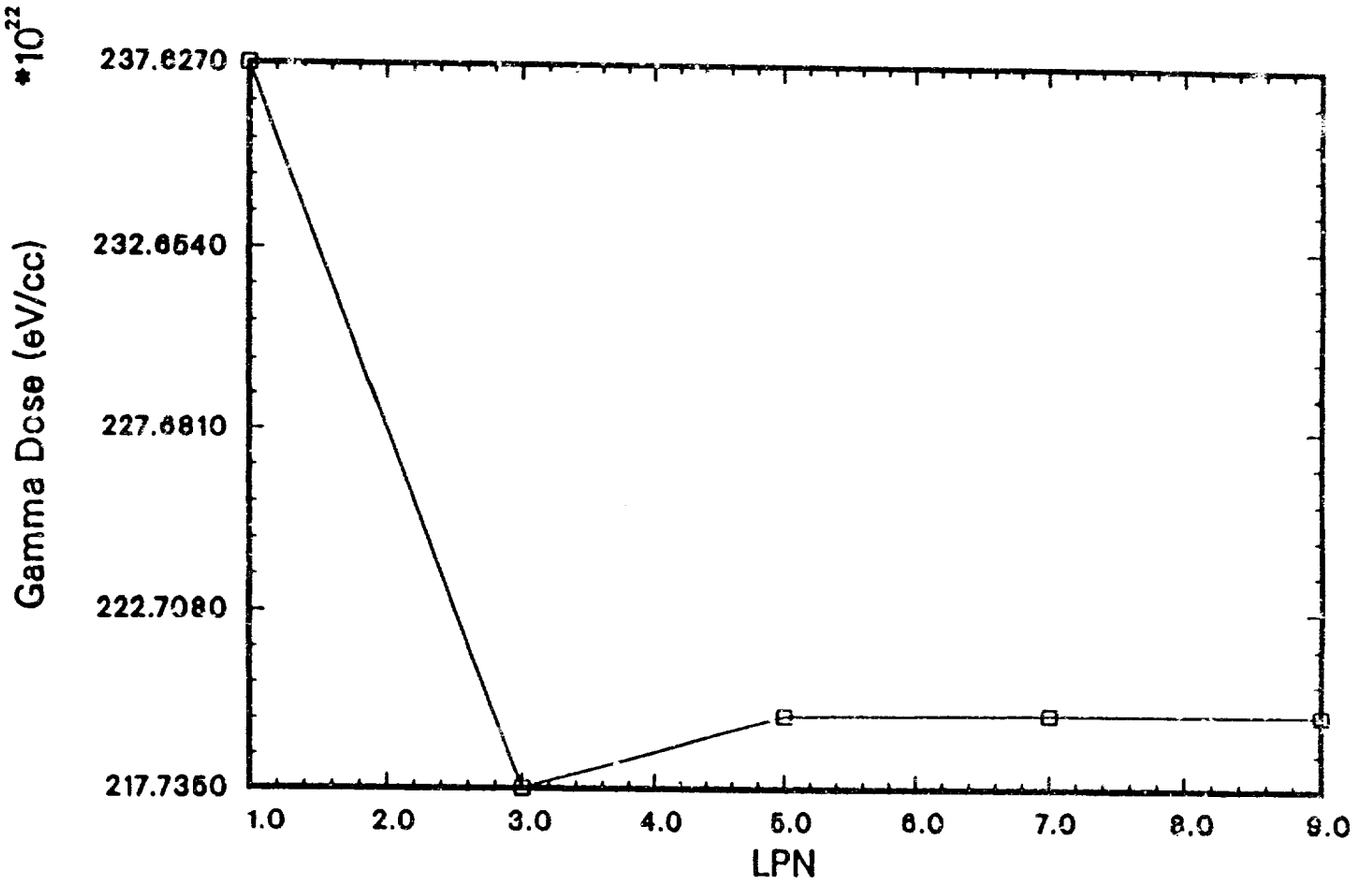

Figure 6.9. Gamma Dose At 77.00 CM vs LPN.
Tungsten - Lithium Hydride Shield.

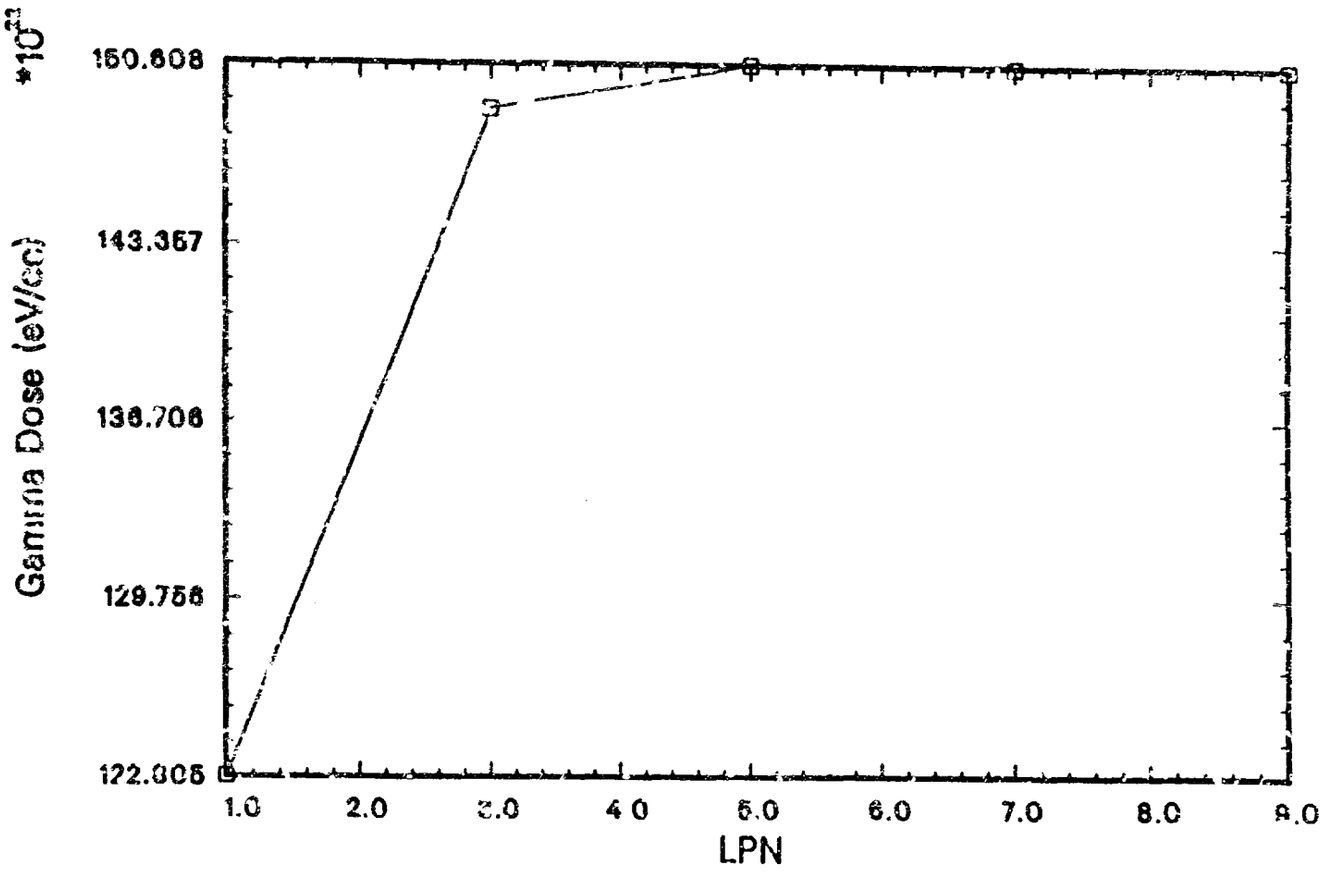

Figure 6.10. Gamma Dose At 100.02 CM vs LPN.
Tungsten - Lithium Hydride Shield.

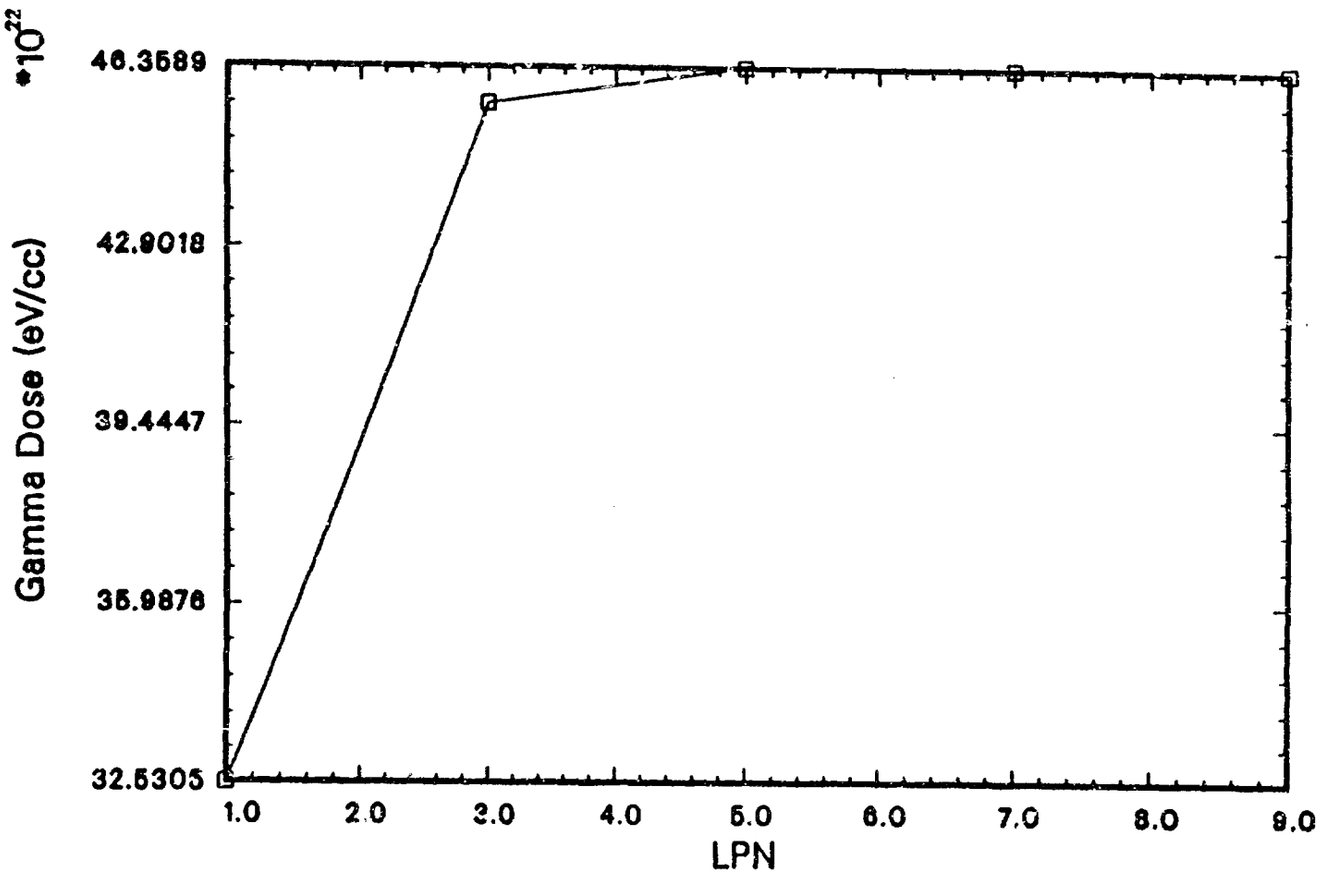

Figure 6.11. Gamma Dose at 130.00 CM vs LPN.
Tungsten - Lithium Hydride Shield.

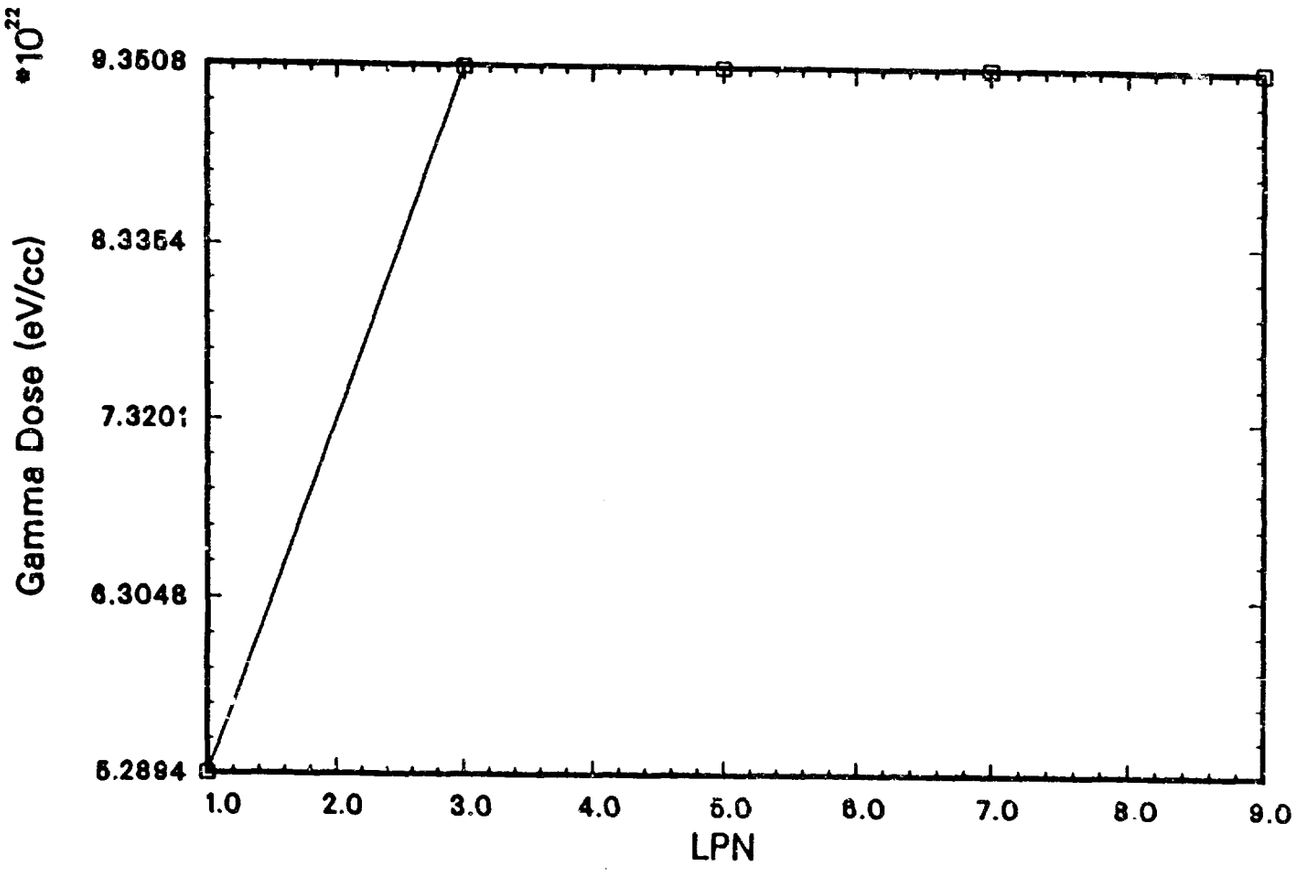

Figure 6.12. Gamma Dose At 77.00 CM vs LPN.
Tungsten - Boron Carbide Shield.

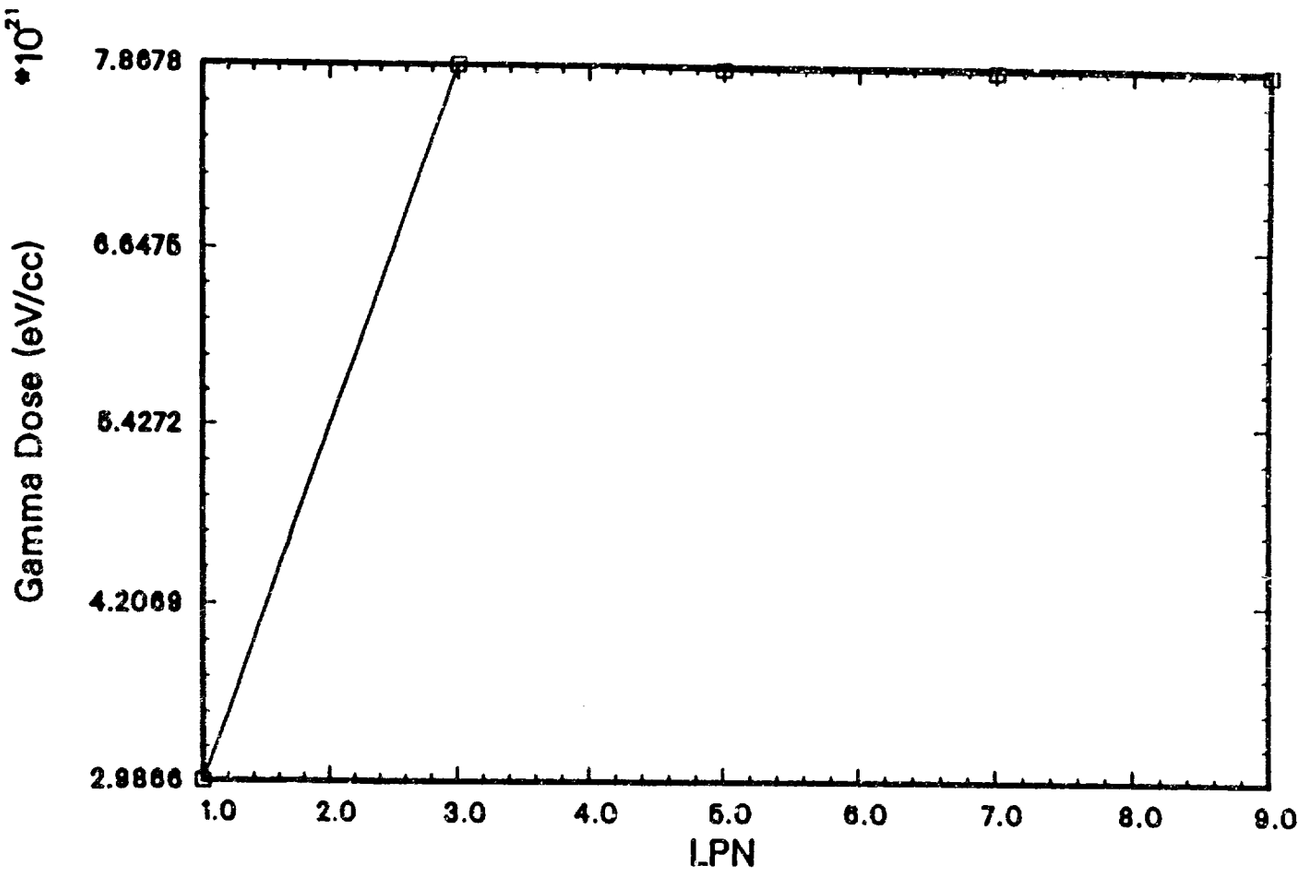

Figure 6.13. Gamma Dose at 100.02 CM vs LPN.
Tungsten - Boron Carbide Shield.

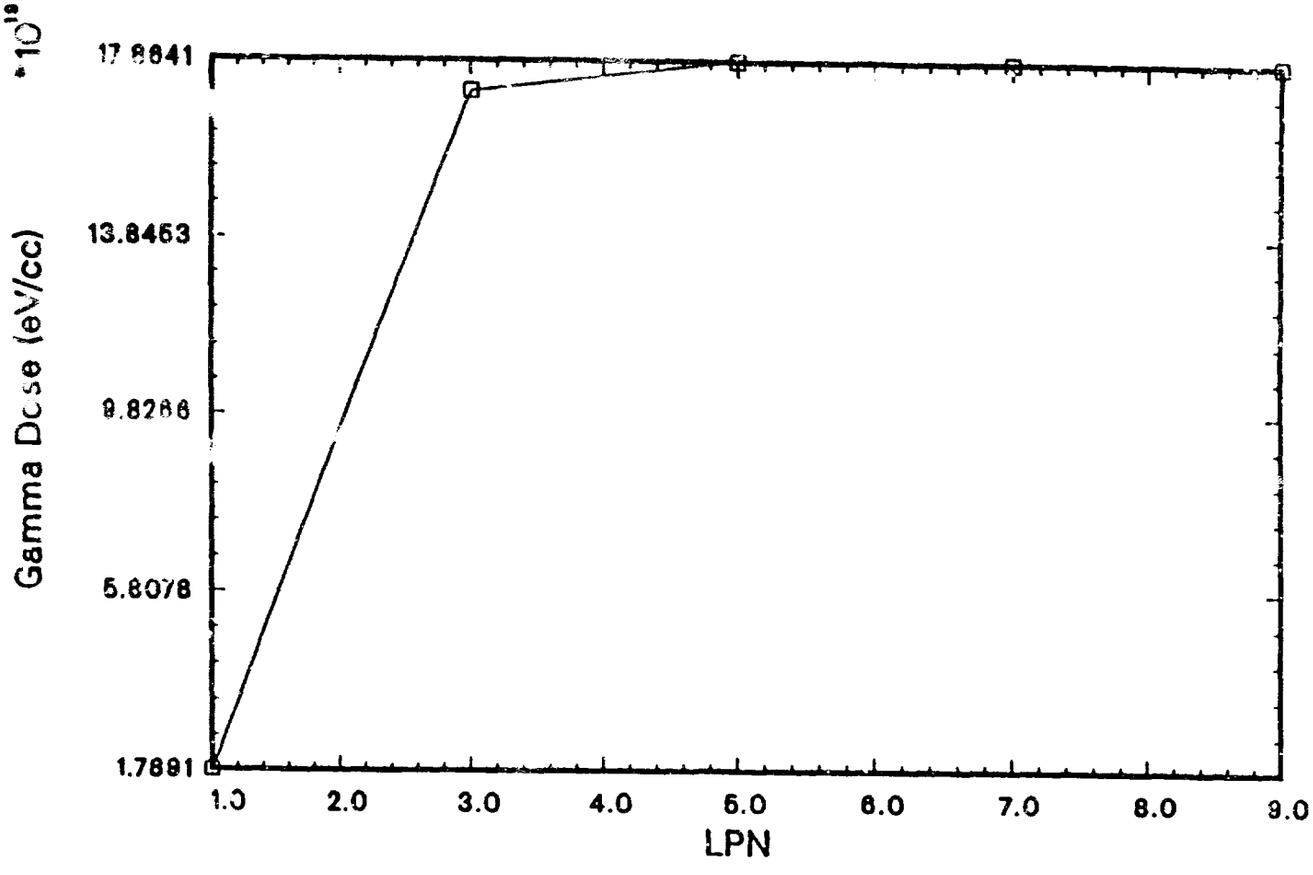

Figure 6.14.. Gamma Dose At 130.00 CM vs LPN.
Tungaten - Boron Carbide Shield.

6.3 Coarse Mesh Model With Shield. The FEMP codes provide a very useful input parameter which can save substantial computational time. In the case of shield design, a core model can be represented by a fine coarse grid without the shield. This grid is much smaller than the material's mean free path. Most numerical algorithms produce a more accurate answer when more mesh spacing is introduced. As in any computational scheme, the accuracy may not change beyond a certain number of mesh points, or the change may be very insignificant. When the fine mesh has been selected and the FEMP code executed, the output can be stored to be used for latter runs. FEMP provides the storage of the group dependent flux to be stored on unit 10 (or tape 10 as the manual calls it). This parameter, ISTRT, is set in the 1$$ array (See Appendix C). Also, the k_{eff} calculated for the fine mesh can be used in another run. This input, XK, or eigenvalue estimate, can be put into the input deck in the 2** array. Using the fine mesh gives a good definition of the flux profile from the core. For shielding, this is more important than the criticality calculation. When the model with the shield attached is set up, there is no need to use fine mesh spacing in the core if the output from the previous run, stored on unit 10, is used as the initial guess. Actually, this is not a guess at all, and the code will need no iterations to improve on this answer. A coarse mesh spacing may then be used, as long as the mesh spacing chosen is no longer than the shortest material mean free

path in each material zone. However, to ensure that the shield is is giving an accurate answer for the flux profile in it, a fine mesh spacing may then be for the shield only.

A fine grid may also be initially used to check for differences in the flux definition, and/or the critically convergence, between a fine or course grid. If both runs are done before modeling the reactor with the shield attached, and the answers are insignificantly different, then there is no need to store the flux, calculated by the fine mesh, on unit 10 and use it for the shielding calculations. The coarse core grid model can be used with the shield, allowing it to generate its own core flux profile, since it can converge with the same accuracy as the flux input from unit 10 generated by the fine mesh.

6.3.1 FEMP1D Reactor Model. Figure 6.15 shows the core configuration used for the FEMP1D shielding analysis. The core is composed of 4 material zones. The atom densities calculated for this run were calculated using the formula:

$$N_i = \sum_j V_j N_{ij}.$$

Where: V_j is the fraction of super zone volume occupied by the j^{th} zone.

N_{ij} is the nuclide atom density in j^{th} zone.

N_i is the atom density in the super zone.

N was calculated for the FEMP2D runs. The materials used for FEMP1D can be related to the FEMP2D materials as shown in Table 6.2. Zones 5, 6, and 7 comprise the shield, and

Table 6.2 Relationship of FEMP1D Zones to FEMP2D Zones.

FEMP1D ZONE	FEMP2D ZONES
Zone 1	Zones 14 and 26
Zone 2	Zones 15 and 27
Zone 3	Zones 16, 22, and 28.
Zone 4	Zone 20

have different compositions depending on whether the B_4C or the LiH shield is being analyzed. The materials used in FEMP2D can also relate to FEMP1D as shown in Table 6.3.

Using this information the volume averaged smeared atom densities where calculated as shown in Appendix B. Table 6.4 shows the nuclide composition of these materials.

Table 6.3. Relationship of FEMP1D Materials to FEMP2D.

FEMP1D Material	FEMP2D Materials
Material 1	Material 2
Material 2	Materials 7, 8, 11, 12
Material 3	Material 5
Material 4	Material 13

Once the atom densities and zones are set up then the FEMP1D input file is set up as shown in Appendix C. For shielding optimization for both volume and mass, the gamma shields (W or Be) were moved at 10 cm increments up and down

the shield. A comparison was made as to the shield thickness that satisfied the dose constraints. This is discussed in detail in Section 8.

Table 6.4 Core Material Composition for FEMP1D.

Nuclide	Material Number	Atoms/Barn/Cm
Niobium	1	1.1425 E-02
Zirconium	1	1.1541 E-04
Lithium 6	1	6.8148 E-04
Lithium 7	1	8.4050 E-03
Nitrogen	2	1.5015 E-02
Uranium 235	2	1.3461 E-02
Uranium 238	2	1.5539 E-03
Tungsten 182	2	1.4963 E-04
Tungsten 183	2	3.5321 E-04
Tungsten 184	2	6.9613 E-04
Tungsten 186	2	7.0644 E-04
Niobium	2	1.1407 E-02
Zirconium	2	1.1523 E-04
Lithium 6	2	5.9377 E-04
Lithium 7	2	7.3232 E-03
Beryllium	2	7.5108 E-03
Carbon	2	3.7554 E-03
Niobium	3	5.5046 E-02
Zirconium	3	5.5602 E-04
Lithium 6	4	3.4748 E-03
Lithium 7	4	4.2856 E-02

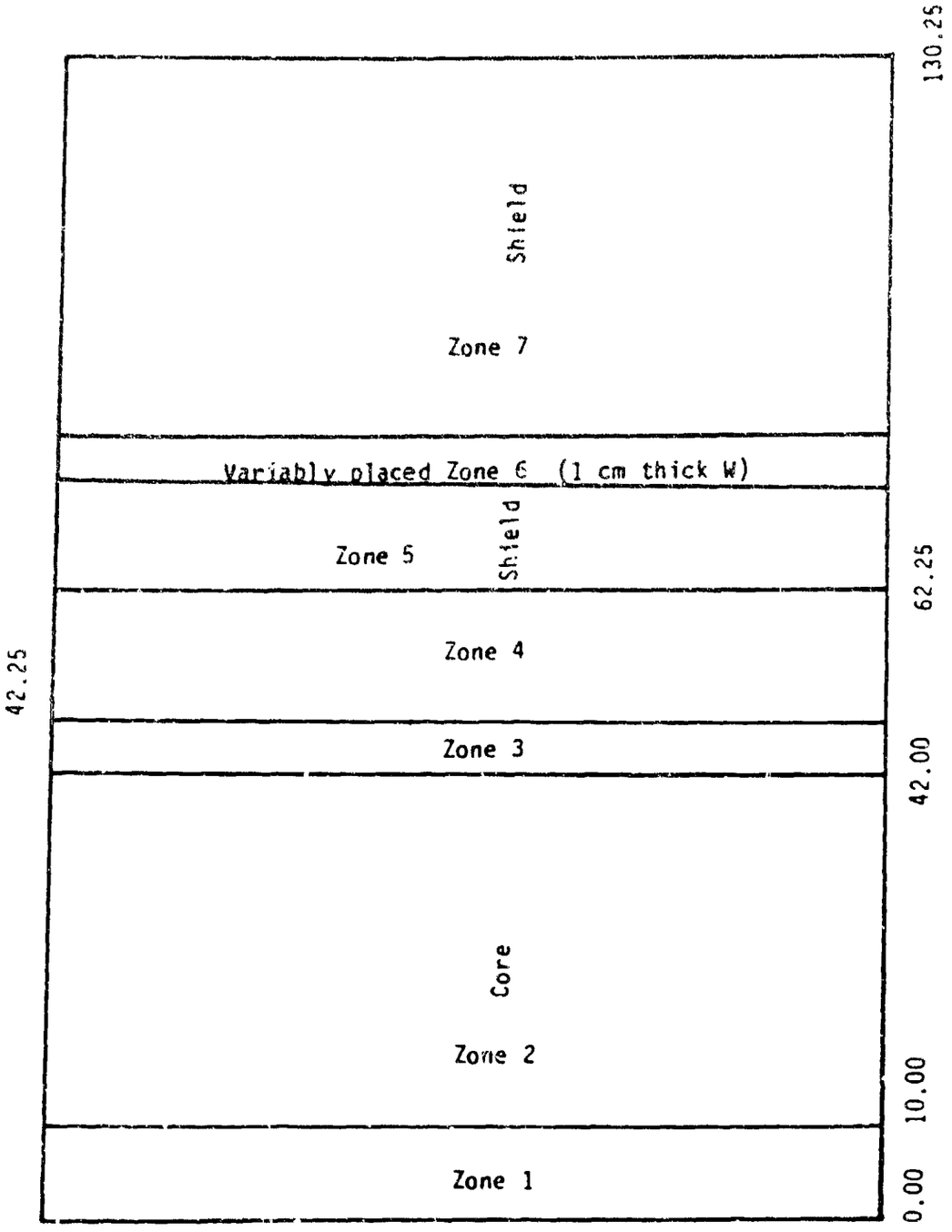

Figure 6.15. FEMP1D Reactor Model.

7.0 Generating Dose Response Functions

FEMP2D and FEMP1D will generate gamma and neutron radiation fluxes which may be multiply by a dose rate conversion factor to produce a radiation dose. A dose is the absorbed energy deposited in the medium by the radiation. Radiation damage is measured in different units. A gray is the SI derived unit of absorbed dose, but the unit most commonly used is the rad (Radiation Absorbed Dose). A rad is equal to an absorbed dose of 100 ergs of energy per gram of matter. Conversely, 1Gy = 100 ergs. The dose requirements for this reactor is 5×10^5 rads for gammas and 1×10^{13} Nvt, or neutron fluence which is the time integrated neutron flux. Both of these requirements are for a seven year period and are set for silicon, the primary medium for microelectronics. The neutron radiation is the 1 MeV equivalent dose. Therefore, the shield must be able to protect the payload at a dose plane 25 meters from the reactor core for these requirements to successfully complete a required mission. The code used for generating dose rate conversion factors for this analysis is called RFCC. Appendix G shows the RFCC input manual.

7.1 Setting up RFCC. Appendix G has an input manual for RFCC, two sample input files, two sample output files, and a sample FEMP1D input deck using the information generated by these RFCC input files. The first input data set generates the neutron flux to dose conversion factor. For this

analysis, the first parameter, IRFC, was set to 1. This instructed the code that it is to generate multigroup response functions only. If IRFC had been set to zero or 2, then the rest of the input deck would have been put into arrays using the FIDAS input scheme. The next input is ICASE, the response function case number. It is set to 1. This input deck is to generate flux to dose conversion factors. The next parameter, IMG, tells the code what response function to generate. In the sample input file, IMG is set to 9, which generates the dose rate conversion factors for human tissue. (The manual is not clear on this.) The next parameter, NG, is the number of energy groups for which conversion factors are to be generated. This number is set to 16. Next, both the upper and lower bounds of each energy group has to be entered. Actually, the code is clever enough to assume the lower bound for energy group one is the upper bound for energy group two, and the lower energy bound for group two is the upper group to group three, etc. Therefore, if there are 16 neutron energy groups, there must be 17 entries to define the group structure to the code, the last being the lowest energy bound in the lowest energy group.

Dose conversion factors can be generated again at this point for another group structure and/or a different material such as silicon. If only the 16 neutron group conversion factors are desired, set the next three parameters after the lowest energy bound of the lowest

energy group to zeros. This sets ICASE=IMG=NG=0 and terminates the run.

The output file simply states the energy group number, the upper and lower bounds for that energy group, and the dose rate conversion factor for that energy group (averaged). The units of the dose rate conversion factor are in Rem/hr/(n/sec-cm^2). Appendix G shows the sample output file generated with the input deck described above. This same process is done to generate dose rate conversion factors for gamma radiation.

7.2 Using the Output of RFCC in FEMP1D. Both FEMP1D and FEMP2D can use the output of RFCC. FEMP2D uses this data in the 37** array while FEMP1D uses it in the 35** array. Since the inputs are similar for both codes, only the FEMP1D input will be discussed.

In the 1$$ array, the last input parameter is called NRF. This is the number of response functions that are going to be input into the 35** array. For this analysis, NRF is set to 2 because the response function for neutron radiation (the set of dose rate conversion factors generated by RFCC for neutron radiation), and the response function for gammas (the set of dose rate conversion factors generated by RFCC for gamma radiation) will be input.

Consider the neutron dose rate conversion factors first. RFCC generated 16 conversion factors. One conversion factor for each energy group. These sixteen will be the first 16 entries in the 35** array as shown in

Appendix G. Since the code expects 16+8=24 energy groups (16 neutron groups and 8 gamma groups), then the last 8 entries for the first response function are zero. This is basically telling the code that the first group of response functions are for neutrons only.

Next the entries must be made for the 8 gamma groups. Again the code expects 24 entries since that is the total number of energy groups. Since the first 16 are neutron energies, and they are not of any interest in the second response function, the first sixteen entries must be zero. FEMP permits efficient input of repeated quantities. Since there are zeros in the last 8 entries for the first response function, and there are 16 zeros in the beginning of the inputs for the second response function, there are 24 repeating zeros in this array. The sample input deck in Appendix G shows an entry "24R0.0". This is telling the code to enter zero 24 consecutive times. Finally, the last eight entries in this array are the eight dose rate conversion factors generated by RFCC.

When the FEMP code using this input deck is run, there will be columns near the end of the output deck labeled "RESP 1" and "RESP 2". These columns represent the total radiation dose produced by neutrons (RESP 1) and the total dose produced by gammas (RESP 2). RESP 1 is the sum of the neutron flux for each energy group multiplied by the dose rate conversion factor for that corresponding energy group. RESP 2 is the sum of the gamma flux multiplied by the

corresponding dose rate conversion factor for each energy group. This output parameter can be calculated for different positions in the reactor and shield to see the radiation level at a particular position. For the shielding analysis the values were printed as different positions in the shield to determine the position in the shield where the radiation was attenuated to the specified levels.

8.0 Shield Optimization

Designing a shield for a space nuclear reactor must include many considerations. Shields must be structurally stable. They must be able to attenuate the radiation levels for a least the proposed duration of the reactor mission. Considered for this analysis are the following layered shield concepts: the traditional LiH and W shield, a Be/LiH shield, a W/B_4C shield, and a Be/B_4C shield. Many considerations, such as thermal expansion and material compatibility, can make the shield unacceptable. However, if the shield material cannot attenuate the radiation to acceptable levels within a certain mass and volume constraint, it is eliminated as a candidate shielding material regardless of its other material properties.

When the shielding material is selected, then its weight must be calculated to determine the feasibility of using the material as a shield. Also, volume is a major constraint since some of the early space nuclear reactors may be launched in the space shuttle. If the launch vehicle is the space shuttle, then it is possible that the limited volume of the shuttle bay may determine the shield design. Therefore, with the candidate shielding material investigated, both volume and mass were the criteria for optimization.

8.1 Tungsten and Lithium Hydride Shield. A layered W/LiH shield has been advocated as the lightest shield for space

nuclear reactors. W, because of its high electron density, has the ability to interact with gamma rays much more than any of the other three materials. Unfortunately, its high density means it is heavier than the other materials with in the same volume. The dominant probability for all W isotopes' neutron cross sections is scattering.

In the 16 group cross section set, the major cause of secondary gammas in ^{182}W for high energy neutrons is inelastic scattering. The probability is the highest in the higher energy ranges, specifically, the upper 5 groups ranging from 1 MeV to 17.33 Mev. Energy group 5 has a cross section of about 2 barns for the lowest probability in these groups, whereas energy group 3 has a cross section of about 3.15 barns for the highest probability.

^{182}W has many resonances for absorption (which produces gammas) probability from about 5×10^{-3} MeV. Therefore a thermal neutron, or neutron in group 16 defined in cross section set use for this analysis, has a good probability of secondary gamma production. These resonance peaks are extremely sharp, which implies that they have a narrow energy range. But they are numerous indicating a neutron that escapes one resonance is likely to encounter another as soon as it interacts reducing its energy. From 5 keV to energy group one, the probability of absorption decreases to below 0.8 barns. This indicates that as W is moved far enough away from the core, and the neutrons have lost some of their energy through collision in the LiH, this

interaction becomes more important.

For ^{183}W the neutron absorption cross section gets very low at the higher energy ranges. Like ^{182}W, the inelastic cross section ranges around 3 barns for the five highest energy groups, with the lowest probability at about 2.1 barns for energy group 1, and about 3.3 barns for group 3.

^{184}W and ^{186}W demonstrate the same behavior. This implies that for fast groups there is much more secondary gamma production caused primarily by the inelastic scattering, but in the lower energy groups, there is some secondary gamma production due to neutron absorption.

The Li modeled in this shield is composed of two isotopes, ^{6}Li and ^{7}Li. Since Li has a low atomic number indicating few orbiting electrons, its gamma attenuating characteristics are not significant. For neutrons. ^{6}Li doesn't have a large cross section for absorption at the high energy groups, however, for the lower groups, the probability goes up significantly. The concern for this reaction is that absorption could cause an exothermic reaction, described in Section 2.2, heating up the shield and possibility effecting its stability. ^{6}Li's elastic scattering probability is not very high except in energy group 7 where it peaks to about 5.5 barns.

^{7}Li has similar elastic scattering characteristics, except that, although energy group 7 is the maximum, the peak is only about 4.8 barns. The absorption probability for ^{7}Li is very low for every energy group in the sixteen

group structure.

In combination with the Li in the LiH shield is the ultimate neutron attenuator, hydrogen. Hydrogen is desired because of the neutron energy lost per collision, a result of the hydrogen atom and the neutron being roughly the same size. Therefore, the higher the hydrogen content in a neutron shielding material, the more effective the neutron shield is.

Be was used in combination with LiH for one shield model. Be has a peak elastic scattering probability of about six barns for the lowest energy group, and about 2-5 barns in the high to the intermediate energy groups. It has a very low absorption probability although it does have a troublesome (n, 2n) reaction starting at about 2.8 MeV. The use of a Be/LiH shield implies that there is no gamma shield. This is actually the case since Be's atomic number is only 4 which indicates that it isn't much better for gamma attenuation than Li. The trade off in question in using this layered shield is to determine if the Be/LiH shield would be a better overall shield than the W/LiH shield since, although W is a much better gamma shield, W produces secondary gamma which also have to be attenuated.

Be was also used layered with B_4C. Boron has a large absorption cross section for thermal neutrons. However, for high energy neutrons, this is not the case. In fact, for ^{10}B the absorption probability is less than one barn until the neutron energy level reaches the intermediate energy

ranges. In the lower energy ranges, the probability climbs well over 100 barns. ^{11}B has a very small absorption probability for all energy groups. From intermediate to the lower energies, it has a scattering probability of from 4 to 5 barns. This will help reduce the neutron energy so that the absorption probability from ^{10}B can dominate.

Finally, carbon is a strength giving material that also aids in the B_4C shield. It has almost no absorption cross section, but it does have a scattering cross section from about 3.5 to 4.7 barns from energy groups 6 to 16. These collisions also help reduce the neutron energy so that the neutron is more likely to be absorbed in the ^{10}B isotope.

8.2 Dose Specifications. The shielding analysis for this thesis was set up to determine what shielding configuration for both mass and/or volume yielded the satisfactory dose limits. The dose requirements for gamma rays was set at 5 X 10^5 rads. For neutrons, it was set at 1 X 10^{13} Nvt, the time integrated flux. Both requirements are for seven years. The dose plane is 25 m from the reactor core, and the half cone angle to be protected is 17 degrees. Since 25 m >> 27.5 cm, the reactor radius, then the radiation can be considered to originate from a point source, i.e., the reactor "looks" like a point source at 25 m.

Assuming the radiation distribution is isotropic, or equally likely in all directions, the streaming attenuation factor (SF) can be calculated as follows:

$$SF = \frac{A_{shield}}{4\pi R^2} = \frac{\pi r_{sh}^2}{4\pi R^2} = \frac{r_{sh}^2}{4R^2}.$$

r_{sh} ≡the radius of the shield, ≈ 55.3 cm.
R ≡the distance from the core to the dose plane, 25 m.

$$SF = \frac{55.3^2}{4[(25)(10^2)]^2} = 1.2232x10^{-4}$$

The SF describes the divergent nature of the radiation once it leaves the shield's surface. The inverse of the SF yields the dose in the shield 25 meters from the dose plane.

$$\frac{1}{SF} = 8.1750x10^3.$$

Adjusting the gamma dose with the SF yields:

$$(5 \times 10^5)(8.1750 \times 10^3) = 4.0875 \times 10^9 \text{ rads.}$$

Adjusting for the neutron fluence yields:

$$(1 \times 10^{13})(8.1750 \times 10^3) = 8.1750 \times 10^{16} \text{ nvt.}$$

Since the radiation unit rad is defined as 100 ergs of energy deposited in a gram of material, the gamma dose needs to be correlated to the material for which it applies. In this case, silicon is the material to be protected since its integrity must be maintained for the electronic circuits in the payload to function. Also the units of the energy deposition can be changed to match the dose rate conversion factors input into the code. To get rads into units of rads silicon, the following conversion factor is used:

1 rad = (100 ergs/gm)(2.42 gm/cc)=242 ergs/cc,

where 2.42 gm/cc is the density of silicon.

$$(242 \text{ ergs/cc})(6.2418 \times 10^{11} \text{ eV/erg}) = 1.5105 \times 10^{14} \text{ eV/cc}$$

$$\text{therefore, 1 rad} = 1.5105 \times 10^{14} \text{ eV/cc.}$$

The dose rate in rads silicon is:

$$DR \text{ (rad Si)} = (4.0875 \times 10^{9})(1.5105 \times 10^{14})$$

$$= 6.1742 \times 10^{23} \text{ eV/cc,}$$

where eV/cc are the energy deposition units to match the dose rate conversion factors.

The two dose limits are now established for this analysis. They are:

for neutrons: 8.1750×10^{16} nvt

for gammas: 6.1742×10^{23} eV/cc.

8.3 Determination of Shield Boundaries. The shield models subjected to the above constraints was composed of 67 cm of the neutron attenuating material and 1 cm of the gamma attenuation material. FEMP1D can be required to print the flux and/or dose for neutrons and gammas at points throughtout the core or shield. This analysis only required the dose print out in the shield. The points chosen began at 14.75 cm in the shield and ended at 67.75 cm at intervals of 0.535 cm. These values are displayed in the FEMP1D output file. The column headed "XOUT" is the distance the point in question is in the shield added to the core length. For example, the point 14.75 cm in the shield corresponds to 62.25 + 14.75 = 77.00 in the XOUT column.

The output file then prints out the dose at specified

points. For this analysis, 100 points were chosen for the printout. The code was instructed to do this by setting the parameter "NPOUT" in the 1$$ array to 100. The 34** array then had to contain the position of the 100 points. There are two ways to do this. All 100 points can be input by hand, i.e., 77.000, 77.535, 78.071, ...,130.000. If the points in question are equally spaced (they can be spaced unequally if desired), then the code allows the use of a handy interpolation scheme making inputs much faster. To get 100 points between 77.000 and 130.000 an input in the 34** array may have an entry "98I77.0 130.0" telling the code to enter 98 equally spaced points between 77.0 and 130.0. Thus, the spacing is 0.535 between each point. This scheme may also be used in the other arrays defining mesh spacing for FEMP2D and FEMP1D.

If the neutron and gamma dose was of interest is at a point 15.285 cm in the shield, then it could be found in the output file by looking at the XOUT column for this value:

$$62.25 + 15.285 = 77.535.$$

On the same page in the output file that has the XOUT column, the left hand column displays a sequence of numbers 1, 2, 3, ..., etc. These can be considered as the position numbers for each value in the XOUT column. The last parameters (before the accounting information) will have the following format:

POSN	RESP 1	RESP2
1	1.9071E+17	2.1774E+24
2	1.6180E+17	1.6705E+24
3	1.3904E+17	1.6762E+24
.	.	.
.	.	.
.	.	.
100	3.5523E+12	4.5663E+23

The dose rates for a point 15.285 cm in the shield is 1.6180 X 10^{17} nvt for neutrons and 1.6705 X 10^{24} eV/cc for gammas.

It is easy to see how to utilize this scheme to determine the point in the shield in which the dose constraints are satisfied. Just read down the column under RESP 1 until the its value is less than or equal to 8.1750E+16. That is the position where the neutron dose is attenuated to the allowable level. Then read down the column headed RESP 2 until the value is less than or equal to 6.1742E+23 for the gammas. This is the point where the gamma rays are attenuated to the specified level. (RESP 1 and RESP 2 do not always have to be for neutrons and gammas respectively; they can be the other way around as determined by input file manipulation.) The point with the largest position number, is the minimum shield thickness to attenuate both the neutron and gamma radiation to an acceptable level. Its thickness can be determined by looking at the section of the output file that has the XOUT values in it, and matching the corresponding position number with the XOUT value and subtracting 62.25, e core length, from it.

Since the shield thickness is now known, the next question is the shield radius. The cone half angle determines this. The cone half angle of 17 degrees implies that any neutrons or gammas leaking out the angle do not contribute to the radiation dose at the dose plane since space is essentially a vacuum and there would little scattering outside the cone angle back in. The shield places the payload in a protective "shadow" in which the radiation levels are acceptable. This also makes the shield much lighter since the core does not need a sphere shaped or 4 pi shield protecting in all directions.

Figures 8.1a and 8.1b show that the shield thickness is constant for the radius core. The shield is essentially a "layered cake" of neutron and gamma shield materials behind the reactor core. Then the layered cake materials make an angle of about 76.6 degrees intersecting the cone angle. The thicknesses in the tapered zones are constant with each other. Since the gamma shield is 1 cm in the shield behind the core, it is also 1 cm in the wings intersecting the cone angle. Some shield designs tapper the gamma shield into a point, (in effect, making it a three point volumetric zone instead of a rectangular volumetric zone) however, doing this requires some intuition [Engle, 1984]. To be sure that the shield designs analyzed in this thesis meet the dose criteria, the gamma shield maintained the same relative thickness in the shield wing as behind the core. The points where each part of the layered shield intersect the cone

Gamma Shield Next to Core.

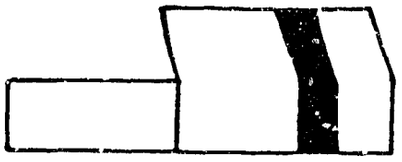

Gamma Shield Away From the Core.

Figure 8.1a and 8.1b. Core and Shield Configurations.

angle is determined so that the shield's mass and volume can be calculated.

The volumes and masses were calculated using a shield volume code, SHVOL.FOR, written in FORTRAN 77 specifically for this thesis. It calculates the intersection points for each segment of the shield and then calculates the shield's mass and volume using a volume of revolution mapping technique. Appendix F describes the code, its input and output in detail.

As the gamma shielding material is moved up and down the shield, the mass and volume changes in two ways. If the two shields in Figures 8.1a and 8.1b are the same volume, then moving the gamma shield away from the core increases its volume since the gamma shield must be extended

in the wing portion of the shield to intersect the cone half angle. It will displace a volume that was once occupied by the neutron shield. Gamma shields are more dense, therefore, they weigh more. Hence, a heavier material is replacing a lighter material increasing the shield's total weight. However, if by moving the gamma shield decreases the neutron shield material enough such that much less of it is needed to attenuate the gamma and neutron radiation to the specified levels, the overall shield mass can decrease. This happens because the neutron and gamma interactions are energy dependent. Moving the gamma material away changes the neutron energy incident to it from the core, i.e., the neutron material. The consequences of this could be, for example, that there is less secondary gamma production, which has to be attenuated by the neutron shield. Since the characteristics of the neutron shielding material dictate that it isn't a very good gamma shield, it usually takes a substantial amount of neutron shield material to attenuate the gamma rays. Therefore, the lower the secondary production, the better. Inelastic scattering can also reduce the neutron energy substantially. If the gamma shield is placed in an energy dependent flux such that the probability of inelastic scattering is larger, then it can help the neutron shield inasmuch as there need not be as much of it to attenuate the Nvt to the acceptable dose. These are the trade offs that are important in this analysis.

8.4 Shield Analysis. There were four shielding configurations considered in this analysis: W/LiH, W/B_4C, Be/LiH, and Be/B_4C. W and Be are considered the gamma shielding materials, whereas LiH and B_4C are considered the neutron shielding materials. This is a bit misleading since Be does not a high atomic number, and therefore, it is not a good gamma shield. It is Be's neutron attenuating characteristics that do not produce secondary gammas that make it a desirable material to look at. In the shields with no W, the neutron materials will be used to attenuate gammas.

The gamma shielding material is moved up and down the shield in ten cm increments to determine the best shield configurations satisfying the dose requirements. If a shield configuration could not meet the dose requirements, it was discarded. Also, the possibility exist where the gamma shielding material was positioned at a point beyond were the dose constraints were met. For example, if the gamma shielding material were placed 50 cm from the core, and the gamma and neutron dose was satisfied at 46.4 cm, then that shielding configuration was thrown out. The neutron material was basically shielding both gammas and neutrons by itself.

Two considerations are used for shielding. Attenuating the dose for silicon and attenuating the dose for humans. FEMP1D was ran before the shield was put into place to calculate the radiation dose not attenuated out of the

reactor core. One run was made for silicon dose. The dose was calculated to be:

1.0114×10^{19} nvt for neutrons, and

1.1777×10^{25} eV/cc for gammas.

The number of doses can be calculated as:

No of Doses = dose/(allowed dose).

The allowed dose for gammas is 0.5×10^{6} rads. Therefore the calculated flux is:

$(1.1777 \times 10^{25}$ eV/cc)/(1.5105 eV/cc/rad)$=7.7968 \times 10^{10}$ rads.

The number of doses is:

$$\text{No of Doses} = 7.7968 \times 10^{10}/0.5 \times 10^{6}$$

$$= 1.5594 \times 10^{5}, \text{ for gammas.}$$

For neutrons, the number of doses is:

$$\text{No of Doses} = 1.0114 \times 10^{19}/10^{13}$$

$$= 1.0114 \times 10^{6}.$$

Taking the ratio of the number of doses for neutrons and gammas yields:

$$1.0144 \times 10^{6}/1.5594 \times 10^{5} = 6.4858.$$

This implies that it is 6.486 times as hard to shield neutrons as it is gammas for silicon. If this is done for humans, it is 66.32 times as hard to shield for neutrons for gammas.

9.0 Results

In the four shield configurations analyzed in this thesis, a one cm thick slice of W or Be was moved down the shield starting at the core and moving at 10 cm increments through the shield to point 60 cm from the core. The shields were first checked with the FEMP1D output files to see at what point in the shield where the dose levels were satisfied. Once that point was identified, then SHVOL.FOR was used to calculate the volume and mass of each of the different material zones in the shield and to calculate the total shield mass (see Appendix F). If the gamma shielding material was moved to a point beyond which the neutron shielding material could attenuate the gamma radiation by itself, then that point, and the remaining point/points, if any, was/were not tabulated in the volume and mass calculations.

9.1 Volume and Mass Calculations. In the shielding analysis, if the radiation levels were not attenuated through the shield after a shield thickness of 67.75 cm, then that shield configuration was thrown out, and it was not considered in the volume and mass calculations. The only exception was for the LiH shield with no gamma shielding material. Using only LiH, it took a thickness of 97.16 cm to finally get the gamma dose under 6.1742×10^{23} eV/cc. Figures 9.1 through Figures 9.8 show the results of this analysis. The shield thickness was calculated on a

line of symmetry bisecting the core and shield. Table 9.1 shows the calculated shield thickness, mass and volume of the shields containing only LiH and B_4C.

Table 9.1. LiH and B_4C Shields.

Material	Thickness	Volume	Mass
LiH	97.16 cm	1,097,378.94 cc	850.47 kg
B_4C	35.63 cm	286,032.80 cc	720.80 kg

Since these materials are primarily neutron shielding materials, adding W or any other gamma attenuating material to these shielding configurations must reduce the mass or volume for the overall shield configuration to justify using it.

For the W/LiH shielding configuration, putting the W next to the core never satisfied the gamma dose criteria. It was therefore discarded for the mass and volume calculations. Table 9.2 shows the results of the W/LiH calculations with the W at positions of 10, 20, 30, 40, 50, and 60 cm from the core. The lightest of these configurations was when the W was at 40 cm from the core. This also yielded the least volume for this configuration. It is interesting to note that with the W at 60 cm, there is no LiH behind the W which implies that the W attenuated the gamma flux inside the 1 cm thick boundary. This was the case. Therefore, for W at 60 cm, only a 0.79 cm W slab was

needed.

Table 9.2. W/LiH Shield Configurations.

W Position (cm)	Thickness (cm)	Volume (cc)	Mass (kg)
10	67.21	646,544.25	637.07
20	63.47	598,009.41	616.26
30	59.18	535,226.11	592.47
40	50.08	437,407.84	528.39
50	51.15	449,504.50	557.55
60	60.79	564,234.71	618.79

*The W positioned next to the core did not satisfy the gamma dose within a shield thickness of 67.75 cm.

Table 9.3 gives the results of the W/B_4C shielding configurations. Table 9.1 shows that the B_4C shield with no W satisfied the dose requirements at 35.63 cm. When the W was moved to 40 cm, the dose for both neutrons and gammas was attenuated by just the B_4C. Therefore, the W/B_4C configurations with W at 40 cm or more did not yield a smaller volume or a lesser mass than the shield with B_4C only. All configurations of the layered W/B_4C shield with the W 40 cm or more from the core were not considered for optimization, so their volumes and masses were not calculated.

With the Be/B_4C shield configuration, the doses were satisfied at 35.629 cm into the shield for all the runs with the Be 10 to 30 cm from the core. Table 9.4 shows the results of the Be/B_4C runs.

Table 9.3. W/B_4C Shield Configurations.

W Position (cm)	Thickness (cm)	Volume (cc)	Mass (kg)
0	31.35	245,313.65	727.07
10	27.60	211,176.00	655.35
20	27.60	211,176.06	670.57
30	30.28	235,485.58	636.52

*Positions 40 through 60 put the W beyond the point where B_4C meets dose criteria by itself.

Table 9.4. Be/B_4C Shield Configurations.

Be Position (cm)	Thickness (cm)	Volume (cc)	Mass (kg)
0	36.164	291,248.32	729.59
10	35.629	286,032.00	715.87
20	35.629	286,032.03	715.26
30	35.629	286,032.10	714.61

*Positions 40 through 60 puts the Be beyond the point where B_4C meets dose criteria by itself.

For the shield configurations of Be/LiH, none met the gamma dose criteria within a maximum shield thickness of 67.750 cm. Therefore, they were not considered for the optimization.

Table 9.2 shows both the mass and shield volume are minimal at 40 cm for the W/LiH shielding configurations,

Table 9.3 shows a minimum volume with W at 10 cm from the core for W/B_4C shield configurations. However, since the volume and mass are almost the same for the 10 and 20 cm positions, there might be a minimum volume existing somewhere between 10 and 20 cm. However, for the calculated points, 10 cm is the optimum point for volume with the W/B_4C shielding configurations.

The Be/B_4C shielding configurations yielded some interesting results. The shield thickness is almost the same for all the shield configurations. It is thickest when the Be it next to the core. In this position, the neutron dose was met 27.598 cm in the shield, and the gamma dose was satisfied with a shield thickness of 36.164 cm. With B_4C only, the neutron dose was met at 28.1340 cm, and the gamma dose was met at 35.63 cm. Therefore, with the Be next to the core, there was a slightly better attenuation of neutrons in the high energy range, but not for high energy gammas. This trade off was not favorable for the Be/B_4C configurations. When the Be was moved away from the core, the dose rates were satisfied with a shield thickness of 35.629 cm for all configurations. This is the same thickness that the B_4C shield attenuated the radiation as shown in Table 9.1. Since both of these materials have a low atomic number, the driving factor for attenuation the radiation to an acceptable dose was the gamma rays. Adding Be did not effect the shield thickness. However, since Be

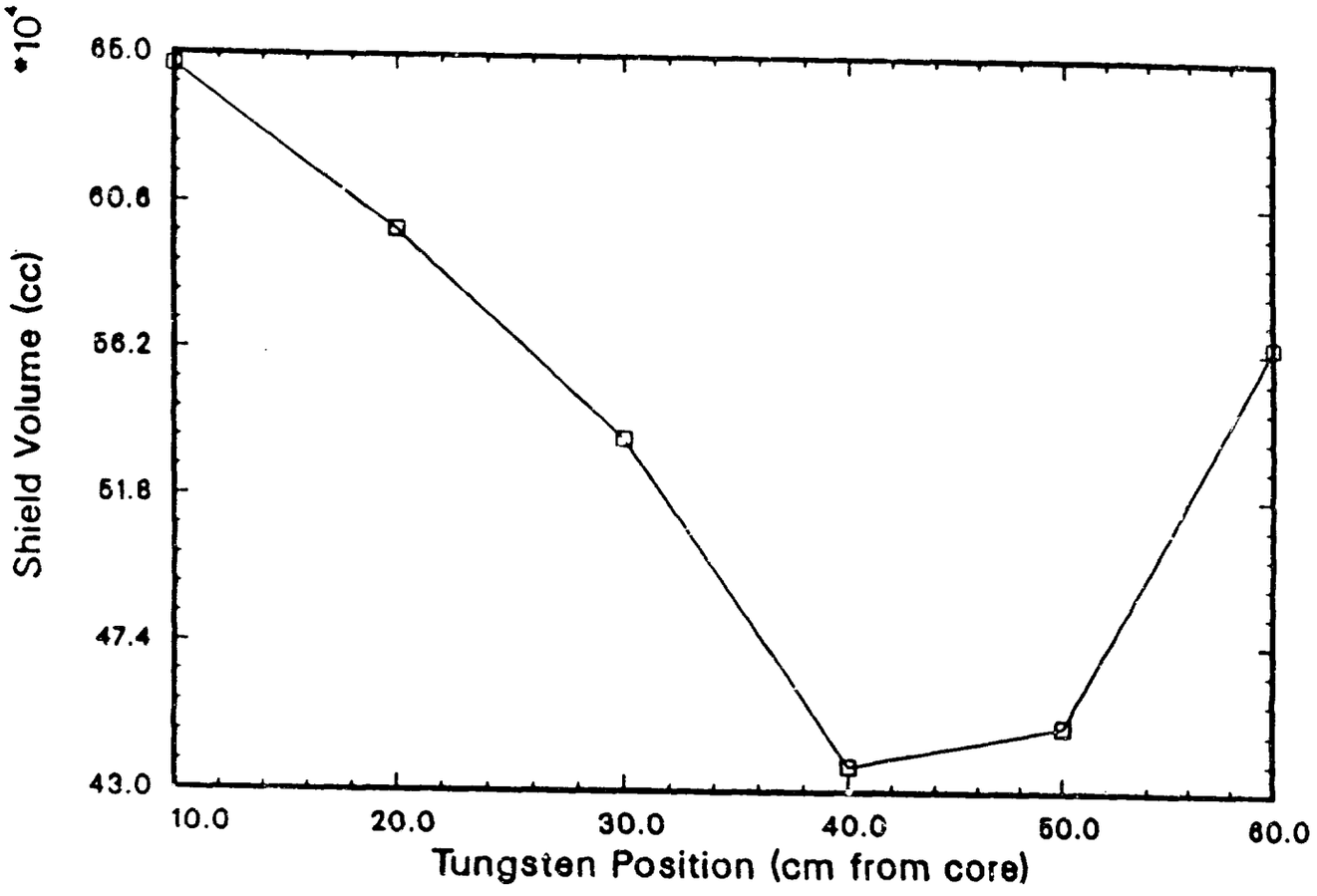

Figure 9.1. Shield Volume vs Tungsten Position.
Tungsten - Lithium Hydride Shield.

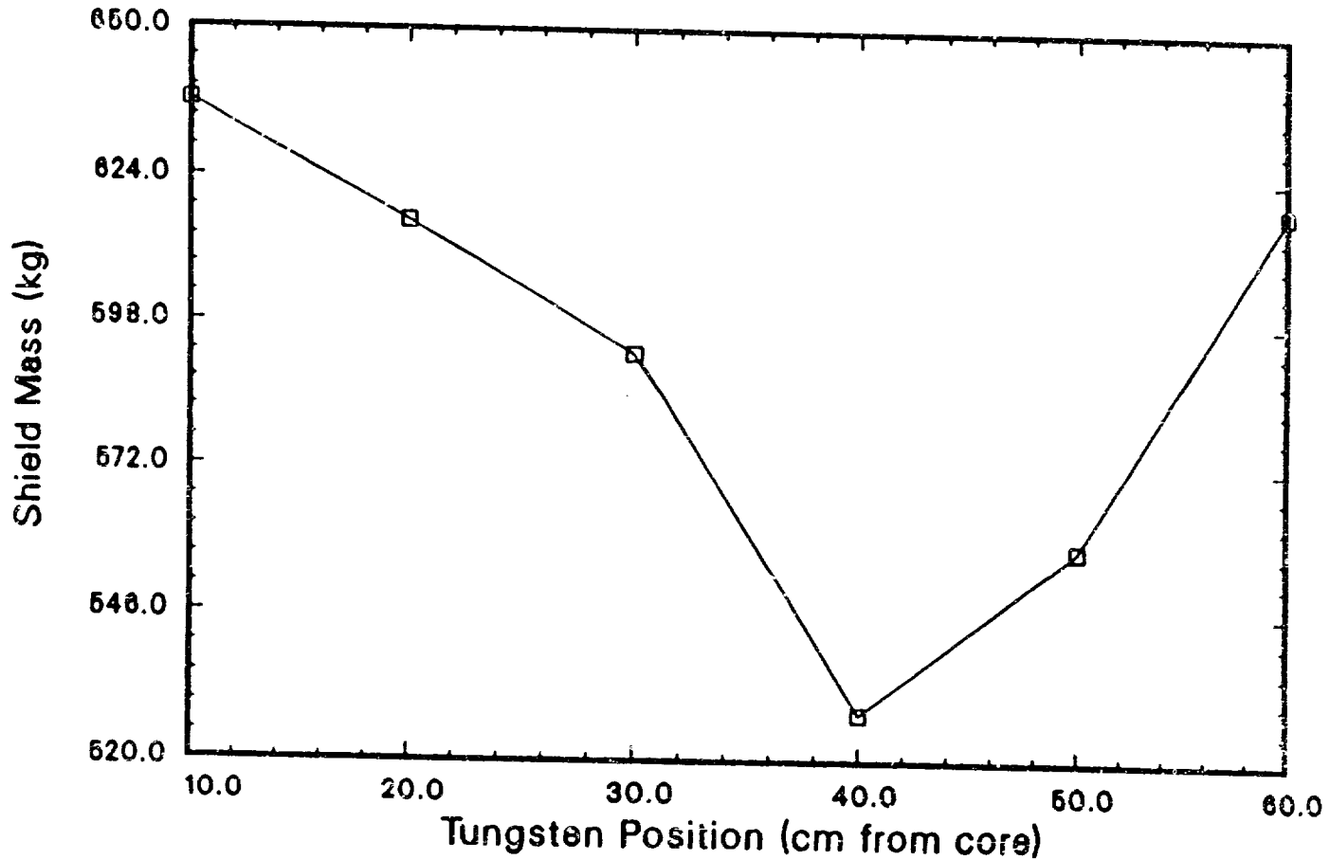

Figure 9.2. Shield Mass vs Tungsten Position
Tungsten - Lithium Hydride Shield.

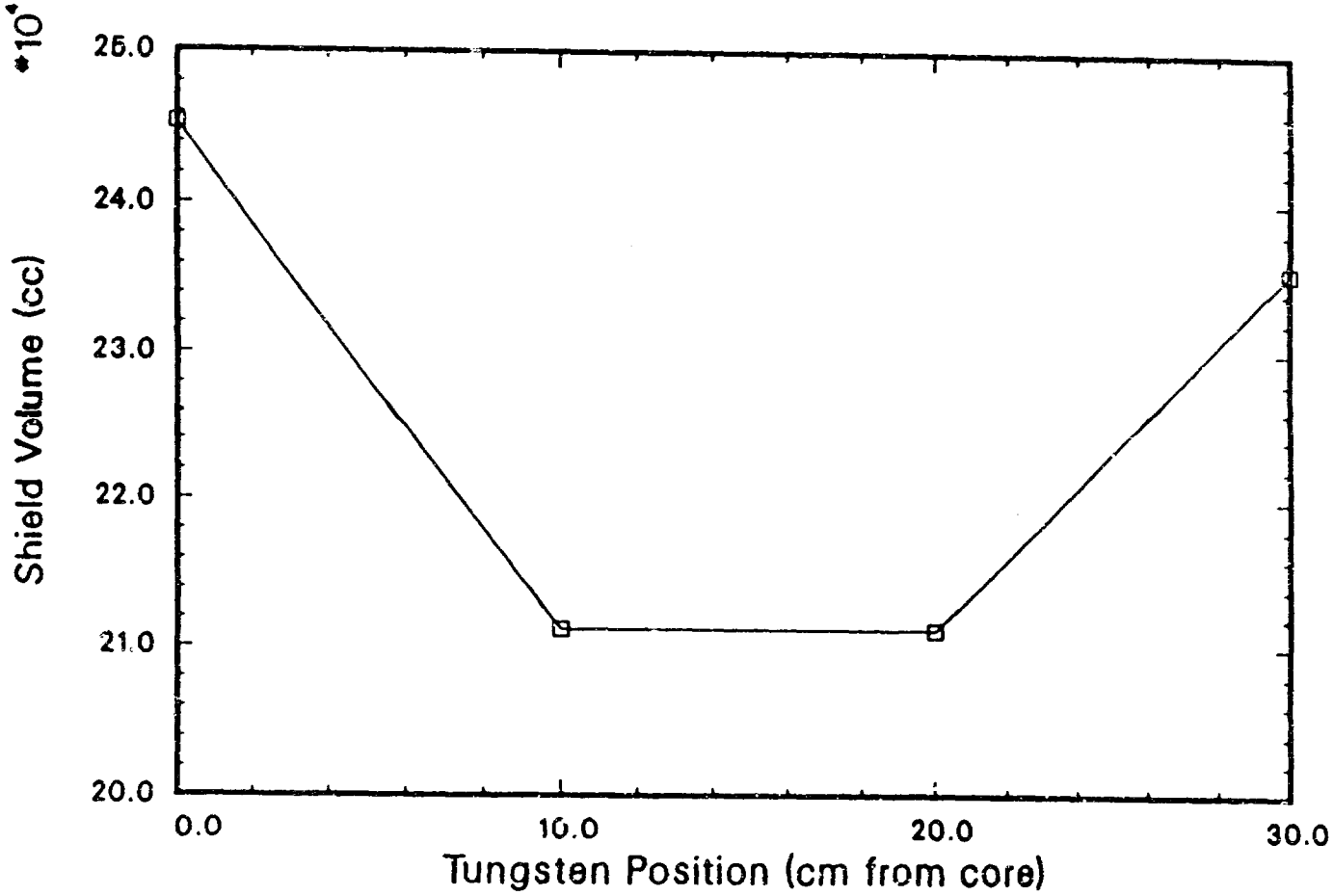

Figure 9.3. Shield Volume vs Tungsten Position.
Tungsten - Boron Carbide Shield.

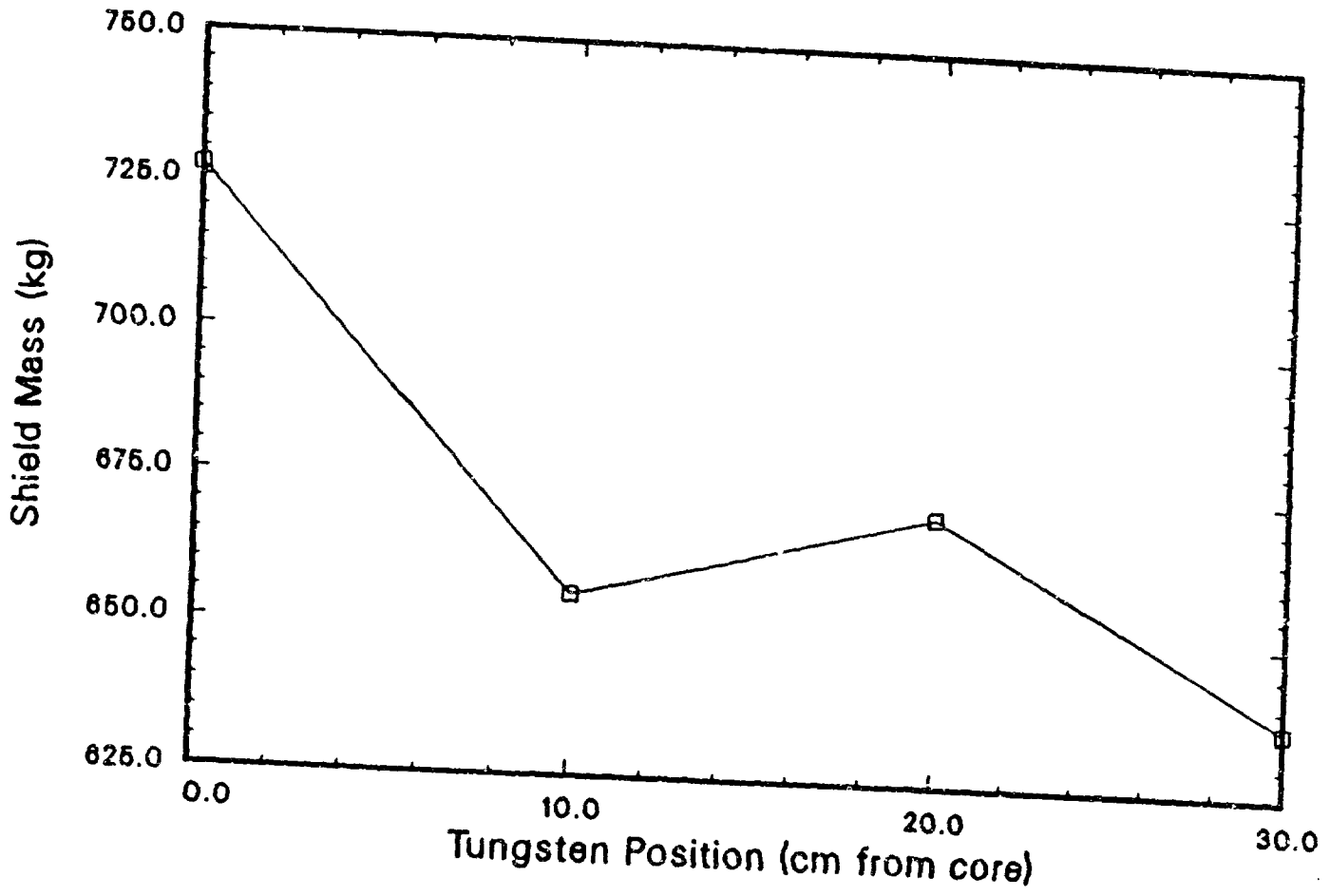

Figure 9.4. Shield Mass vs Tungsten Position.
Tungsten - Boron Carbide Shield.

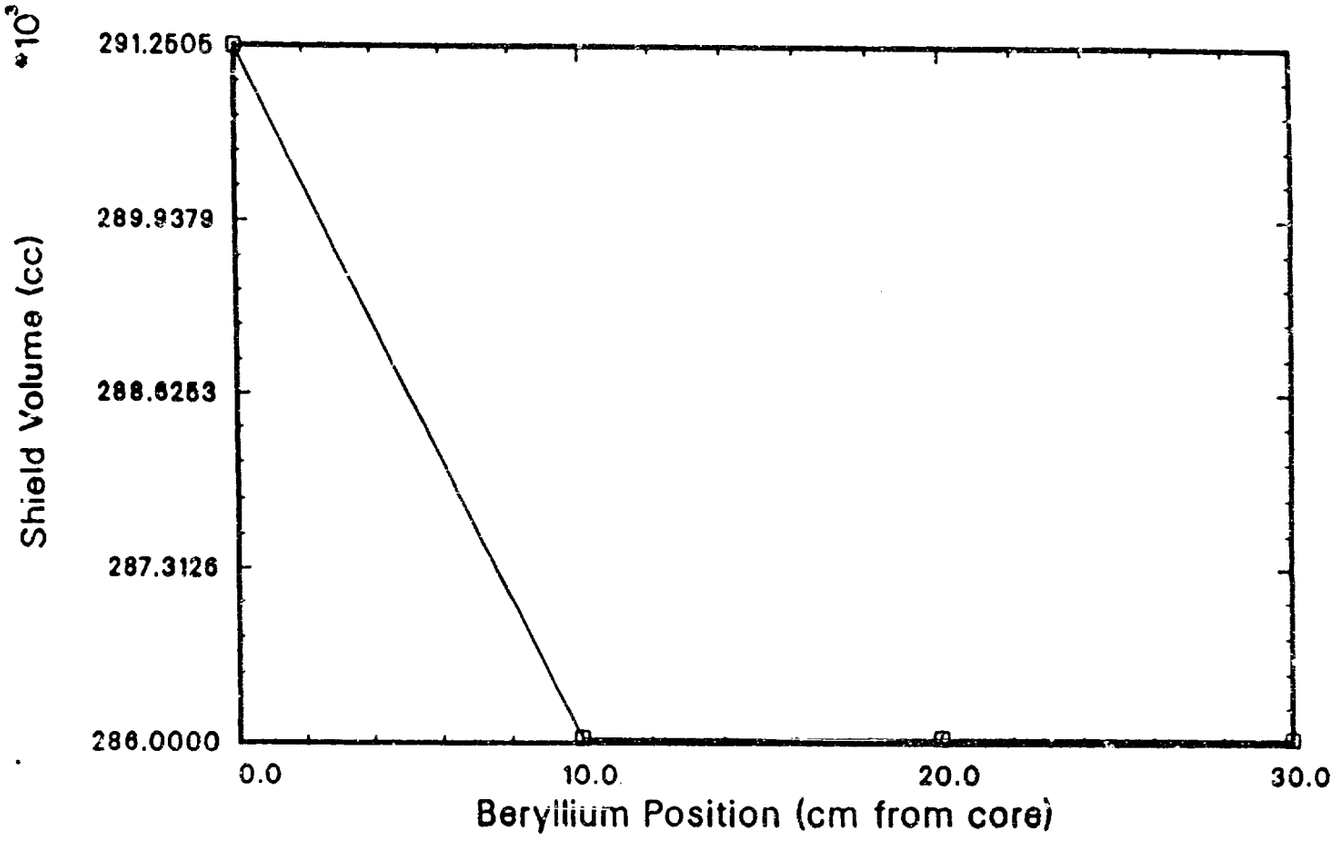

Figure 9.5. Shield Volume vs Beryllium Position.
Beryllium - Boron Carbide Shield.

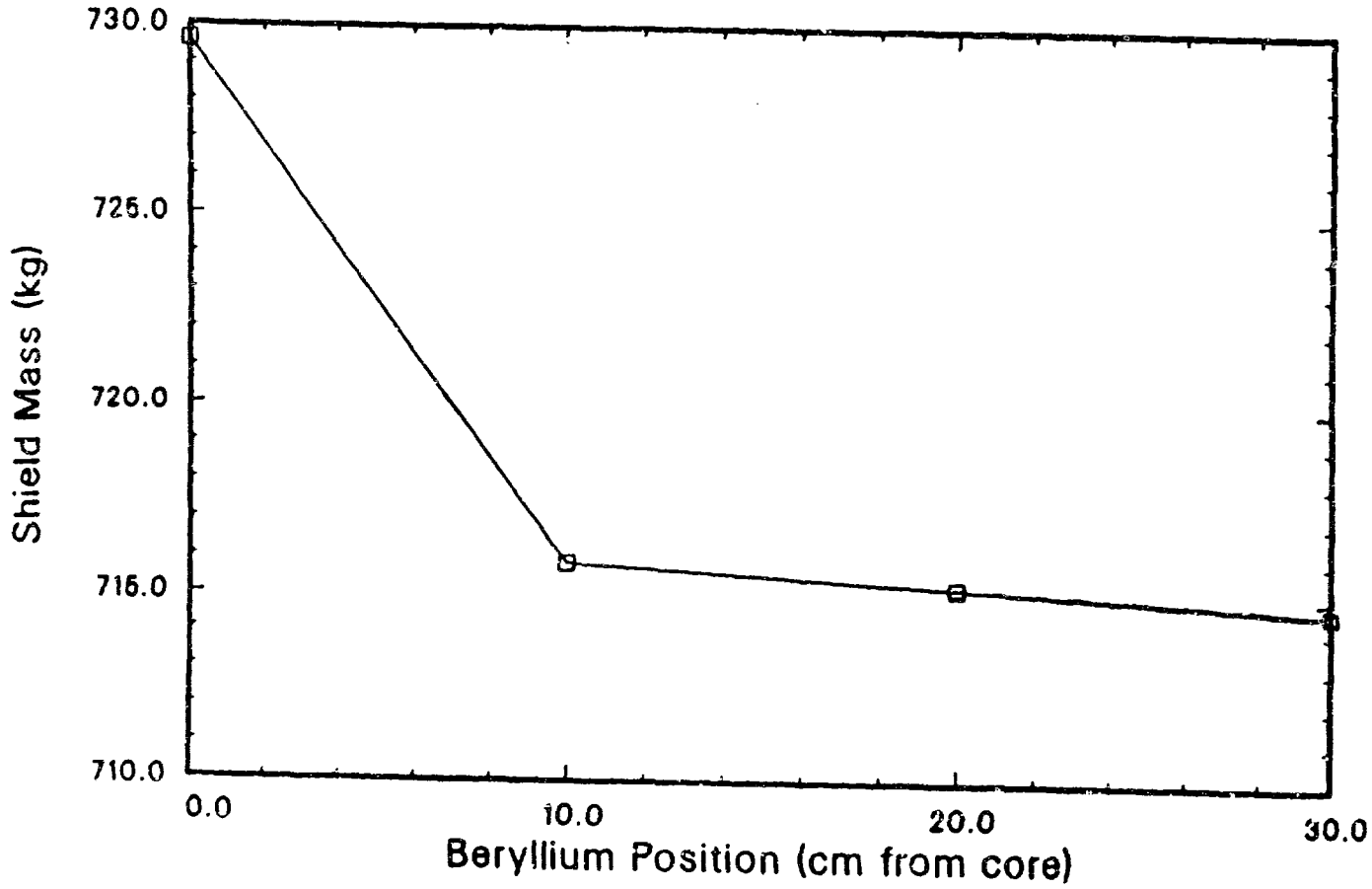

Tigure 9.6. Shield Mass vs Beryllium Position.
Beryllium - Boron Carbide Shield.

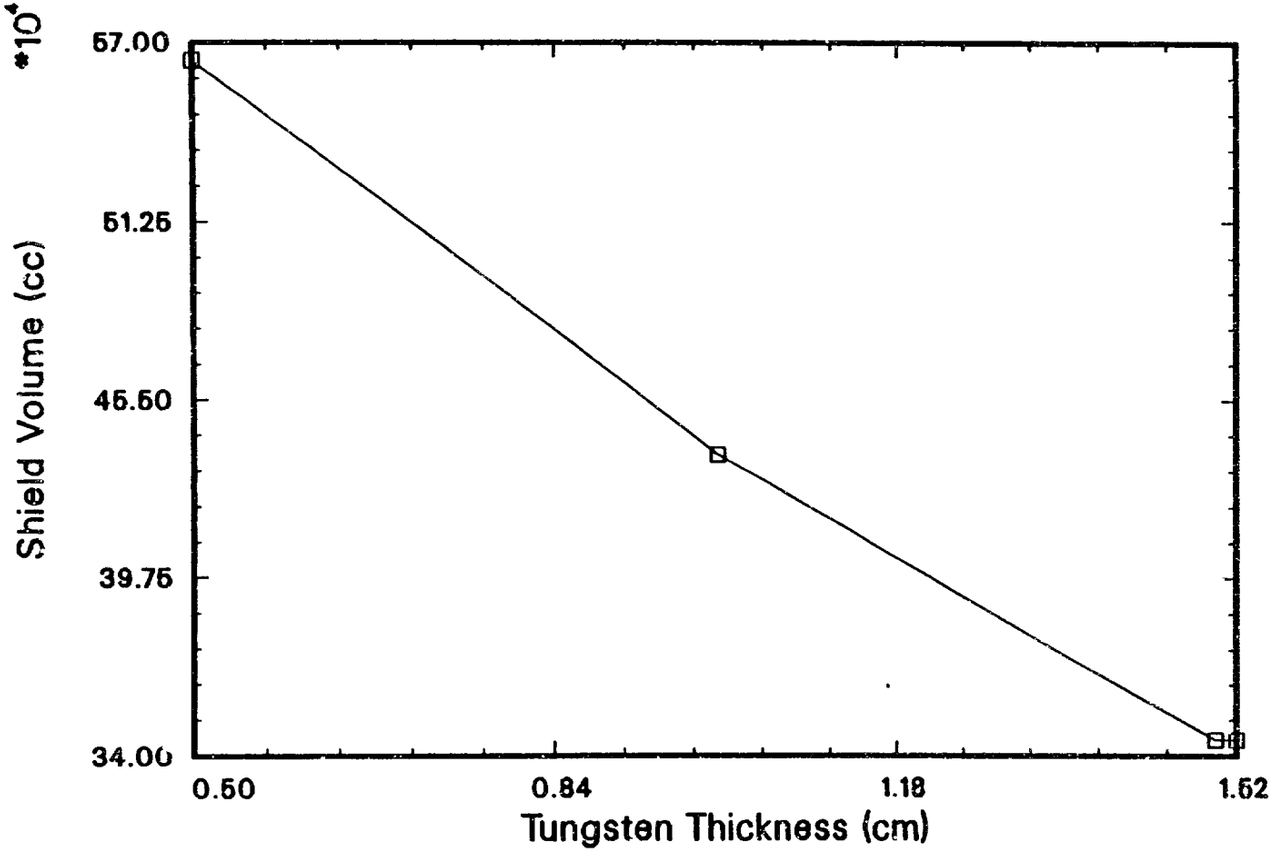

Figure 9.7. Shield Volume vs Tungsten Thickness.
Tungsten 40 cm From Core.

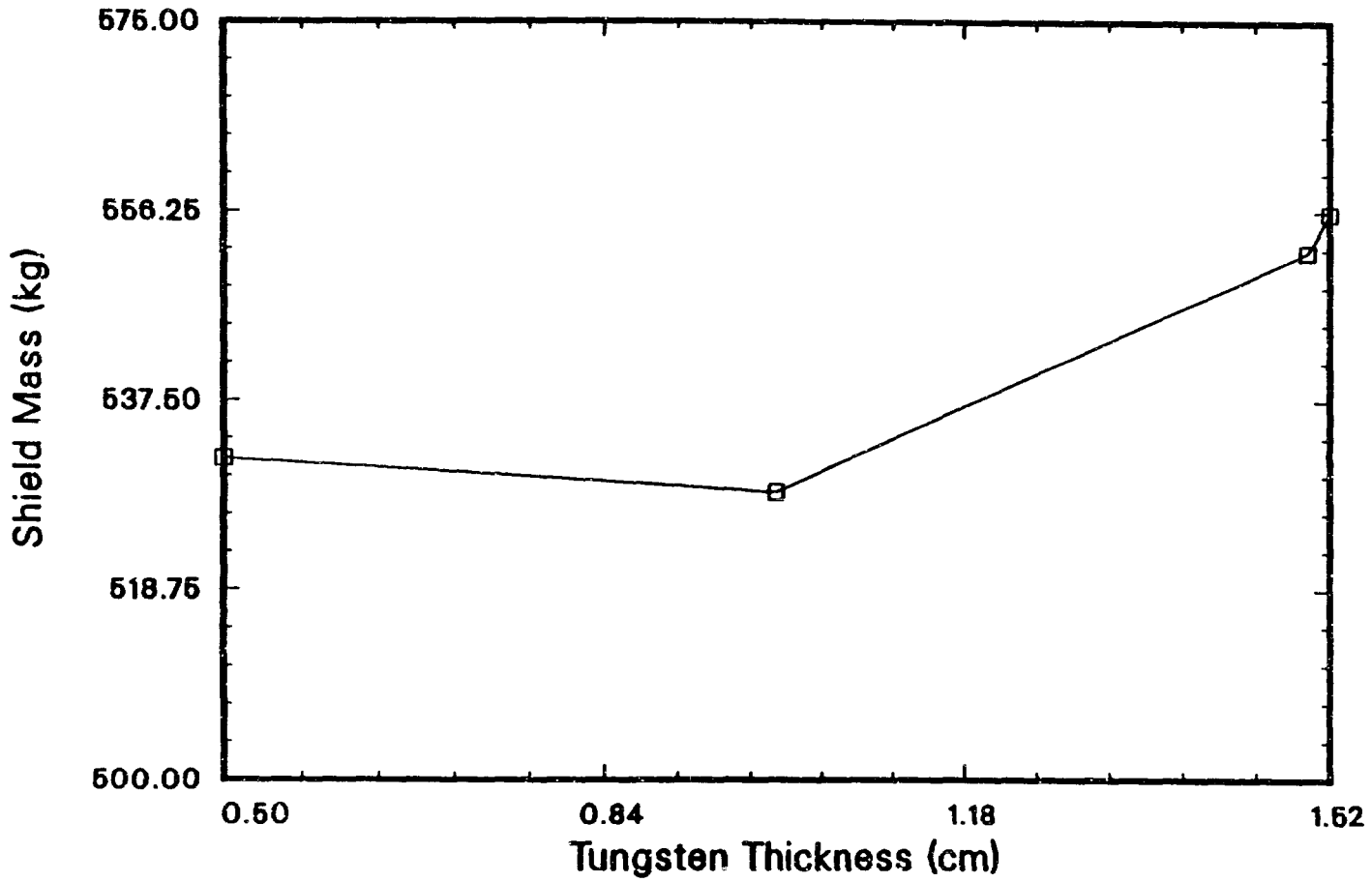

Figure 9.8. Shield Mass vs Tungsten Thickness.
Tungsten 40 cm From Core.

has a lower density, moving the Be away from the core allowed Be to replace B_4C in larger segments causing the shield mass to go down.

For all the shielding volumes, the W/B_4C configuration was the best with the W at 10 cm appearing to be an optimum. The configurations for mass, however, did not compare favorable with the W/LiH configuration at 40 cm.

The W/LiH shield was the lightest configuration. To determine the optimum for lightest shield, a closer examination of the W/LiH configuration with the W at 40 cm was done. Table 9.5 shows the optimum calculations for

Table 9.5. Optimum Shield Mass Calculations.

Thickness W (cm)	Volume (cc)	Mass (kg)
0.5	564,234.60	531.74
1.0	437,408.22	528.39
1.5	345,098.29	552.26
1.52*	345,089.22	556.09

* The dose criteria was met at this W thickness.

shield mass. Clearly, the lightest shield is with W at a thickness of 1 cm, 40 cm from the core. Figures 9.9a and 9.9b show the optimum shield configurations and reactor core.

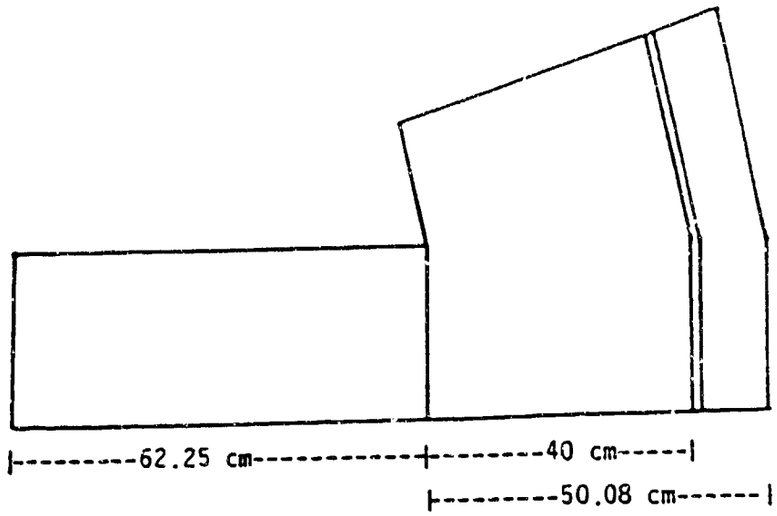

Figure 9.9a. W/LiH Optimum Weight Shield Configuration.

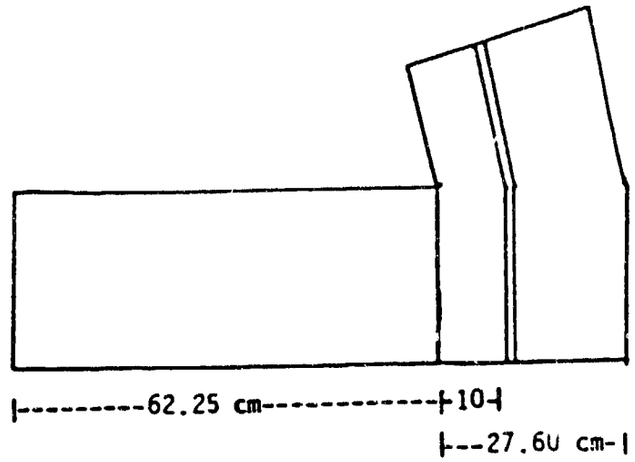

Figure 9.9b. W/B_4C Optimum Volume Shield Configuration.

10.0 Conclusion

Two shields were identified in this analysis that are of primary concern for the launching of a space nuclear reactor. A W/LiH configuration was found to be the lightest weight shield. Its mass was calculated to be 528.39 kg. The SP-100 shield was calculated to be about 681 kg. The difference in mass can be accounted for by noting that the LiH in the SP-100 is in a stainless steel honeycomb, and there is aluminum in the shield for thermal conduction. There is also much more W in the SP-100 shield. Also, the shield has an insulation material which adds more weight.

The shield with the smallest volume was found to be a W/B_4C shield with the W at a position of 10 cm from the core. This shield's mass was calculated to be 655.35 kg. The volume for the W/B_4C shield was found to be 211,176 cc. The volume of the W/LiH optimum weight shield was calculated to be 437,407.84 cc. Since the W/LiH shield has twice the volume than that of the B_4C shield, the 126.96 kg difference in mass may be more acceptable when considering a volume constraint for the launch vehicle or the material characteristics of the different shielding materials.

Figure 9.3 shows the shield volume vs W position for the W/B_4C configurations. The figure is a linear graphical representation of the calculated volumes. If a more detailed examination was done between the W at 10 cm and 20 cm, there might be a optimum volume somewhere in that region. Future research could verify this. Appendix D

shows the 25 neutron and 12 gamma groups and the 16 neutron and 8 gamma groups used in this analysis. Future work could be done using this group structure with a more refined cross section set which may yield a clearer picture of the dominate interactions in the shielding materials. Different thickness of different gamma shielding materials may identify a more optimum shield volume. One such material is borated beryllium oxide. Also, the shield could be modeled with a stainless steel matrix for the LiH and with aluminum thermal strips embedded to verify the necessary W thickness to attenuate the gammas.

It has been shown that a B_4C shield would not be a catastrophic liability in shield mass for the reactor analyzed. However, since it can withstand higher temperatures, it could be a material to consider for higher power space reactors. A temperature analysis incorporated in a radiation shielding analysis could determine the maximum thermal power that a space nuclear reactor could produce using B_4C. This could yield significant results for the next generation of high powered space nuclear reactors.

REFERENCES

Akerhielm, F.,"Boron and Boron Compounds." Engineering Compendium on Radiation Shielding, Vol II. Berlin/Hiedelberg Germany: Springer - Verlag, 1975.

Anderson, R. V. et al., "Space Reactor Electric Systems Subsystem Technology Assessment." ESG-DOE-13398 (Rockwell International), Canoga Park, CA, 29 March 1983.

Barattino, William J., Coupled Radiation Transport/Thermal Analysis of the Radiation Shield For a Space Nuclear Reactor. Diss. University of New Mexico, 1985. Wright-Patterson AFB, OH: AFIT, 1985.

Cember, Herman, Introduction to Health Physics. Oxford: Pergamon Press, 1982.

Conversation with Dr. Charles Stein, Air Force Weapons Laboratory, October 1986.

Conversation with Ward Engle, Oak Ridge National Laboratory, 1984.

Dix, G. P., and Voss, S. S., "The Pied Piper - A Historical Overview of the U.S. Space Power Reactor Program." Space Nuclear Power Systems. Malabar, Fl: Orbit Book Company, 1985.

Duderstadt, J. J. and Hamilton, L. J., Nuclear Reactor Analysis. New York: John Wiley and Sons, Inc., 1976.

Henry, Allan F. Nuclear-Reactor Analysis. Cambridge, Mass: MIT Press, 1975.

Hildebrand, F. B. Advanced Calculus for Applications. Englewood Cliffs, New Jersey: Prentice-Hall, Inc., 1976.

Hubbell, J. H. and Berger, M. J., "Photon Atomic Cross Sections." Engineering Compendium on Radiation Shielding, Vol I. Berlin/Hiedelberg Germany: Springer-Verlag, 1968.

Koenig, Daniel R., Experience Gained From the Space Nuclear Rocket Program (ROVER), LA-10062-H, Los Alamos National Laboratory, Los Alamos, NM, 1986.

McDaniel, Patrick J. NE-511 Nuclear Reactor Analysis Class Notes, the University of New Mexico, 1984.

Schaeffer, N. M., ed. Reactor Shielding for Nuclear Engineers. Washington D. C.: U. S. Atomic Energy Commission.

Selph, W., "Interaction Processes." Engineering Compendium on Radiation Shielding, Vol I. Berlin/Hiedelberg Germany: Springer-Verlag, 1968.

Simons, et al., ed. Illustrated Home Reference. Nashville, Tennessee: The Southwestern Company, 1973.

Voss, S. S. SNAP Reactor Overview, AFWL-TN-84-14, Air Force Weapons Laboratory, Kirtland AFB, NM, 1984.

Weast, ed. CRC Handbook of Chemistry and Physics. 56th ed. Cleveland, Ohio: CRC Press, 1975.

Weidner, Richard T., and Sells Robert L. Elementary Physics: Classical and Modern. Boston: Allyn and Bacon, Inc., 1975.

Welch, F. H., "Metallic and Saline Hydrides " Engineering Compendium on Radiation Shielding, Vol II. Berlin/Hiedelberg Germany: Springer - Verlag, 1975.

Wright, William E., "Accomplishments and Plans of the SP-100 Program." Space Nuclear Power Systems. Malabar, Fl: Orbit Book Company, 1985.

APPENDIX A

CALCULATIONS OF EFFECTIVE RADII

Calculation of the effective radii used for FEMP2D.

First the effective radius of the hexagonal center control rod is calculated.

The area of a hexagon can be calculated by using the following formula:

$$Area = n\ r^2\ tan\frac{\pi}{n}.$$

Where n=6, the number of sides in a hexagon.
r is the radius from the center of the hexagon to the intersection point of the sides.

$$Area = (6)(2.325)^2 tan(\frac{\pi}{6})$$

$$Area = 18.7256\ cm^2.$$

The effective radius is calculated:

$$r = \sqrt{\frac{Area}{\pi}}$$

$$r = \sqrt{\frac{18.7256}{\pi}}$$

$$r_{eq} = 2.4414\ cm.$$

Therefore:

$$r_1 = 2.4414\ cm.$$

We must work backward to calculate r_2 by calculating r_3.
r_3 is a concentric cylinder from r_2 to the outside edge of the six hexagonal control rods.

We have 1 safety plug and 6 control rods within the area of concern.

This total area is:

$$(7)(18.7256) = 131.0794\ cm^2.$$

There are 300, 72/96% enriched pins.
Fuel pin radius (including cladding): $\frac{1.05}{2} = 0.5250$ cm.
This total area:

$$(300)\pi(0.5250)^2 = 259.7704\ cm^2.$$

The pitch to diameter ratio is: $\frac{P}{D} = 1.07$.

Therefore:

$$Pitch = (1.07)(1.05) = 1.1235\ cm.$$

Since the fuel is in a trangular pitch, consider the triangular cell:
The area of a triangle may be calculated by:

$$Area = \frac{1}{2}a^2 sin(\theta)$$

Where a=pitch
θ=60 degrees $=\frac{\pi}{3}$ radians.
First, calculate the area of the trangular cell:

$$Area = \frac{1}{2}(1.1235)^2 sin(\theta)$$

$$= 0.5466\ cm^2.$$

Second, calculate the area of the fuel pins (in the trangular cell).

$$Area = (\frac{1}{6} + \frac{1}{6} + \frac{1}{6})\pi r_{fp}^2.$$

Where r_{fp} is the radius of the fuel pins.

$$Area = \frac{1}{2}\pi(0.5250)^2$$

$$= 0.4330\ cm^2$$

This leads to two very important ratios (which are the inverse of each other) .

$A_{fp} \equiv$ the area of the fuel pins in the trangular cell.
$A_{tot} \equiv$ the total area of the trangular cell.

$$\frac{A_{fp}}{Atot} = \frac{0.4330}{0.5466} = 0.7921.$$

$$\frac{A_{tot}}{A_{fp}} = 1.2624.$$

The total area occupied by 300 fuel pins, wire spacer, and coolant is:

$$\frac{A_{tot}}{A_{fp}} A_{fp} = (1.2624)(259.7704) = 327.9428\ cm^2$$

The total area in question including the 7 hexagonal rods is:

$$327.9428 + 131.0794 = 459.0222\ cm^2.$$

The equivalent radius, r_3:

$$r_3 = \sqrt{\frac{459.0222}{\pi}} = 12.0877\ cm^2.$$

r_2 is the "inner radius" of the concentric cylinder from r_1 to the inside

of the six hexagonal control rods.
It can be calculated by substracting the diameter of one of the hexagonal control rods from r_3.
Recalling that r for one of the hexagonal elements (not the equivalent radius) was 2.325 cm, then:

$$r_2 = r_3 - [(2)(2.325)] = 12.0877 - 4.650 = 7.4377\ cm.$$

r_4 will bound all fuel rods, safety plug, control rods, wire spacer, and coolant channels.

$$Total\ fuel\ pins = 396 + 300 = 696.$$

Total fuel pin area:

$$A_{fps} = 696\pi(0.5250)^2 = 602.6674\ cm^2.$$

Fuel pin and coolant area:

$$A_t = (1.2624)(602.6674) = 760.8074\ cm^2.$$

The total area bounded by r_4:

$$A_{tot} = 760.80784 + (7)(18.7256) = 891.8866\ cm^2.$$

Therefore:

$$r_4 = \sqrt{891.8866\pi} = 16.8492\ cm^2.$$

r_5 and r_6 are chosen to be:

$$r_5 = 18.4500\ cm^2$$

$$r_6 = 27.5000\ cm^2.$$

APPENDIX B

ATOM DENSITY CALCULATIONS FOR

FEMP1D AND FEMP2D

Atom densities for this thesis was calculated using the following formula:

$$N\left(\frac{atom}{barn \cdot cm}\right) = \frac{\rho \cdot N_a}{M_a}$$

Where: $N_a \equiv$ Avogadro's Number, $6.022045x10^{23}$ $\frac{atoms}{gm\ atom}$ *or* $\frac{molecules}{gram\ mole}$.

$M_a \equiv$ Molecular weight $\frac{gm}{gm\ atom}$ *or* $\frac{gm}{gm\ mole}$.

$\rho \equiv$Nuclide density $\frac{gm}{cc}$.

This Appendix shows the calculated atom densities for FEMP1D and FEMP2D runs.

Sample Calculation For Lithium:

Lithium has two isotopes: Lithium 6 and Lithium 7.
Lithium 6 composes 7.5% of natural lithium,
Lithiun 7 composis 92.7% of natural lithium.

$$\rho = 0.534\left(\frac{gm}{cc}\right)$$

$$M_a = 6.941\left(\frac{gm}{gm\ atom}\right).$$

$$N_{Li} = \frac{(0.534)(6.022045x10^{23})}{6.941} = 4.6331x10^{22}\left(\frac{atoms}{cc}\right)$$

$$N_{Li} = \left[4.6331x10^{22}\left(\frac{atoms}{cc}\right)\right]\left[10^{-24}\left(\frac{cm^2}{barn}\right)\right]$$

$$N_{Li} = 4.6331x10^{-2}\left(\frac{atoms}{barn \cdot cm}\right)$$

$$N_{^6Li} = (0.075)(4.6331x10^{-2}) = 3.4748x10^{-3}\left(\frac{atoms}{barn \cdot cm}\right)$$

$$N_{^7Li} = (0.925)(4.6331x10^{-2}) = 4.2856x10^{-2}\left(\frac{atoms}{barn \cdot cm}\right)$$

ATOM DENSITIES FOR FEMP2D RUNS
Not Smeared

ATOMS/BARN/CM	NUCLIDE
5.5046E-02	NB-93
5.5802E-04	NAT-ZR
2.1970E-02	B-10
8.7881E-02	B-11
2.7463E-02	C-12 (For boron carbide)
3.4748E-04	LI-6
4.2856E-03	LI-7
7.6179E-02	BE
3.8090E-02	C-12 (For beryllium carbide)
For 96% enriched fuel.	
3.3226E-02	N-14
3.1913E-02	U-235
1.3129E-03	U-238
For 72% enriched fuel.	
3.3131E-02	N-14
2.3939E-02	U-235
9.1920E-03	U-238
1.6627E-02	W-182
9.0403E-03	W-183
1.9389E-02	W-184
1.8081E-02	W-186

Sample calculation of a smeared atom density.

From Table 5.3, consider the atom density of boron-10.
It will be smeared in zone 1. Consider only the ratio of the areas since the heights cancel in the area ratio of the volumes.
Zone 1 total area is 18.7256 cm^2.
The area in this zone occupied by the boron is 14.3469 cm^2.

The smeared atom density for this zone:

$$N_{^{10}B}(Smeared) = \left(\frac{14.3469}{18.7256}\right)(2.1970x10^{-2})$$

$$N_{^{10}B}(Smeared) = 1.6883x10^{-2}\left(\frac{atoms}{barn \cdot cm}\right)$$

MIXING TABLE; SMEARED ATOM DENSITIES FOR FEMP2D RUNS

MATERIAL	ATOMS/BARN/CM	NUCLIDE
1	1.1288E-02	NB-93
1	1.1402E-04	NAT-ZR
1	1.6833E-02	B-10
1	6.7331E-02	B-11
1	2.1041E-02	C-12
2	1.1425E-02	NB-93
2	1.1541E-04	NAT-ZR
2	6.8148E-04	LI-6
2	8.4050E-03	LI-7
3	1.1370E-02	NB-93
3	1.1485E-04	NAT-ZR
3	6.6304E-03	B-10
3	2.6522E-02	B-11
3	8.2882E-03	C-12
3	4.1300E-04	LI-6
3	5.0937E-03	LI-7
4	2.7792E-02	NB-93
4	2.8073E-04	NAT-Z
4	1.6154E-03	LI-6
4	1.9924E-02	LI-7
5	5.5046E-02	NB-93
5	5.5602E-04	NAT-ZR
6	1.1288E-02	NB-93
6	1.1402E-04	NAT-ZR
6	5.8366E-02	BE
6	2.9183E-02	C-12
7	1.7246E-02	N-14
7	1.6564E-02	U-235
7	6.8146E-04	U-238
7	7.4583E-04	W-182
7	4.0552E-04	W-183
7	8.6972E-04	W-184
7	8.1105E-04	W-186
7	1.1425E-02	NB-93
7	1.1541E-04	NAT-ZR
7	6.8148E-04	LI-6
7	8.4050E-03	LI-7

MIXING TABLE; SMEARED ATOM DENSITIES FOR FEMP2D RUNS

MATERIAL	ATOMS/BARN/CM	NUCLIDE
8	1.0040E-02	U-235
8	4.1305E-04	U-238
8	4.5137E-04	W-182
8	2.4541E-04	W-183
8	5.2635E-04	W-184
8	4.9084E-04	W-186
8	1.1370E-02	NB-93
8	1.1485E-04	NAT-ZR
8	4.1300E-04	LI-6
8	5.0937E-03	LI-7
8	2.2990E-02	BE
8	1.1495E-02	C-12
9	2.7792E-02	NB-93
9	2.8073E-04	NAT-ZR
9	1.6154E-03	LI-6
9	1.9924E-02	LI-7
9	6.6386E-04	B-10
9	2.6555E-03	B-11
9	8 3984E-04	C-12
10	7 179E-02	BE
10	3.5090E-02	C-12
11	1.7197E-02	N-14
11	1.2425E-02	U-235
11	4.7711E-03	U-238
11	7.4583E-04	W-182
11	4.0552E-04	W-183
11	8.6972E-04	W-184
11	8.1105E-04	W-186
11	1.1425E-02	NB-93
11	1.1541E-04	NAT-ZR
11	8.4050E-03	LI-7
12	7.5313E-03	U-235
12	2.8919E-03	U-238
12	4.5137E-04	W-182
12	2.4541E-04	W-183
12	5.2635E-04	W-184
12	4.9084E-04	W-186
12	1.1370E-02	NB-93
12	1.1485E-04	NAT-ZR
12	4.1300E-04	LI-6
12	5.0937E-03	LI-7
12	1.1495E-02	C-12

MIXING TABLE; SMEARED ATOM DENSITIES FOR FEMP1D RUNS.

MATERIAL	ATOMS/BARN/CM	NUCLIDE
1	1.1425E-02	NB-93
1	1.1541E-04	NAT-ZR
1	6.8148E-04	LI-6
1	8.4050E-03	LI-7
2	1.5015E-02	N-14
2	1.3461E-02	U-235
2	1.5539E-03	U-238
2	6.4963E-04	W-182
2	3.5321E-04	W-183
2	6.9613E-04	W-184
2	7.0644E-04	W-186
2	1.1407E-02	NB-93
2	1.1523E-04	NAT-ZR
2	5.9377E-04	LI-6
2	7.3232E-03	LI-7
2	7.5108E-03	BE
2	3.7554E-03	C-12
3	5.5046E-02	NB-93
3	5.5602E-04	NAT-ZR
4	3.4748E-03	LI-6
4	4.2856E-02	LI-7

SHIELDING MATERIALS: *

MATERIAL	ATOMS/BARN/CM	NUCLIDE
LiH	4.4042E-3	LI-6
"	5.4317E-2	LI-7
"	5.8721E-2	H
Boron Carbide	2.1970E-2	B-10
	8.7881E-2	B-11
	2.9463E-2	C
Tungsten	1.6627E-2	W-182
"	9.0403E-3	W-183
"	1.9389E-2	W-184
"	1.8081E-2	W-186
Be	1.2349E-1	Be

*The atom densities for the shielding materials are not smeared.

APPENDIX C

FEMP1D AND FEMP2D DATA

FEMP1D and FEMP2D Codes.

FEMP1D and FEMP2D have demonstrated accuracy several times in comparison with results from other state-of-the-art codes used in the Air Force Weapons Laboratory and at Science Applications International Corporation. Dr Charles Sparrow, an IPA from Mississippi State University, with the Weapons Laboratory has produced nearly identical results for K_{eff} calculations using XSDRNPM as computed with FEMP1D. Dr. Sparrow calculates a K_{eff} of 0.9985 (with a Vitamin E cross section) for a specific reactor model. This results was duplicated using FEMP1D and with a different cross section set. This verifies the valitidy of both cross section sets as well as demostrates the accuracy of both codes. The FEMP cross section used in this comparison is the same set use for this thesis.

At the Weapons Lab, a model of the STAR-C reactor was analyzed using FEMP2D. The results duplicated the K_{eff} calculated by G. A. Technologies using MCNP. Also, Jim Mims, at Science Applications International Corporation in Albuquerque, has analyzed a gas-cooled pellet reactor with the same atom densities using both a Los Alamos code, TWODANT, and FEMP2D. The K_{eff} calculated by the two codes agreed up to the first decimal point. The cross section sets and the group structures were different. This gives credence to some of the state-of-the-art reactor codes being used at this time.

PROGRAM FEMP2D

INPUT DATA

TITLE CARD(18A4)

DATA BLOCK NO. 0 (PROBLEM DEFINITION)

1$ ARRAY(34)

NGEOM=1, (X,Y) GEOMETRY
=2, (R,Z) GEOMETRY
=3, (R,T GEOMETRY

NOUTR=1, INHOMOGENEOUS SOURCE
2, INHOMOGENEOUS SOURCE WITH FISSION
3, FISSION EIGENVALUE
4, FISSION EIGENVALUE SEARCH

MADJ=0, FORWARD PROBLEM
=1, ADJOINT PROBLEM

LPN=SPHERICAL HARMONIC ORDER

NMAT=NUMBER OF MATERIAL MIXTURES

NNG=NUMBER OF NEUTRON GROUPS

NPG=NUMBER OF PHOTON GROUPS

MPN=PN ORDER OF CROSS SECTIONS RETAINED

IHT=TOTAL CROSS SECTION POSITION (ANISN TAPE)

IHS=WITHIN GROUP SCATTER CROSS SECTION POSITION (ANISN TAPE)

LTBL=CROSS SECTION TABLE LENGTH (ANISN TAPE)

MTL=MIXING TABLE LENGTH

MCRD=NUMBER OF MATERIAL CROSS SECTIONS TO BE READ FROM CARDS

MANSN=NUMBER OF MATERIAL CROSS SECTIONS TO BE READ IN ANISN FORMAT FROM TAPE15

MAMPX=NUMBER OF MATERIAL CROSS SECTIONS TO BE READ IN AMPX WORKING LIBRARY FORMAT FROM TAPE16

NBYTE=1, FOR VAX FORTRAN COMPATIBILITY
=8, FOR CRAY FORTRAN COMPATIBILITY

NX=NUMBER OF X MESH POINTS

NY=NUMBER OF Y MESH POINTS

NZONE=NUMBER OF MATERIAL ZONES IN PROBLEM

IB(1)=0, LEFT BOUNDARY IS VACUUM
=1, LEFT BOUNDARY IS REFLECTING
=2, LEFT BOUNDARY HAS SOURCE INCIDENT

IB(2)=0, RIGHT BOUNDARY IS VACUUM
=1, RIGHT BOUNDARY IS REFLECTING
=2, RIGHT BOUNDARY HAS SOURCE INCIDENT

IB(3)=0, BOTTOM BOUNDARY IS VACUUM
=1, BOTTOM BOUNDARY IS REFLECTING
=2, BOTTOM BOUNDARY HAS SOURCE INCIDENT

IB(4)=0, TOP BOUNDARY IS VACUUM
=1, TOP BOUNDARY IS REFLECTING
=2, TOP BOUNDARY HAS SOURCE INCIDENT

ISTRT=1, SET FLUX EQUAL TO ZERO EVERYWHERE
=2, SET FLUX EQUAL TO 1.0 EVERYWHERE
=3, SET FLUX EQUAL TO FUNDAMENTAL MODE BASED ON BC'S
=4, SET FLUX EQUAL TO INPUT FROM TAPE10

IT1MX=MAXIMUM NUMBER OF INNER ITERATIONS

IT3MX=MAXIMUM NUMBER OF OUTER ITERATIONS FOR FISSION PROBLEMS

IACC=0, NO FISSION SOURCE ACCELERATION
1, SINGLE STEP CHEBYCHEV ACCELERATION
2, MULTIPLE STEP CHEBYCHEV ACCELERATION

NPOW=NUMBER OF POWER ITERATIONS PERFORMED BEFORE ACCELERATION

IUPS=0, NO UPSCATTER SCALING
=1, OVER-RELAXATION SCALING
=2, MATRIX INVERSION SCALING

NS=NUMBER OF SOURCE SPECTRA

NBYTE=1, FOR VAX FORTRAN COMPATIBILITY
=8, FOR CRAY FORTRAN COMPATIBILITY

NX=NUMBER OF X MESH POINTS

NY=NUMBER OF Y MESH POINTS

NZONE=NUMBER OF MATERIAL ZONES IN PROBLEM

IB(1)=0, LEFT BOUNDARY IS VACUUM
=1, LEFT BOUNDARY IS REFLECTING
=2, LEFT BOUNDARY HAS SOURCE INCIDENT

IB(2)=0, RIGHT BOUNDARY IS VACUUM
=1, RIGHT BOUNDARY IS REFLECTING
=2, RIGHT BOUNDARY HAS SOURCE INCIDENT

IB(3)=0, BOTTOM BOUNDARY IS VACUUM
=1, BOTTOM BOUNDARY IS REFLECTING
=2, BOTTOM BOUNDARY HAS SOURCE INCIDENT

IB(4)=0, TOP BOUNDARY IS VACUUM
=1, TOP BOUNDARY IS REFLECTING
=2, TOP BOUNDARY HAS SOURCE INCIDENT

ISTRT=1, SET FLUX EQUAL TO ZERO EVERYWHERE
=2, SET FLUX EQUAL TO 1.0 EVERYWHERE
=3, SET FLUX EQUAL TO FUNDAMENTAL MODE BASED ON BC'S
=4, SET FLUX EQUAL TO INPUT FROM TAPE10

IT1MX=MAXIMUM NUMBER OF INNER ITERATIONS

IT3MX=MAXIMUM NUMBER OF OUTER ITERATIONS FOR FISSION PROBLEMS

IACC=0, NO FISSION SOURCE ACCELERATION
1, SINGLE STEP CHEBYCHEV ACCELERATION
2, MULTIPLE STEP CHEBYCHEV ACCELERATION

NPOW=NUMBER OF POWER ITERATIONS PERFORMED BEFORE ACCELERATION

IUPS=0, NO UPSCATTER SCALING
=1, OVER-RELAXATION SCALING
=2, MATRIX INVERSION SCALING

NS=NUMBER OF SOURCE SPECTRA

IPX=-2, DO NOT PRINT CROSS SECTIONS
=-1, PRINT 1D CROSS SECTIONS
= N, PRINT 2D CROSS SECTIONS THRU PN

NPOUT=NUMBER OF POINTS F FLUX PRINT

IPFLX=-2, PRINT FLUX AT CALCULATION MESH POINTS
(NO RESTART TAPE)
-1, PRINT FLUX AT REQUESTED OUTPUT POINTS
(NO RESTART TAPE)
0, DO NOT PRINT FLUX OUTPUT (NO RESTART TAPE)
1, PRINT FLUX AT REQUESTED OUTPUT POINTS
2, PRINT FLUX BY GROUP AT CALCULATION MESH POINTS
3, RESTART TAPE ONLY

NRF=NUMBER OF CARD INPUT RESPONSE FUNCTIONS

2* ARRAY

EPS=CONVERGENCE TOLERANCE ON FLUX

EPSK=CONVERGENCE TOLERANCE ON EIGENVALUE

XK=EIGENVALUE ESTIMATE

SNORM=SOURCE NORMALIZATION

T

DATA BLOCK NO. 1 (MIXING TABLE)

10$ ARRAY(MTL)

MATERIAL NUMBERS

11$ ARRAY(MTL)

NUCLIDE NUMBERS

12* ARRAY(MTL)

NUMBER DENSITIES (ATOMS/BARN/CM)

13$ ARRAY(MCRD)

NUCLIDE IDS FOR CROSS SECTIONS INPUT ON CARDS

14* ARRAY(NOG)

CHI SPECTRUM

15* ARRAY(NNG+1)

NEUTRON GROUP BOUNDS

16* ARRAY(NPG+1)

GAMMA GROUP BOUNDS

17* ARRAY(NOG)

GROUP VELOCITIES

T

DATA BLOCK NO. 2 (CROSS SECTIONS-ONE BLOCK FOR EACH NUCLIDE/MATERIAL)

20* ARRAY(NOG*4)

NOTE THE 1D CROSS SECTIONS ARE STORED IN THE FOLLOWING ORDER

1. TOTAL
2. TOTAL FISSION YIELD(NU*SIGF)
3. ABSORPTION
4. GROUP FRACTIONAL YIELD(CHI)

1D CROSS SECTIONS FOR THIS MATERIAL

21* ARRAY(NOG*NOG)

P0 SCATTERING ARRAY FOR THIS NUCLIDE

22* ARRAY(NOG*NOG)

P1 SCATTERING ARRAY FOR THIS NUCLIDE

T

DATA BLOCK NO. 3 (MESH POINTS AND MATERIAL ZONES)

30* ARRAY(NX)

X MESH POINTS

31* ARRAY(NY)

Y MESH POINTS

32$ ARRAY(NZONE)

MACROSCOPIC MATERIALS BY ZONE

33$ ARRAY(NX-1)*(NY-1)

ZONE NUMBERS BY MESH INTERVAL

34* ARRAY(NMAT)

TRANSVERSE DIMENSIONS FOR BUCKLING CORRECTION BY MATERIAL

35* ARRAY(NPOUT)

OUTPUT X MESH POINTS FOR FLUX PRINT OUT

36* ARRAY(NPOUT)

OUTPUT Y MESH POINTS FOR FLUX PRINT OUT

37* ARRAY(NOG*NRF)

RESPONSE FUNCTIONS

T

DATA BLOCK NO. 4 (INHOMOGENEOUS SOURCES)

40* ARRAY(NOG*LPN1)

LEFT BOUNDARY SOURCE SPECTRUM

41* ARRAY(NOG*LPN1)

RIGHT BOUNDARY SOURCE SPECTRUM

42* ARRAY(NOG*LPN1)

BOTTOM BOUNDARY SPECTRUM

43* ARRAY(NOG*LPN1)

TOP BOUNDARY SPECTRUM

44* ARRAY(NOG*NS)

FIXED SOURCE SPECTRA

45$ ARRAY(NX-1)*(NY-1)

INHOMOGENEOUS SOURCES BY MESH INTERVAL

T

```
Sample Input File for FEMP2D.
1$$ 2   3   0   1
    13  16  8   1
    3   4   0   85
    0   0   85  1
    27  42  42  1
    0   0   0   3
    200 25  0   0
    0   0  -2   0
    3   0

2** 1.0E-4 1.0E-4 1.0 1.0 T

10$$ 5R1   4R2   7R3   4R4  2R5
     4R6   11R7  13R8  7R9  2R10
     11R11 13R12 2R13

11$$ 41093 40000 5010 5011 6012
     41093 40000 3006 3007
     41093 40000 5010 5011 6012 3006 3007
     41093 40000 3006 3007
     41093 40000
     41093 40000 4009 6012
     7014  92235 92238 74182 74183 74184 74186 41093 40000
           3006  3007
     7014  92235 92238 74182 74183 74184 74186 41093 40000
           3006  3007  4009  6012
     41093 40000 3006 3007 5010 5011 6012
     4009  6012
     7014  92235 92238 74182 74183 74184 74186 41093 40000
           3006  3007
     7014  92235 92238 74182 74183 74184 74186 41093 40000
           3006  3007  4009  6012
     3006  3007
12** 1.1288E-2 1.1402E-4 1.6833E-2 6.7331E-2 2.1041E-2
     1.1425E-2 1.1541E-4 6.8148E-4 8.4050E-3
     1.1370E-2 1.1485E-4 6.8304E-3 2.6522E-2 8.2882E-3 4.1300E-4
               5.0937E-3
     2.7792E-2 2.8073E-4 1.6154E-3 1.9924E-2
     5.5046E-2 5.5602E-4
     1.1288E-2 1.1402E-4 5.8366E-2 2.9183E-2
     1.7246E-2 1.6564E-2 6.8146E-4 7.4583E-4 4.0552E-4 8.6972E-4
               8.1105E-4 1.1425E-2 1.1541E-4 6.8148E-4 8.4050E-3
     1.0453E-2 1.0040E-2 4.1305E-4 4.5137E-4 2.4541E-4 5.2635E-4
               4.9084E-4 1.1370E-2 1.1485E-4 4.1300E-4 5.0937E-3
               2.2990E-2 1.1495E-2
     2.7792E-2 2.8073E-4 1.6154E-3 1.9924E-2 6.6386E-4 2.6555E-3
               8.2984E-4
     7.6179E-2 3.8090E-2
     1.7197E-2 1.2425E-2 4.7711E-3 7.4583E-4 4.0552E-4 8.6972E-4
               8.1105E-4 1.1425E-2 1.1541E-4 6.8148E-4 8.4050E-3
     1.0423E-2 7.5313E-3 2.8919E-3 4.5137E-4 2.4541E-4 5.2635E-4
               4.9084E-4 1.1370E-2 1.1485E-4 4.1300E-4 5.0937E-3
               2.2990E-2 1.1495E-2
     3.4748E-3 4.2856E-2 T
```

```
30** 0.0000  1.0000  2.0000
     2.4414  3.0000  4.0000  5.0000  6.0000  7.0000
     7.2048  8.0000  9.1000 10.2000 11.3000
    12.0876 13.2000 14.3000 15.4000
    16.8792 18.0000
    18.4500 19.9500 21.4500 22.9500 24.4500 25.9500
    27.5000

31** 0.0000  1.0000  2.0000  3.0000  4.0000  5.0000  6.0000
             7.0000  8.0000  9.0000
     9.7500
    10.0000 11.2000 12.4000 13.6000 14.8000
    16.0000 17.6000 19.2000 20.8000 22.4000 24.0000 25.6000
            27.2000 28.8000 30.4000 32.0000 33.6000 35.2000
    36.0000 37.2000 38.4000 39.6000 40.8000
    42.0000
    42.2500 45.5833 48.9167 52.2500 55.5833 58.9167
    62.2500

32$$ 1  2  3  2  4  5
     1  2  3  2  4  10
     6  7  8  7  9  10
     6  11 12 7  9  10
     6  7  8  7  9  10
     5  5  5  5  5  10
     13 13 13 13 13 13

33$$ 3R1  6R2   5R3   4R4   2R5   6R6   9Q26
     3R7  6R8   5R9   4R10  2R11  6R12
     3R13 6R14  5R15  4R16  2R17  6R18  4Q26
     3R19 6R20  5R21  4R22  2R23  6R24 12Q26
     3R25 6R26  5R27  4R28  2R29  6R30  4Q26
     3R31 6R32  5R33  4R34  2R35  6R36
     3R37 6R38  5R39  4R40  2R41  6R42  5Q26

36** 62.25 T
```

PROGRAM FEMP1D

INPUT DATA

TITLE CARD(18A4)

DATA BLOCK NO. 0 (PROBLEM DEFINITION)

1$ ARRAY

NGEOM=1, SLAB GEOMETRY
=2, CYLINDRICAL GEOMETRY
=3, SPHERICAL GEOMETRY

NOUTR=1, INHOMOGENEOUS SOURCE
2, INHOMOGENEOUS SOURCE WITH FISSION
3, FISSION EIGENVALUE

MADJ=0, FORWARD PROBLEM
=1, ADJOINT PROBLEM

LPN=SPHERICAL HARMONIC ORDER

NMAT=NUMBER OF MATERIAL MIXTURES

NNG=NUMBER OF NEUTRON GROUPS

NPG=NUMBER OF GAMMA GROUPS

MPN=PN ORDER OF CROSS SECTIONS RETAINED

IHT=TOTAL CROSS SECTION POSITION
(ANISN TAPE)

IHS=WITHIN GROUP SCATTER CROSS SECTION POSITION
(ANISN TAPE)

LTBL=CROSS SECTION TABLE LENGTH (ANISN TAPE)

MTL=MIXING TABLE LENGTH

MCRD=NUMBER OF MATERIAL CROSS SECTIONS TO BE
READ FROM CARDS

MANSN=NUMBER OF MATERIAL CROSS SECTIONS TO BE
READ IN ANISN FORMAT FROM TAPE15

MAMPX=NUMBER OF MATERIAL CROSS SECTIONS TO BE
READ IN AMPX WORKING LIBRARY FORMAT FROM
TAPE16

NBYTE=1, FOR VAX FORTRAN COMPATIBILITY
=8, FOR CRAY FORTRAN COMPATIBILITY

NX=NUMBER OF MESH POINTS

NZONE=NUMBER OF MATERIAL ZONES IN PROBLEM

IBL=0, LEFT BOUNDARY IS VACUUM
=1, LEFT BOUNDARY IS REFLECTING
=2, LEFT BOUNDARY HAS SOURCE INCIDENT

IBR=0, RIGHT BOUNDARY IS VACUUM
=1, RIGHT BOUNDARY IS REFLECTING
=2, RIGHT BOUNDARY HAS SOURCE INCIDENT

ISTRT=1, SET FLUX EQUAL TO ZERO EVERYWHERE
=2, SET FLUX EQUAL TO 1.0 EVERYWHERE
=3, SET FLUX EQUAL TO INPUT FROM TAPE10

ITMX2=MAXIMUM NUMBER OF MIDDLE ITERATIONS

ITMX3=MAXIMUM NUMBER OF OUTER ITERATIONS FOR
FISSION PROBLEMS

IACC=0, NO FISSION SOURCE ACCELERATION
1, SINGLE STEP CHEBYCHEV ACCELERATION
2, MULTIPLE STEP CHEBYCHEV ACCELERATION

NPOW=NUMBER OF POWER ITERATIONS PERFORMED BEFORE
STARTING THE CHEBYCHEV ACCELERATION

IUPS=0, NO UPSCATTER SCALING
=1, OVER-RELAXATION SCALING
=2, MATRIX INVERSION SCALING

NS=NUMBER OF SOURCE SPECTRA

IPX=-2, DO NOT PRINT CROSS SECTIONS
=-1, PRINT 1D CROSS SECTIONS
= N, PRINT 2D CROSS SECTIONS THRU PN

NPOUT=NUMBER OF POINTS FOR FLUX PRINT

IPFLX=0, DO NOT PRINT FLUX OUTPUT
1, PRINT FLUX AT REQUESTED OUTPUT POINTS
2, PRINT FLUX BY GROUP AT CALCULATION MESH POINTS

NRF=NUMBER OF CARD INPUT RESPONSE FUNCTIONS

2* ARRAY

EPSK=CONVERGENCE TOLERANCE ON EIGENVALUE

XK=EIGENVALUE ESTIMATE

SNORM=SOURCE NORMALIZATION

T

DATA BLOCK NO. 1 (MIXING TABLE)

10$ ARRAY(MTL)

MATERIAL NUMBERS

11$ ARRAY(MTL)

NUCLIDE NUMBERS

12* ARRAY(MTL)

NUMBER DENSITIES (ATOMS/BARN/CM)

13$ ARRAY(MCRD)

NUCLIDE IDS FOR CROSS SECTIONS INPUT ON CARDS

14* ARRAY(NOG)

CHI SPECTRUM

15* ARRAY(NNG+1)

NEUTRON GROUP BOUNDARIES

16* ARRAY(NPG+1)

GAMMA GROUP BOUNDARIES

17* ARRAY(NOG)

GROUP AVERAGE VELOCITIES

T

DATA BLOCK NO. 2 (CROSS SECTIONS-ONE BLOCK FOR EACH NUCLIDE/MATERIAL)

20* ARRAY(NOG*4)

NOTE THE 1D CROSS SECTIONS ARE STORED IN THE FOLLOWING ORDER

1. TOTAL
2. TOTAL FISSION YIELD(NU*SIGF)
3. ABSORPTION
4. GROUP FRACTIONAL YIELD(CHI)

1D CROSS SECTIONS FOR THIS MATERIAL

21* ARRAY(NOG*NOG)

P0 SCATTERING ARRAY FOR THIS NUCLIDE

22* ARRAY(NOG*NOG)

P1 SCATTERING ARRAY FOR THIS NUCLIDE

T

DATA BLOCK NO. 3 (MESH POINTS AND MATERIAL ZONES)

30* ARRAY(NX)

X MESH POINTS

31$ ARRAY(NZONE)

MACROSCOPIC MATERIALS BY ZONE

32$ ARRAY(NX-1)

ZONE NUMBERS BY MESH INTERVAL

33* ARRAY(NMAT)

TRANSVERSE DIMENSIONS FOR BUCKLING CORRECTION BY MATERIAL

34* ARRAY(NPOUT)

OUTPUT X MESH POINTS FOR FLUX PRINT OUT

35* ARRAY(NOG*NRF)

RESPONSE FUNCTIONS

T

DATA BLOCK NO. 4 (INHOMOGENEOUS SOURCES)

40* ARRAY((LPN+1)*NOG)

LEFT BOUNDARY SOURCE SPECTRUM

41* ARRAY((LPN+1)*NOG)

RIGHT BOUNDARY SOURCE SPECTRUM

42* ARRAY(NOG*NS)

FIXED SOURCE SPECTRA

43$ ARRAY(NX-1)

INHOMOGENEOUS SOURCES BY MESH INTERVAL

T

```
Sample Input file for FEMP1D.
1$$ 2  3   0  5
    4 16   8  3
    3  4   0 21
    0  0  21  1
   64  4   0  0
    2 500 10  0
    0  0   0 -2
    1  1   2

2** 1.0E-5  1.009  3.3787E+22 T

3023 4R1 12R2 2R3 2R4

11$$ 41093  40000  3006  3007
     7014   92235  92238 74182  74183  74184  74186  41093
            40000  3006  3007   4009   6012
     41093  40000
     3006   3007


12** 1.1425E-2 1.1541E-4 6.8148E-4 8.4050E-3
     1.5015E-2 1.3461E-2 1.5539E-3 6.4983E-4 3.5321E-4 6.9613E-4
               7.0644E-4 1.1407E-2 1.1523E-4 5.9377E-4 7.3232E-3
               7.5108E-3 3.7554E-3
     5.5046E-2 5.5802E-4
     3.4748E-3 4.2856E-2 T

30** 0.0000   1.0000   2.0000   3.0000   4.0000   5.0000   6.0000
              7.0000   8.0000   9.0000
    10.0000  11.0000  12.0000  13.0000  14.0000  15.0000  16.0000
             17.0000  18.0000  19.0000  20.0000  21.0000  22.0000
             23.0000  24.0000  25.0000  26.0000  27.0000  28.0000
             29.0000  30.0000  31.0000  32.0000  33.0000  34.0000
             35.0000  36.0000  37.0000  38.0000  39.0000  40.0000
             41.0000
   42.0000
   42.2500   43.2500  44.1500  45.2500  46.2500  47.2500  48.2500
             49.2500  50.2500  51.2500  52.2500  53.2500  54.2500
             55.2500  58.2500  57.2500  58.2500  59.2500  60.2500
             61.2500
   62.2500

31$$ 1 2 3 4

32$$ 10R1 32R2 1R3 2CR4
```

```
33** 31.0 31.0 F0.0

34**  62.25

35**  1.779579-4 1.480736-4 1.273286-4 1.289578-4
      1.175837-4 8.307393-5 4.780253-5 3.073550-5
      1.741842-5 8.706003-6 4.805043-6 3.608882-6
      3.675812-6 3.845325-6 4.405964-6 3.675043-6
      24R0.0
      8.783468-6 4.167297-6 2.620405-6 1.510685-6
      7.532709-7 3.860888-7 2.692778-7 4.511449-7 T
```

APPENDIX D

ENERGY GROUP DEFINITION

FEMP2D Energy group structure:

THIS LIBRARY HAS A 25 GROUP NEUTRON STRUCTURE

GROUP	RANGE
1	1.733000E+07---6.065000E+06
2	6.065000E+06---3.011000E+06
3	3.011000E+06---1.920000E+06
4	1.920000E+06---1.002000E+06
5	1.002000E+06---6.081000E+05
6	6.081000E+05---2.972000E+05
7	2.972000E+05---1.831000E+05
8	1.831000E+05---1.110000E+05
9	1.110000E+05---4.086000E+04
10	4.086000E+04---2.187000E+04
11	2.187000E+04---1.503000E+04
12	1.503000E+04---7.101000E+03
13	7.101000E+03---3.354000E+03
14	3.354000E+03---1.584000E+03
15	1.584000E+03---4.540000E+02
16	4.540000E+02---2.144000E+02
17	2.144000E+02---1.013000E+02
18	1.013000E+02---3.726000E+01
19	3.726000E+01---1.067000E+01
20	1.067000E+01---5.043000E+00
21	5.043000E+00---1.855000E+00
22	1.855000E+00---8.764000E-01
23	8.764000E-01---4.139000E-01
24	4.139000E-01---9.999000E-02
25	9.999000E-02---1.000000E-05

THIS LIBRARY HAS A 12 GROUP GAMMA STRUCTURE

GROUP	RANGE
1	1.400000E+07---8.000000E+06
2	8.000000E+06---6.000000E+06
3	6.000000E+06---4.000000E+06
4	4.000000E+06---2.000000E+06
5	2.000000E+06---1.500000E+06
6	1.500000E+06---1.000000E+06
7	1.000000E+06---7.000000E+05
8	7.000000E+05---4.000000E+05
9	4.000000E+05---2.000000E+05
10	2.000000E+05---1.000000E+05
11	1.000000E+05---6.000000E+04
12	6.000000E+04---1.000000E+04

FEMP1D Energy group structure:

THIS LIBRARY HAS A 16 GROUP NEUTRON STRUCTURE

GROUP	RANGE
1	1.733000E+07---6.065000E+06
2	6.065000E+06---3.011000E+06
3	3.011000E+06---1.920000E+06
4	1.920000E+06---1.002000E+06
5	1.002000E+06---6.081000E+05
6	6.081000E+05---2.972000E+05
7	2.972000E+05---1.831000E+05
8	1.831000E+05---1.110000E+05
9	1.110000E+05---4.086000E+04
10	4.086000E+04---2.187000E+04
11	2.187000E+04---7.101000E+03
12	7.101000E+03---3.354000E+03
13	3.354000E+03---1.584000E+03
14	1.584000E+03---3.726000E+01
15	3.726000E+01---9.999000E-02
16	9.999000E-02---1.000000E-05

THIS LIBRARY HAS A 8 GROUP GAMMA STRUCTURE

GROUP	RANGE
1	1.400000E+07---4.000000E+06
2	4.000000E+06---2.000000E+06
3	2.000000E+06---1.000000E+06
4	1.000000E+06---4.000000E+05
5	4.000000E+05---2.000000E+05
6	2.000000E+05---1.000000E+05
7	1.000000E+05---6.000000E+04
8	6.000000E+04---1.000000E+04

APPENDIX E

TRANSPORT EQUATION, LEGENDRE POLYNOMIAL DERIVATION

Boltzmann transport equation:

$$\nabla \cdot \Omega \Psi(\mathbf{r}, E, \Omega) + \Sigma_t(\mathbf{r}, E)\Psi(\mathbf{r}, E, \Omega) = S(\mathbf{r}, E, \Omega) + \int_{\Omega'} \int_{E'} \Sigma_s(\mathbf{r}, E' \rightarrow E, \Omega' \rightarrow \Omega)\Psi(\mathbf{r}, E', \Omega')dE'd\Omega' + \int_{\Omega'} \int_{E'} \frac{\chi(E)}{4\pi} \nu\Sigma_f(E')\Psi(\mathbf{r}, E', \Omega')dE'd\Omega'.$$

This equation is three dimensional, energy dependent, and represents steady-state, i.e., $dn/dt = 0$ *or* $\frac{\partial \Psi}{\partial t} = 0$.

$\Psi(\mathbf{r}, E, \Omega) \equiv$ neutron angular flux density.

$\Sigma_t(\mathbf{r}, E) \equiv$total interaction cross section.

$\Sigma_s(\mathbf{r}, E' \rightarrow E, \Omega' \rightarrow \Omega) \equiv$ scattering cross section for transfer from energy E' and direction Ω' to energy E and direction Ω.

$\nu\Sigma_f(E') \equiv$number of neutrons produced per fission times the fission cross section for a neutron of energy E'. (In the laboratory system, fission is isotropic, or having a tendency in all directions.)

$S(\mathbf{r}, E\Omega) \equiv$the time independent source density of neutrons at position r, with energy E, and moving in the direction, Ω.

This equation is a function of six independent variables: Three position coordinates, $\mathbf{r} = \mathbf{r}(x\mathbf{i} + y\mathbf{j} + z\mathbf{k})$ and two angular directions, $\Omega = \Omega(\theta, \phi)$.

Before developing a transport equation for this geometry, let's

review the following:
A spatial derivative is a gradient.
The gradent is a vector normal to the surface at the point at which the gradient is to be evaluated.

The gradient of a scalar function is the result of the application of the del operator;

$$\nabla = \mathbf{i}\frac{\partial}{\partial x} + \mathbf{j}\frac{\partial}{\partial y} + \mathbf{k}\,\frac{\partial}{\partial z},\ \textit{in Cartesian coordinates.}$$

In one dimensional geometry in the z direction only:

$$\mu = \cos(\theta)$$
$$\theta = \cos^{-1}\mu$$
$$d\Omega = -2\pi d\mu$$

In 1-D geometry, the solid angle changes its characteristics:

$$\mathbf{\Omega} = \mathbf{\Omega}(\theta, \phi).$$

For 1-D geometry, the physical process does not depend on ϕ.

$$\mathbf{\Omega} = \Omega_x \mathbf{i} + \Omega_y \mathbf{j} + \Omega_z \mathbf{k}$$

$$\Omega_x = \mathbf{\Omega} \cdot \mathbf{i}$$

$$\Omega_y = \mathbf{\Omega} \cdot \mathbf{j}$$

$$\Omega_z = \mathbf{\Omega} \cdot \mathbf{k} = \mu$$

Which defines

$$\mathbf{\Omega} \cdot \mathbf{k} = \mu$$

By problem selection:

$$\frac{\partial \Psi}{\partial x} = 0$$

$$\frac{\partial \Psi}{\partial y} = 0$$

Therefore:

$$\mathbf{\Omega} \cdot \nabla \Psi = \mathbf{\Omega} \cdot \frac{\partial \Psi}{\partial z} \mathbf{i} = \mathbf{\Omega} \cdot \mathbf{i} \frac{\partial \Psi}{\partial z} = \mu \frac{\partial \Psi}{\partial z}$$

Another helpful tool is Legendre polynomials.
The following in a derivation of Legendre polynomials using a power series solution.

Legendre Functions of Order p are solutions of the differential equations:

$$(1-x^2)\frac{d^2y}{dx^2} - 2x\frac{dy}{dx} + p(p+1)y = 0$$

p is real and nonnegative.

Assume a solution: $y(x) = \sum_{k=0}^{\infty} B_k x^{2k+s}$

$$y' = \sum_{k=0}^{\infty} B_k(2k+s)x^{2k+s-1}$$

$$y'' = \sum_{k=0}^{\infty} B_k(2k+s)(2k+s-1)x^{2k+s-2}$$

Plugging into the orginal equation:

$$\sum_{k=0}^{\infty} B_k(2k+s)(2k+s-1)x^{2k+s-2} - \sum_{k=0}^{\infty} B_k(2k+s)(2k+s-1)x^{2k+s}$$

$$-2\sum_{k=0}^{\infty} B_k(2k+s)x^{2k+s} + p(p+1)\sum_{k=0}^{\infty} B_k x^{2k+s} = 0.$$

Grouping terms:

$$\sum_{k=0}^{\infty} B_k(2k+s)(2k+s-1)x^{2k+s-2}$$

$$+\sum_{k=0}^{\infty} B_k[p(p+1) - 2(2k+s) - (2k+s)(2k+s-1)]x^{2k+s} = 0.$$

Let k=k-1 in the second summation:

$$\sum_{k=0}^{\infty} B_k(2k+s)(2k+s-1)x^{2k+s-2}$$

$$+\sum_{k=1}^{\infty} B_{k-1}[p(p+1)-2(2k+s-2)(2k+s-3)]x^{2k+s-2}=0.$$

Expanding the first summation until the indices are the same, and then combining under one summation yields:

$$B_0(s)(s-1)x^{s-2}+\sum_{k=1}^{\infty}\{B_k(2k+s)(2k+s-1)+$$

$$B_{k-1}[p(p+1)-2(2k+s-2)-(2k+s-2)(2k+s-3)]\}x^{2k+s-2}=0.$$

Considering the terms grouped with B_0;
$B_0 \neq 0$
$x^{s-2} \neq 0$

Then: $(s)(s-1)=0$
The solutions are s=0, and s=1.

From this a recurrence formula can be developed:

$$(2k+s)(2k+s-1)B_k=-B_{k-1}[p(p+1)-2(2k+s-2)-(2k+s-2)(2k+s-3)]$$

$$B_k=-\frac{(p-s-2k+2)(p+s+2k-1)}{(2k+s)(2k+s-1)}B_{k-1}$$

For s=0:

$$B_0(0)=-\frac{(p-2k+2)(p+2k-1)}{2k(2k-1)}B_{k-1}$$

Running out a few terms:

$$B_1(0) = -\frac{(p-2+2)(p+2-1)}{(2)(1)}B_0 = -\frac{p(p+1)}{(2)(1)}B_0.$$

$$B_2(0) = -\frac{(p-2)(p+3)}{(2)(2)(4-1)}B_1 = \frac{(p-2)(p+3)}{(4)(3)}B_1$$

$$= \left[\frac{-p(p+1)}{(2)(1)}B_0\right]\left[\frac{(p-2)(p+3)}{(4)(3)}\right]$$

$$= \frac{p(p+1)(p-2)(p+3)}{(4)(3)(2)(1)}B_0.$$

or

$$B_k(0) = \frac{(-1)^k B_0}{(2k)!}[p(p-2)\cdots(p-2k+2)][(p+1)(p+3)\cdots(p+2k-1)]$$

Now, consider $s=1$:

$$B_k(1) = -\frac{(p-1-2k+2)(p+1+2k-1)}{(2k+1)(2k)}B_{k-1}$$

$$B_k(1) = -\frac{(p-2k+1)(p+2k)}{(2k+1)(2k)}B_{k-1}$$

Therefore:
for $s_1 = 0$

$$y_1 = B_0 \sum_{k=1}^{\infty} B_k(0)x^{2k}$$

and for $s_2 = 1$

$$y_2 = B_0 x + \sum_{k=1}^{\infty} B_k(1)x^{2k+1}$$

So now we have:

$$u_p(x) = 1 - \frac{p(p+1)}{2!}x^2 + \frac{p(p-2)(p+2)(p+3)}{4!}x^4 + \cdots$$

and

$$v_p(x) = x - \frac{(p-1)(p+2)}{3!}x^3 + \frac{(p-1)(p-3)(p+2)(p+4)}{5!}x^5 + \cdots$$

So the general solution of $(1-x^2)\frac{d^2y}{dx^2} - 2x\frac{dy}{dx} + p(p+1)y = 0$ can be written as:

$$y = c_1 u_p(x) + c_2 v_p(x).$$

The following Legendre polynomials are readily found to be:

$$P_0(x) = 1$$
$$P_1(x) = x$$

This will be shown with the following functions:

$P_n(x) = \frac{u_n(x)}{u_n(1)}$ when n is even or equal zero.

$P_n(x) = \frac{v_n(x)}{v_n(1)}$ when n is odd.

Examples:

$$P_0(x) = \frac{u_0(x)}{u_0(1)}.$$

$$u_0(x) = 1 - \frac{(0)(0+1)}{2!}x^2 + \frac{(0)(0-2)(0+2)(0+3)}{4!}x^4 + \cdots$$

$$u_0(1) = 1 - \frac{(0)(0+1)}{2!}(1^2) + \frac{(0)(0-2)(0+2)(0+3)}{4!}(1^4) + \cdots$$

$u_0(x) = 1$
$u_0(1) = 1$
Therefore, $P_0(x) = \frac{1}{1} = 1$.

$$P_1(x) = \frac{v_1(x)}{v_1(C)}$$

$$v_1(x) = x - \frac{(1-1)(1+2)}{3!}(3)^3 + \frac{(1-1)(1-3)(1+2)(1+4)}{5!}x^5 + \cdots$$

$$v_1(1) = 1 - \frac{(1-1)(1+2)}{3!}(1^3) + \frac{(1-1)(1-3)(1+2)(1+4)}{5!}(1^5) + \cdots$$

Therefore $P_1(x) = \frac{x}{1} = x$.

It has been shown that for a 1 dimensional slab, the transport equation,

$$\nabla \cdot \mathbf{\Omega}\Psi(\mathbf{r}, E, \mathbf{\Omega}) + \Sigma_t(\mathbf{r}, E)\Psi(\mathbf{r}, E, \mathbf{\Omega}) =$$

$$S(\mathbf{r}, E, \mathbf{\Omega}) + \int_{\mathbf{\Omega}'} \int_{E'} \Sigma_s(\mathbf{r}, E', \mathbf{\Omega}' \rightarrow E, \mathbf{\Omega})\Psi(\mathbf{r}, E', \mathbf{\Omega}')dE'd\mathbf{\Omega}'$$

$$+ \int_{\mathbf{\Omega}'} \int_{E'} \frac{\chi(E)}{4\pi}\nu\Sigma_f(E')\Psi(\mathbf{r}, E', \mathbf{\Omega}')dE'd\mathbf{\Omega}'$$

Simplifies to:

$$\mu\frac{\partial}{\partial z}\Psi(z, E, \mu) + \Sigma_t(z, E)\Psi(z, E, \mu) =$$

$$S(z, E, \mu) + \int_{\mathbf{\Omega}'} \int_{E'} \Sigma_s(z, \mathbf{\Omega}', E' \rightarrow \mathbf{\Omega}, E)\Psi(z, E', \mu')dE'd\mathbf{\Omega}' +$$

$$\frac{\chi(E)}{4\pi} \int_{\mathbf{\Omega}'} \int_{E'} \nu\Sigma_f(E')\Psi(z, E', \mu')dE'd\mathbf{\Omega}'.$$

We assume that both differential scattering and the flux can be expanded in spherical harmonics.

$$\Psi(z, E', \mu) = \sum_{l=0}^{\infty} \frac{2l+1}{2}\phi_l(z, E')P_l(\mu).$$

Where

$$\phi_l(z, E') = \int_{-1}^{1} \Psi(z, E', \mu)P_l(\mu)d\mu$$

And

$$\Sigma_s(z, E' \rightarrow E, \mathbf{\Omega}' \rightarrow \mathbf{\Omega}) = \sum_{l=0}^{\infty} \frac{2l+1}{4\pi}\Sigma_{sl}(z, E')P_l(\mathbf{\Omega} \cdot \mathbf{\Omega}').$$

$\Omega \cdot \Omega' = \mu_0 \equiv$the cosine of the angle of scatter in the laboratory system.

$$\Sigma_s(z, E' \to E, \Omega' \to \Omega) = \sum_{l=0}^{\infty} \frac{2l+1}{4\pi} \Sigma_{sl}(z, E') P_l(\mu_0).$$

Source:

$$S(z, E, \Omega) = \sum_{l=0}^{\infty} S_l(z, E) \frac{2l+1}{4\pi} P_l(\mu)$$

Plugging in:

$$\mu \frac{\partial}{\partial z} \sum_{l=0}^{\infty} \frac{2l+1}{4\pi} \phi(z, E') P_l(\mu) + \Sigma_t(z, E) \sum_{l=0}^{\infty} \frac{2l+1}{4\pi} \phi(z, E) P_l(\mu)$$

$$= \int_{\Omega'} \int_{E'} 2\pi \sum_{l=0}^{\infty} \frac{2l+1}{4\pi} \Sigma_{sl}(z, E') P_l(\mu_0) \sum_{l=0}^{\infty} \frac{2l+1}{4\pi} \phi_l(z, E) P_l(\mu) dE' d\Omega'$$

$$+ \sum_{l=0}^{\infty} \frac{2l+1}{4\pi} S_l(z, E) P_l(\mu).$$

Note:

$$P_l(\mu_0) \equiv P_l(\Omega \cdot \Omega') = P_l(\mu) P_l(\mu') + 2 \sum_{m=1}^{l} \frac{(l-m)!}{(l+m)!} P_l^m(\mu) P_l^m(\mu') cos[m(\phi - \phi')]$$

And

$$P_l^m(\mu) = (1-\mu^2)^{m/2} \frac{d^m}{d\mu^m} P_l(\mu)$$

The $P_l^m(\mu)$ are called the associated Legendre polynomials.

The transport equation now becomes:

$$\mu\frac{\partial}{\partial z}\sum_{l=0}^{\infty}\frac{2l+1}{4\pi}\phi_l(z,E')P_l(\mu)+\Sigma_t(z,E)\sum_{l=0}^{\infty}\frac{2l+1}{4\pi}\phi_l(z,E)P_l(\mu)=$$

$$\int_{\Omega'}\int_{E'}2\pi\sum_{l=0}^{\infty}\frac{2l+1}{4\pi}\Sigma_{sl}(z,E)\{[P_l(\mu)P_l(\mu')+2\sum_{n=1}^{l}\frac{(l-n)!}{(l+n)!}P_l^n(\mu)P_l^n(\mu')cos[n(\phi-\phi')]\}$$

$$\cdot\sum_{l=0}^{\infty}\frac{2l+1}{4\pi}\phi_l(z,E)P_l(\mu)dE'd\Omega'$$

$$+\int_{\Omega'}\int_{E'}\frac{\chi(E)}{4\pi}\nu\Sigma_f(E')\sum_{n=0}^{\infty}\frac{2n+1}{4\pi}\phi_n(z,E)P_n(\mu)dE'd\Omega'$$

$$+\sum_{l=0}^{\infty}\frac{2l+1}{4\pi}S_l(z,E)P_l(\mu)$$

Separating the above equation into the following terms for easier simplification:

Term 1:

$$\mu\frac{\partial}{\partial z}\sum_{l=0}^{\infty}\frac{2l+1}{4\pi}\phi_l(z,E')P_l(\mu)$$

Term 2:

$$\Sigma_t(z,E)\sum_{l=0}^{\infty}\frac{2l+1}{4\pi}\phi_l(z,E)P_l(\mu)$$

Term 3:

$$\int_{\Omega'}\int_{E'}2\pi\sum_{l=0}^{\infty}\frac{2l+1}{4\pi}\Sigma_{sl}(z,E)\{[P_l(\mu)P_l(\mu')+2\sum_{n=1}^{l}\frac{(l-n)!}{(l+n)!}P_l^n(\mu)P_l^n(\mu')cos[n(\phi-\phi')]\}$$

$$\cdot\sum_{l=0}^{\infty}\frac{2l+1}{4\pi}\phi_l(z,E)P_l(\mu)dE'd\Omega'$$

Term 4:

$$\int_{\Omega'}\int_{E'}\frac{\chi(E)}{4\pi}\nu\Sigma_f(E')\sum_{n=0}^{\infty}\frac{2n+1}{4\pi}\phi_n(z,E)P_n(\mu)dE'd\Omega'$$

Term 5:

$$\sum_{l=0}^{\infty} \frac{2l+1}{4\pi} S_l(z,E) P_l(\mu)$$

Note: $\int_{\Omega'} d\Omega' = \int_{-1}^{1} d\mu' \int_{0}^{2\pi} d\phi'$.

Taking this to simplify term 3:

$$\int_0^{2\pi} cos(\phi - \phi') d\phi' = \int_0^{2\pi} [cos\phi cos\phi' + sin\phi sin\phi'] d\phi'$$

$$= [cos\phi sin\phi' - sin\phi cos\phi' \,|_0^{2\pi}$$

$$= cos\phi\{sin(2\pi) - sin(0)\} - sin\phi\{cos(2\pi) - cos(0)\} = 0.$$

Term 3 now becomes:

$$\int_{E'} \int_{\mu'} 2\pi \sum_{l=0}^{\infty} \frac{2l+1}{4\pi} \Sigma_{sl}(z,E') P_l(\mu') P_l(\mu) \cdot \sum_{n=0}^{\infty} \frac{2n+1}{4\pi} \phi_n(z,E) P_n(\mu') d\mu' dE'.$$

The transport equation now looks like this:

$$\mu\frac{\partial}{\partial z}\sum_{l=0}^{\infty}\frac{2l+1}{4\pi}\phi_l(z,E')P_l(\mu)+\Sigma_t(z,E)\sum_{l=0}^{\infty}\frac{2l+1}{4\pi}\phi_l(z,E)P_l(\mu)=$$

$$\int_{E'}\int_{\mu'}2\pi\sum_{l=0}^{\infty}\frac{2l+1}{4\pi}\Sigma_{sl}(z,E')P_l(\mu')P_l(\mu)\cdot\sum_{n=0}^{\infty}\frac{2n+1}{4\pi}\phi_n(z,E)P_n(\mu')d\mu'dE'$$

$$+\int_{\Omega'}\int_{E'}\frac{\chi(E)}{4\pi}\nu\Sigma_f(E')\sum_{n=0}^{\infty}\frac{2n+1}{4\pi}\phi_n(z,E)P_n(\mu)dE'd\Omega'$$

$$+\sum_{l=0}^{\infty}\frac{2l+1}{4\pi}S_l(z,E)P_l(\mu).$$

Term 4 can be rewritten by using: $\int_{\Omega'}d\Omega'=\int_{-1}^{1}d\mu'\int_{0}^{2\pi}d\phi'$.

$$\int_{E'}\int_{-1}^{1}\int_{0}^{2\pi}\frac{\chi(E)}{4\pi}\nu\Sigma_f(E')\sum_{n=0}^{\infty}\frac{2n+1}{4\pi}\phi_n(z,E')P_n(\mu)d\phi'd\mu'dE'=$$

$$\int_{E'}\frac{\chi(E)}{4\pi}\nu\Sigma_f(E')\sum_{n=0}^{\infty}\frac{2n+1}{4\pi}\phi_n(z,E')P_n(\mu)[2\pi][2]dE'=$$

$$\int_{E'}\frac{\chi(E)}{4\pi}\nu\Sigma_f(E')\sum_{n=0}^{\infty}(2n+1)\phi_n(z,E')P_n(\mu)dE'.$$

Expanding this to only its first summation term, i.e., n=0, and recalling $P_o(\mu)=1$ yields:

$$\int_{E'}\frac{\chi(E)}{4\pi}\nu\Sigma_f(E')[(2)(0)+1]\phi_0(z,E')(1)dE'=$$

$$\int_{E'} \frac{\chi(E)}{4\pi} \nu\Sigma_f(E')\phi_0(z,E')dE'.$$

For term 1 use:

$$(2l+1)\mu P_l(\mu) = (l+1)P_{l+1}(\mu) + lP_{l-1}(\mu)$$
$$\mu P_l(\mu) = \frac{(l+1)P_{l+1}(\mu) + lP_{l-1}(\mu)}{2l+1}$$
$$\mu P_l(\mu) = \frac{(l+1)P_{l+1}(\mu)}{2l+1} + \frac{lP_{l-1}(\mu)}{2l+1}$$

Plugging in:

$$\frac{\partial}{\partial z}\sum_{l=0}^{\infty}\frac{2l+1}{4\pi}\phi_l(z,E)\mu P_l(\mu) =$$
$$\frac{\partial}{\partial z}\sum_{l=0}^{\infty}\frac{2l+1}{4\pi}\phi_l(z,E)\left[\frac{(l+1)P_{l+1}(\mu)}{2l+1} + \frac{lP_{l-1}(\mu)}{2l+1}\right] =$$
$$\sum_{l=0}^{\infty}\frac{1}{4\pi}\frac{\partial}{\partial z}\phi_l(z,E)(l+1)P_{l+1}(\mu) + \sum_{l=0}^{\infty}\frac{1}{4\pi}\frac{\partial}{\partial z}\phi_l(z,E)lP_{l-1}(\mu)$$

.....Let m=l+1.....Let K=l-1....
.....l=m-1.....l=K+1....

$$\frac{1}{4\pi}\sum_{m=1}^{\infty}\frac{\partial}{\partial z}\phi_{m-1}(z,E)(m)P_m(\mu) + \frac{1}{4\pi}\sum_{K=-1}^{\infty}\frac{\partial}{\partial z}\phi_{K+1}(z,E)(K+1)P_K(\mu)$$

Consider just the second summation:

$$\sum_{K=-1}^{\infty} \frac{\partial}{\partial z}\phi_{K+1}(z,E)(K+1)P_K(\mu).$$

Expanding the summation one term:

$$\frac{1}{4\pi}\{\frac{\partial}{\partial z}\phi_{(-1+1)}(z,E)(-1+1)P_{-1}(\mu)+\sum_{K=0}^{\infty}\frac{\partial}{\partial z}\phi_{K+1}(z,E)(K+1)P_K(\mu)\}$$

$$= \frac{1}{4\pi}\{0+\sum_{K=0}^{\infty}\frac{\partial}{\partial z}\phi_{K+1}(z,E)(K+1)P_K(\mu)\}$$

$$= \frac{1}{4\pi}\sum_{K=0}^{\infty}\frac{\partial}{\partial z}\phi_{K+1}(z,E)(K+1)P_K(\mu).$$

Therefore we have:

$$\frac{1}{4\pi}\sum_{m=1}^{\infty}\frac{\partial}{\partial z}\phi_{m-1}(z,E)(m)P_m(\mu)+\frac{1}{4\pi}\sum_{K=0}^{\infty}\frac{\partial}{\partial z}\phi_{K+1}(z,E)(K+1)P_K(\mu).$$

Changing the indices to l yields:

$$\frac{1}{4\pi}\sum_{l=1}^{\infty}\frac{\partial}{\partial z}\phi_{l-1}(z,E)(l)P_l(\mu)+\frac{1}{4\pi}\sum_{l=0}^{\infty}\frac{\partial}{\partial z}\phi_{l+1}(z,E)(l+1)P_l(\mu).$$

Consider the third term (already simplified somewhat):

$$\int_{E'}\int_{\mu'} 2\pi \sum_{l=0}^{\infty} \frac{2l+1}{4\pi} \Sigma_{sl}(z,E') P_l(\mu') P_l(\mu) \cdot \sum_{n=0}^{\infty} \frac{2n+1}{4\pi} \phi_n(z,E') P_n(\mu') d\mu' dE'.$$

By orthogonality:

$$\int_{-1}^{1} P_l(\mu') P_n(\mu') d\mu' = \frac{2}{2l+1} \text{ for } l = n$$

$$\int_{-1}^{1} P_l(\mu') P_n(\mu') d\mu' = 0 \text{ when } l \neq n.$$

Using this, term 3 becomes:

$$\int_{E'} 2\pi \sum_{q=0}^{Q} \frac{2q+1}{4\pi} \cdot \frac{2}{2q+1} \Sigma_{sq}(z,E') P_q(\mu) \cdot \sum_{n=0}^{\infty} \frac{2n+1}{4\pi} \phi_n(z,E') dE'$$

$$= \frac{1}{4\pi} \sum_{n=0}^{\infty} (2n+1) P_n(\mu) \int_{E'} \Sigma_{sn}(z,E') \phi_n(z,E') dE'$$

The transport equation now has this form:

$$\frac{1}{4\pi}\sum_{l=1}^{\infty}\frac{\partial}{\partial z}\phi_{l-1}(z,E)(l)P_l(\mu)+\frac{1}{4\pi}\sum_{l=0}^{\infty}\frac{\partial}{\partial z}\phi_{l+1}(z,E)(l+1)P_l(\mu)$$

$$+\Sigma_t(z,E)\sum_{l=0}^{\infty}\frac{2l+1}{4\pi}\phi_l(z,E)P_l(\mu)$$

$$=\frac{1}{4\pi}\sum_{n=0}^{\infty}(2n+1)P_n(\mu)\int_{E'}\Sigma_{sn}(z,E')\phi_n(z,E')dE'$$

$$\int_{E'}\frac{\chi(E)}{4\pi}\nu\Sigma_f(E')\phi_0(z,E')dE'+\sum_{l=0}^{\infty}\frac{2l+1}{4\pi}S_l(z,E)P_l(\mu).$$

Multipling through by 4π yields:

$$\sum_{l=1}^{\infty}\frac{\partial}{\partial z}\phi_{l-1}(z,E)(l)P_l(\mu)+\sum_{l=0}^{\infty}\frac{\partial}{\partial z}\phi_{l+1}(z,E)(l+1)P_l(\mu)$$

$$+\Sigma_t(z,E)\sum_{l=0}^{\infty}(2l+1)\phi_l(z,E)P_l(\mu)$$

$$=\sum_{n=0}^{\infty}(2n+1)P_n(\mu)\int_{E'}\Sigma_{sn}(z,E')\phi_n(z,E')dE'$$

$$\int_{E'}\chi(E)\nu\Sigma_f(E')\phi_0(z,E')dE'+\sum_{l=0}^{\infty}(2l+1)S_l(z,E)P_l(\mu).$$

This is still an exact equation.

To show the development of P_n equations, the following example is presented.
First, we use orthogonality as before:

$$\int_{-1}^{1} P_l(\mu')P_n(\mu')d\mu' = \frac{2}{2l+1} \; for \; l = n$$

$$\int_{-1}^{1} P_l(\mu')P_n(\mu')d\mu' = 0 \; when \; l \neq n.$$

Next, multiply the transport equation by $P_0(\mu)$ and integrate.
This will cause the first summation term to go to zero:

$$\sum_{l=1}^{\infty} l\frac{\partial}{\partial z}\phi_{l-1}(z,E)\int_{-1}^{1} P_l(\mu)P_0(\mu)d\mu = 0.$$

This happened because the summation began at 1, therefore, there was never a P_0 term, and by orthogonality, the other integrated terms yielded zero.

Consider the second summation term:

$$\sum_{l=0}^{\infty}(l+1)\frac{\partial}{\partial z}\phi_{l+1}(z,E)\int_{-1}^{1} P_l(\mu)P_0(\mu)d\mu$$

$$= 2\frac{\partial}{\partial z}\phi_1(z,E) \; for \; l = 0,$$

$$= 0 \; for \; all \; other \; terms.$$

Now the Σ_t term:

$$\int_{-1}^{1} \Sigma_t(z,E) \sum_{l=0}^{\infty} (2l+1)\phi_l(z,E)P_l(\mu)P_0(\mu)d\mu$$

$$= 2\Sigma_t(z,E)\phi_0(z,E) \; for \; l = 0,$$

$$= 0 \; for \; all \; other \; terms.$$

The Σ_{sn} term:

$$\int_{-1}^{1} \sum_{n=0}^{Q} (2n+1)P_n(\mu)P_0(\mu) \int_{E'} \Sigma_{sn}(z,E')\phi_n(z,E')dE'd\mu$$

$$= 2\int_{E'} \Sigma_{s0}(z,E)\phi_0(z,E')dE' \; for \; n = 0,$$

$$= 0 \; for \; all \; other \; terms.$$

Now the $\chi(E)$ term:

$$\int_{-1}^{1} \chi(E) \int_{E'} \nu\Sigma_f(E')\phi_0(z,E')dE' \cdot P_0(\mu)d\mu$$

Recall $P_0(\mu) = 1$, then

$$\int_{-1}^{1} \chi(E) \int_{E'} \nu\Sigma_f(E')\phi_0(z,E')dE'd\mu =$$

$$\chi(E) \int_{E'} \nu\Sigma_f(E')\phi_0(z,E')dE'[1 - (-1)] =$$

$$2\chi(E)\int_{E'}\nu\Sigma_f(E')\phi_0(z,E')dE'$$

Finally, the source term:

$$\int_{-1}^{1}\sum_{l=0}^{\infty}(2l+1)S_l(z,E)P_l(\mu)P_0(\mu)d\mu$$

$$= 2S_0(z,E) \ for \ l=0,$$

$$= 0 \ for \ all \ other \ terms.$$

Dividing through by 2 yields:

$$\frac{\partial}{\partial z}\phi_1(z,E)+\Sigma_t(z,E)\phi_0(z,E) =$$

$$\int_{E'}\Sigma_{s0}(z,E'\rightarrow E)\phi_0(z,E)dE'$$

$$+\chi(E)\int_{E'}\nu\Sigma_f(E')\phi_0(z,E')dE'+S_0(z,E)$$

This process can be continued by multiplying by $P_1(\mu)$ and integrating, and by $P_2(\mu)$ and integrating, etc., until a $P_n(\mu)$ set of equations is obtained.

APPENDIX F

SHIELD VOLUME DATA

Sample input files for the Be/B_4C shield and the W/B_4C shield.

B_4C density	Be density	Cone half angle	Core radius	Core length	Gamma shield position	Gamma shield thickness	Core and shield thickness where the radiation limits are satisfied
2.520	1.848	17.0	27.5	62.25	0.0	1.0	98.414
2.520	1.848	17.0	27.5	62.25	10.0	1.0	97.879
2.520	1.848	17.0	27.5	62.25	20.0	1.0	97.879
2.520	1.848	17.0	27.5	62.25	30.0	1.0	97.879
2.520	1.848	17.0	27.5	62.25	40.0	1.0	97.879
2.520	1.848	17.0	27.5	62.25	50.0	1.0	97.879
2.520	1.848	17.0	27.5	62.25	60.0	1.0	97.879

	W density						
2.520	19.3	17.0	27.5	62.25	0.0	1.0	93.596
2.520	19.3	17.0	27.5	62.25	10.0	1.0	89.848
2.520	19.3	17.0	27.5	62.25	20.0	1.0	89.848
2.520	19.3	17.0	27.5	62.25	30.0	1.0	92.525

Shields with no gamma attenuator:

Boron Carbide Shield with no gamma shield
The volume of the neutron shield is: 286032.00 cc.
The total mass of the shield is: 720.80 kg.

LiH Shield with Tungsten at 80.00 cm.
The volume of the neutron shield is: 1097378.94 cc.
The total mass of the shield is: 850.47 kg.

LiH Shield with Tungsten at 10.00 cm.

The volume of the neutron shield is:	639202.69	cc.
The volume of the gamma shield is:	7341.56	cc.
The mass of the neutron shield is:	495.38	kg.
The mass of the gamma shield is:	141.69	kg.
The total mass of the shield is:	637.07	kg.

LiH Shield with Tungsten at 20.00 cm.

The volume of the neutron shield is:	589760.94	cc.
The volume of the gamma shield is:	8248.47	cc.
The mass of the neutron shield is:	457.06	kg.
The mass of the gamma shield is:	159.20	kg.
The total mass of the shield is:	616.26	kg.

LiH Shield with Tungsten at 30.00 cm.

The volume of the neutron shield is:	535133.19	cc.
The volume of the gamma shield is:	9209.19	cc.
The mass of the neutron shield is:	414.73	kg.
The mass of the gamma shield is:	177.74	kg.
The total mass of the shield is:	592.47	kg.

LiH Shield with Tungsten at 40.00 cm.

The volume of the neutron shield is:	427184.38	cc.
The volume of the gamma shield is:	10223.84	cc.
The mass of the neutron shield is:	331.07	kg.
The mass of the gamma shield is:	197.32	kg.
The total mass of the shield is:	528.39	kg.

LiH Shield with Tungsten at 50.00 cm.

The volume of the neutron shield is:	438212.34	cc.
The volume of the gamma shield is:	11292.16	cc.
The mass of the neutron shield is:	339.61	kg.
The mass of the gamma shield is:	217.94	kg.
The total mass of the shield is:	557.55	kg.

LiH Shield with Tungsten at 60.00 cm.

The volume of the neutron shield is:	554436.81	cc.
The volume of the gamma shield is:	9797.90	cc.
The mass of the neutron shield is:	429.69	kg.
The mass of the gamma shield is:	189.10	kg.
The total mass of the shield is:	618.79	kg.

LiH Shield with Tungsten at 40.00 cm with 0.5 cm of Tungsten.

The volume of the neutron shield is:	559135.75 cc.
The volume of the gamma shield is:	5098.85 cc.
The mass of the neutron shield is:	433.33 kg.
The mass of the gamma shield is:	98.41 kg.
The total mass of the shield is:	531.74 kg.

LiH Shield with Tungsten at 40.00 cm with 1.0 cm of Tungsten.

The volume of the neutron shield is:	427184.38 cc.
The volume of the gamma shield is:	10223.84 cc.
The mass of the neutron shield is:	331.07 kg.
The mass of the gamma shield is:	197.32 kg.
The total mass of the shield is:	528.39 kg.

LiH Shield with Tungsten at 40.00 cm with 1.5 cm of Tungsten.

The volume of the neutron shield is:	329714.47 cc.
The volume of the gamma shield is:	15374.82 cc.
The mass of the neutron shield is:	255.53 kg.
The mass of the gamma shield is:	296.73 kg.
The total mass of the shield is:	552.26 kg.

LiH Shield with Tungsten at 40.00 cm with 1.52 cm of Tungsten.

The volume of the neutron shield is:	329507.72 cc.
The volume of the gamma shield is:	15581.50 cc.
The mass of the neutron shield is:	255.37 kg.
The mass of the gamma shield is:	300.72 kg.
The total mass of the shield is:	556.09 kg.

Boron Carbide Shield with Tungsten at 0.00 cm.

The volume of the neutron shield is:	238824.92	cc.
The volume of the gamma shield is:	6488.73	cc.
The mass of the neutron shield is:	601.84	kg.
The mass of the gamma shield is:	125.23	kg.
The total mass of the shield is:	727.07	kg.

Boron Carbide Shield with Tungsten at 10.00 cm.

The volume of the neutron shield i	203834.44	cc.
The volume of the gamma shield is:	7341.56	cc.
The mass of the neutron shield is:	513.66	kg.
The mass of the gamma shield is:	141.69	kg.
The total mass of the shield is:	655.35	kg.

Boron Carbide Shield with Tungsten at 20.00 cm.

The volume of the neutron shield is:	202927.59	cc.
The volume of the gamma shield is:	8248.47	cc.
The mass of the neutron shield is:	511.38	kg.
The mass of the gamma shield is:	159.20	kg.
The total mass of the shield is:	670.57	kg.

Boron Carbide Shield with Tungsten at 30.00 cm.

The volume of the neutron shield is:	232917.03	cc.
The volume of the gamma shield is:	2568.54	cc.
The mass of the neutron shield is:	586.95	kg.
The mass of the gamma shield is:	49.57	kg.
The total mass of the shield is:	636.52	kg.

Boron Carbide Shield with Be at 0.00 cm.

The volume of the neutron shield is:	284759.59	cc.
The volume of the gamma shield is:	6488.73	cc.
The mass of the neutron shield is:	717.59	kg.
The mass of the gamma shield is:	11.99	kg.
The total mass of the shield is:	729.59	kg.

Boron Carbide Shield with Be at 10.00 cm.

The volume of the neutron shield is:	278690.44	cc.
The volume of the gamma shield is:	7341.56	cc.
The mass of the neutron shield is:	702.30	kg.
The mass of the gamma shield is:	13.57	kg.
The total mass of the shield is:	715.87	kg.

Boron Carbide Shield with Be at 20.00 cm.

The volume of the neutron shield is:	277783.56	cc.
The volume of the gamma shield is:	8248.47	cc.
The mass of the neutron shield is:	700.01	kg.
The mass of the gamma shield is:	15.24	kg.
The total mass of the shield is:	715.26	kg.

Boron Carbide Shield with Be at 30.00 cm.

The volume of the neutron shield is:	276822.91	cc.
The volume of the gamma shield is:	9209.19	cc.
The mass of the neutron shield is:	697.59	kg.
The mass of the gamma shield is:	17.02	kg.
The total mass of the shield is:	714.61	kg.

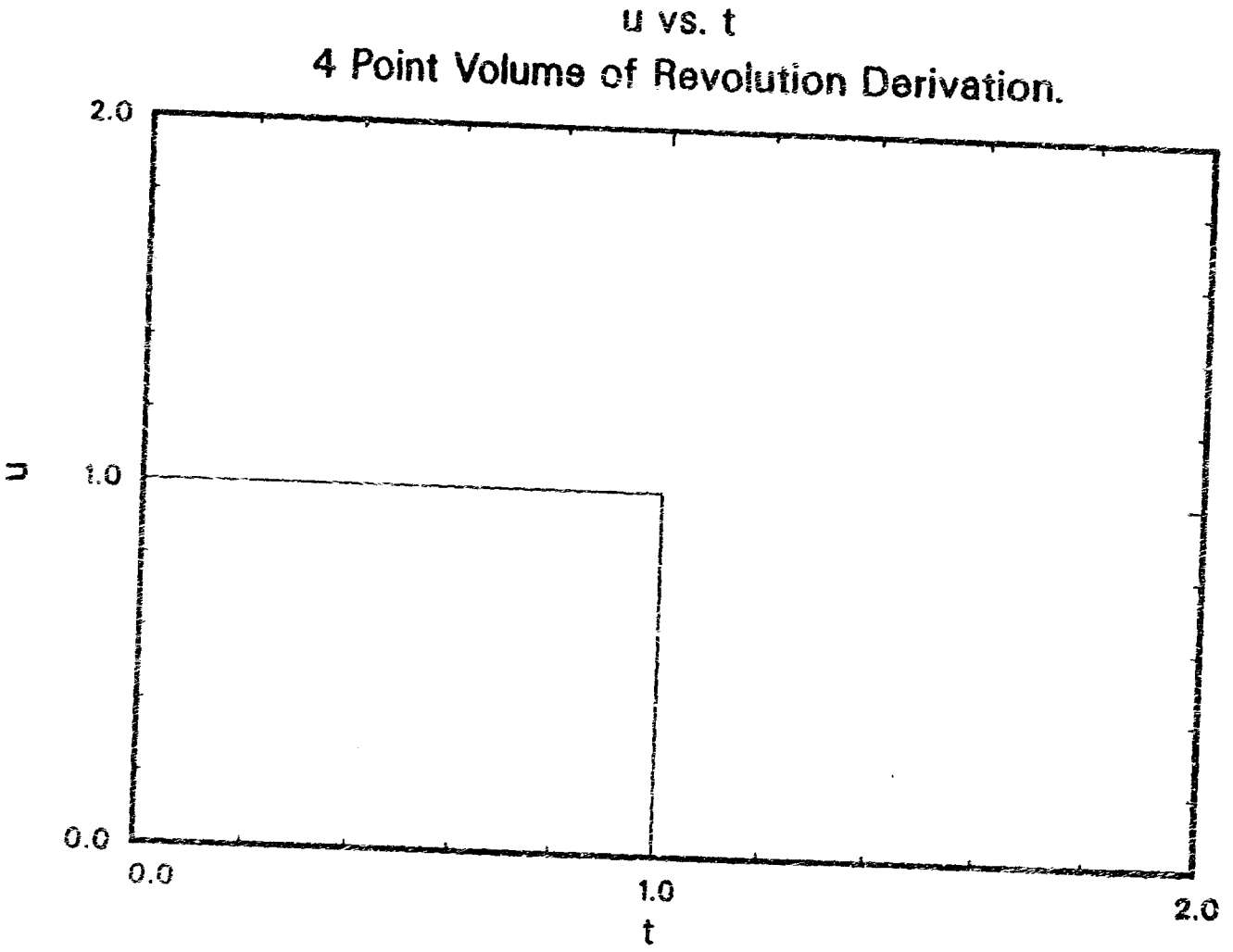
u vs. t
4 Point Volume of Revolution Derivation.
2.0
1.0
0.0
u
0.0
1.0
2.0
t

Derivation of the volume of revolution technique.

$$x = a_x + b_x t + c_x u + d_x tu$$
$$y = a_y + b_y t + c_y u + d_y tu$$
$$u_2 = u_1 = 0;\ u_3 = u_4 = 1$$
$$t_1 = t_2 = 0;\ t_2 = t_4 = 1$$

$x_1 = a_x$
$y_1 = a_y$

$x_2 = a_x + b_x \Rightarrow b_x = x_2 - x_1$
$y_2 = a_y + b_y \Rightarrow b_y = y_2 - y_1$

$x_3 = a_x + c_x \Rightarrow c_x = x_3 - x_1$
$y_3 = a_x + c_y \Rightarrow c_y = y_3 - y_1.$

$x_4 = a_x + b_x + c_x + d_x \Rightarrow dx = x_4 + x_1 - x_2 - x_3$
$y_4 = a_y + b_y + c_y + d_y \Rightarrow dy = y_4 + y_1 - y_2 - y_3.$

Substituting:

$$x = x_1 + (x_2 - x_1)t + (x_3 - x_1)u + (x_4 + x_1 - x_2 - x_3)tu$$

$$y = y_1 + (y_2 - y_1)t + (y_3 - y_1)u + (y_4 + y_1 - y_2 - y_3)tu.$$

$$\frac{\partial x}{\partial t} = (x_2 - x_1) + (x_4 + x_1 + x_2 - x_3)u$$

$$\frac{\partial x}{\partial u} = (x_3 - x_1) + (x_4 + x_1 - x_2 - x_3)t$$

$$\frac{\partial y}{\partial t} = (y_2 - y_1) + (y_4 + y_1 - y_2 - y_3)u$$

$$\frac{\partial y}{\partial u} = (y_3 - y_1) + (y_4 + y_1 - y_2 - y_3)t$$

Let: $\alpha_{xt} = x_2 - x_1$, $\alpha_{xu} = x_3 - x_1$, $B_x = x_4 + x_1 - x_2 - x_3$.
$\alpha_{yt} = y_2 - y_1$, $\alpha_{yu} = x_3 - x_1$, $B_y = y_4 + y_1 - y_2 - y_3$.

Substituting bach into the partials yields:

$$\frac{\partial x}{\partial t} = \alpha_{xt} + B_x u$$

$$\frac{\partial y}{\partial t} = \alpha_{yt} + B_y u$$

$$\frac{\partial x}{\partial u} = \alpha_{xu} + B_x t$$

$$\frac{\partial y}{\partial u} = \alpha_{yu} + B_y t.$$

$$v = 2\pi \int_0^1 \int_0^1 [x_1+(x_2-x_1)t+(x_3-x_1)u+(x_4+x_1-x_2-x_3)ut] J\left(\frac{x,y}{t,u}\right) dtdu.$$

$$J\left(\frac{x,y}{t,u}\right) = \frac{\partial(x,y)}{\partial(u,t)} \equiv \begin{vmatrix} \frac{\partial x}{\partial t} & \frac{\partial x}{\partial u} \\ \frac{\partial y}{\partial t} & \frac{\partial y}{\partial u} \end{vmatrix} = \frac{\partial x}{\partial t} \cdot \frac{\partial y}{\partial u} - \frac{\partial x}{\partial u} \cdot \frac{\partial y}{\partial t}$$

$$= (\alpha_{xt} + B_x u)(\alpha_{yu} + B_y t) - (\alpha_{xt} + B_x t)(\alpha_{yt} + B_y u).$$

$$V = 2\pi \int_0^1 \int_0^1 (x_1 + \alpha_{xt} t + \alpha_{xu} u + B_x t u)$$

$$[(\alpha xt + B_x u)(\alpha_{yu} + B_y t) - (\alpha_{xu} + B_x t)(\alpha_{yt} + B_y u)] dtdu$$

$$V = 2\pi \left| \int_0^1 \int_0^1 [(x_1 + \alpha_{xu} u + B_x t u) \right.$$

$$\left. \{(\alpha_{xt}\alpha_{yu} - \alpha_{xu}\alpha_{yt}) + (\alpha_{xt} B_y - \alpha_{yt} B_x)t + (\alpha_{yu} B_x - \alpha_{xu} B_y)u\}] dtdu \right|$$

Let:

$a = \alpha_{xt}\alpha_{yu} - \alpha_{xu}\alpha_{yt}$

$$b = \alpha_{xt}B_y - \alpha_{yt}B_x$$
$$c = \alpha_{yu}B_x - \alpha_{xu}B_y$$

$$V = 2\pi \left| \int_0^1 \int_0^1 (ax_1 + bx_1 t + cx_1 u + a\alpha_{xt} + b\alpha_{xt}t^2 + c\alpha_{xt}tu + a\alpha_{xu}u + b\alpha_{xu}tu + c\alpha_{xu}u^2 + ab_x tu + bB_x t^2 u + cB_x tu^2)dtdu \right|$$

$$V = 2\pi \left| (ax_1 + \frac{bx_1}{2} + \frac{cx_1}{2} + \frac{a\alpha_{xt}}{2} + \frac{b\alpha_{xt}}{3} + \frac{c\alpha_{xt}}{4} + \frac{a\alpha_{xu}}{2} + \frac{b\alpha_{xu}}{4} + \frac{c\alpha_{xu}}{3} + \frac{aB_x}{4} + \frac{bB_x}{6} + \frac{cB_x}{6}) \right|$$

$$V = \frac{\pi}{6} |(12a + 6[b + c])x_1 + (6a + 4b + 3c)\alpha_{xt} + (6a + 3b + 4c)\alpha_{xu} + (3a + 2[b + c]B_x|$$

Or finally,

$$V = \frac{\pi}{6} |3(4x_1 + 2[\alpha_{xt} + \alpha_{xu}] + B_x)a + (6x_1 + 4\alpha_{xt} + 3\alpha_{xu} + 2B_x)b + (6x_1 + 3\alpha_{xt} + 4\alpha_{xu} + 2B_x)c|$$

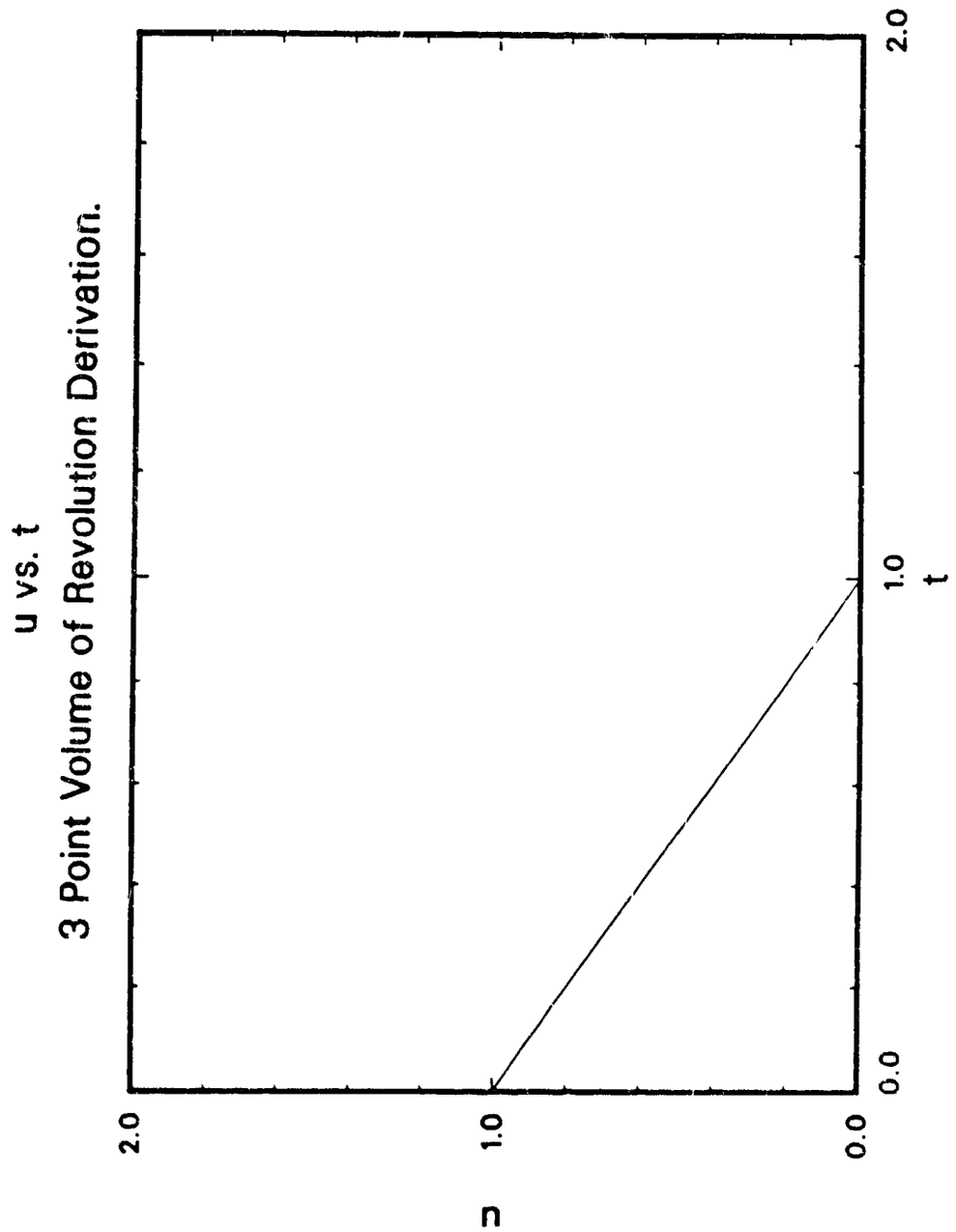
u vs. t
3 Point Volume of Revolution Derivation.
2.0
1.0
0.0
u
2.0
1.0
0.0
t

Much the same is done for a triangle.

$$x = a_x + b_x t + c_x u$$
$$y = a_y + b_y t + c_y u$$
$$u_1 = u_2 = 0;\ u_3 = 1$$
$$t_1 = t_3 - 0;\ t_2 = 1$$

$$x_1 = a_x$$
$$y_1 = a_y$$
$$x_2 = a_x + b_x \Rightarrow b_x = x_2 - x_1$$
$$y_2 = a_y + b_y \Rightarrow b_y = y_2 - y_1$$
$$x_3 = a_x + c_x \Rightarrow c_x = x_3 - x_1$$
$$y_3 = a_y + c_y \Rightarrow c_y = y_3 - y_1$$

$$x = x_1 + (x_2 - x_1)t + (x_3 - x_1)u$$
$$y = y_1 + (y_2 - y_1)t + (y_3 - y_1)u$$

$$\frac{\partial x}{\partial t} = (x_2 - x_1) = \alpha_{xt};\ \frac{\partial y}{\partial t} = (y_2 - y_1) = \alpha_{yt}$$

$$\frac{\partial x}{\partial u} = (x_3 - x_1) = \alpha_{xu};\ \frac{\partial y}{\partial u} = (y_3 - y_1) = \alpha_{yu}$$

$$V = 2\pi \left| \int_0^1 du \int_0^{1-u} dt (x_1 + \alpha_{xt} t + \alpha_{xu} u)(\alpha_{xt}\alpha_{yu} - \alpha_{xu}\alpha_{yt}) \right|$$

$$V = 2\pi \left| (\alpha_{xt}\alpha_{yu} - \alpha_{xu}\alpha_{yt}) \int_0^1 du([1-u]x_1 + [1-u]\alpha_{xu} u + \frac{\alpha_{xt}}{2}[1-u]^2) \right|$$

$$V = 2\pi \left| (\alpha_{xt}\alpha_{yu} - \alpha_{xu}\alpha_{yt}) \int_0^1 (x_1 - x_1 u + \alpha_{xu} u - \alpha_{xu} u^2 + \frac{\alpha_{xt}}{2} - \alpha_{xt} u + \frac{\alpha_{xt}}{2} u^2) du \right|$$

$$V = 2\pi \left| (\alpha_{xt}\alpha_{yu} - \alpha_{xu}\alpha_{yt})(x_1 - \frac{x_1}{2} + \frac{\alpha_{xu}}{2} - \frac{\alpha_{xu}}{3} + \frac{\alpha_{xt}}{2} - \frac{\alpha_{xt}}{2} + \frac{\alpha xt}{6}) \right|$$

$$V = \frac{\pi}{3} |(\alpha_{xt}\alpha_{yu} - \alpha_{xu}\alpha_{yt})(3x_1 + \alpha_{xu} + \alpha_{xt})|$$

$$V = \frac{\pi}{3} |([x_2 - x_1][y_3 - y_1] - [x_3 - x_1][y_2 - y_1])(3x_1 + x_2 + x_3 - 2x_1)|$$

Finally, the volume for a triangle is:

$$V = \frac{\pi}{3} |(x_1 + x_2 + x_3)[(x_2 - x_1)(y_3 - y_1) - (x_3 - x_1)(y_2 - y_1)]|$$

```
      PROGRAM SHIELD VOLUME

      REAL MNEUT,MGAM
      PI=3.141592654
      OPEN(UNIT=10, FILE='SHDAT.DAT', STATUS='OLD')
      OPEN(UNIT=11, FILE='SHDAT.OUT', STATUS='NEW')

C  Input file is SHDAT.DAT
C
C  Input the half angle in degrees.
C  The program will convert it to radians.
C

      COUNT =0.0
      WRITE(11,75)
      WRITE(11,100)
      WRITE(11,100)

10    IF(COUNT.EQ.6.0) THEN
        COUNT=0.0
        WRITE(11,75)
        WRITE(11,100)
        WRITE(11,100)
        ELSE
      END IF

      READ(10,*,END=999)DEN1,DEN2,ANG,CRAD,
     &CLEN,XGAM,TGAM,XMAX
      WRITE(11,1000)XGAM

      ANG=(ANG*PI)/180.0
      P=CRAD/TAN(ANG)
      PNOT=P+CLEN

      PX1=PNOT
      PY1=CRAD

      PX2=PX1+XGAM
      PY2=CRAD

      PX5=PX2+TGAM
      PY5=CRAD

      PX7=XMAX+P
      PY7=CRAD

      R1=SQRT(PX1**2+PY1**2)
      R2=SQRT(PX2**2+PY2**2)
      R3=SQRT(PX5**2+PY5**2)
      R4=SQRT(PX7**2+PY7**2)
```

```
      PX3=R1*COS(ANG)
      PY3=R1*SIN(ANG)

      PX4=R2*COS(ANG)
      PY4=R2*SIN(ANG)

      PX6=R3*COS(ANG)
      PY6=R3*SIN(ANG)

      PX8=R4*COS(ANG)
      PY8=R4*SIN(ANG)


      V1=PI*CRAD**2*(PX2-PX1)
      V2=PI*CRAD**2*(PX5-PX2)
      V3=PI*CRAD**2*(PX7-PX5)


      CALL VOL1(PX1,PY1,PX2,PY2,PX3,PY3,PX4,PY4,V4)
      CALL VOL1(PX2,PY2,PX5,PY5,PX4,PY4,PX6,PY6,V5)
      CALL VOL1(PX5,PY5,PX7,PY7,PX6,PY6,PX8,PY8,V6)

      VNEUT=V1+V3+V4+V6
      VGAM =V2+V5

      MNEUT=VNEUT*DEN1*1.0E-3
      MGAM =VGAM *DEN2*1.0E-3
      TMASS=MNEUT+MGAM

      WRITE(11,105)VNEUT
      WRITE(11,110)VGAM
      WRITE(11,115)MNEUT
      WRITE(11,120)MGAM
      WRITE(11,125)TMASS
      WRITE(11,130)

      COUNT=COUNT+1.0
      GO TO 10

1000  FORMAT('0',10X,'LiH Shield
     &with Tungsten at ',F5.2,' cm.')
25    FORMAT( G12.4)
75    FORMAT('1')
100   FORMAT('0')
105   FORMAT(' ',12X,'The volume of the neutron
     &shield is: ',F10.2,' cc.')
```

```
110     FORMAT(' ',12X,'The volume of the gamma
     &shield is:   ',F10.2,' cc.')
115     FORMAT(' ',12X,'The mass of the neutron
     &shield is:   ',F10.2,' kg.')
120     FORMAT(' ',12X,'The mass of the gamma
     &shield is:     ',F10.2,' kg.')
125     FORMAT(' ',12X,'The total mass of the shield is:
     &     ',F10.2,' kg.')
130     FORMAT(' ',' ')
999     PRINT*,' The output file is called "SHDAT.OUT".'

        STOP
        END

        SUBROUTINE VOL1(Y1,X1,Y2,X2,Y3,X3,Y4,X4,V)

C  This subroutine calculates the volume of a
C  rotated rectangle.

        PI=3.141592654

        AXT=X2-X1
        AXU=X3-X1
        BX=X4+X1-X2-X3

        AYT=Y2-Y1
        AYU=Y3-Y1
        BY=Y4+Y1-Y2-Y3

        A=AXT*AYU-AXU*AYT
        B=AXT*BY-AYT*BX
        C=AYU*BX-AXU*BY

        V=(PI/6.0)*ABS(3.0*(4.0*X1+2.0*(AXT+AXU)+BX)
     &*A+(6.0*X1+4.0*AXT+3.0*AXU+2.0*BX)*B+(6.0*X1+3.0
     &*AXT+4.0*AXU+2.0*BX)*C)

        RETURN
        END

        SUBROUTINE VOL2(Y1,X1,Y2,X2,Y3,X3,V)

C  This subroutine calculates a volume of a rotated triangle.

        PI=3.141592654

        V=(PI/3.0)*ABS((X1+X2+X3)*((X2-X1)*(Y3-Y1)-
     &(X3-X1)*(Y3-Y1)))

        RETURN
        END
```

APPENDIX G

RFCC DATA

The following is two input files for RFCC to calculate neutron flux to dose conversion factors, and gamma dose rate conversion factors for human tissue. The outputs of these runs are put in the sample FEMP1D input file provided in this Appendix in the 35** array as stipulated in the 1$$ array for input variable, NRF.

RFCC neutron input:

```
1
1 9 16
1.733E+7 6.065E+6 3.011E+6 1.920E+6 1.002E+6 6.081E+5
2.972E+5 1.831E+5 1.110E+5 4.086E+4 2.187E+4 7.101E+3
3.354E+3 1.584E+3 3.726E+1 1.000E-1 1.000E-5
 0 0 0
```

RFCC gamma input:

```
1
1 10 8
1.4+7 4.0+6 2.0+6 1.0+6 4.0+5
2.0+5 1.0+5 6.0+4 1.0+4
 0 0 0
```

Neutron RFCC output:

MULTIGROUP REP. OF THE NEUTRON FLUX
TO DOSE EQUIVALENCE RATE CONVERSION FACTOR

GROUP	UPPER E BOUND (EV)	LOWER E BOUND (EV)
1	1.73300E-07	6.06500E+06
2	6.06500E+06	3.01100E+06
3	3.01100E+06	1.92000E+06
4	1.92000E+06	1.00200E+06
5	1.00200E+06	6.08100E+05
6	6.08100E+05	2.97200E+05
7	2.97200E+05	1.83100E+05
8	1.83100E+05	1.11000E+05
9	1.11000E+05	4.08600E+04
10	4.08600E+04	2.18700E+04
11	2.18700E+04	7.10100E+03
12	7.10100E+03	3.35400E+03
13	3.35400E+03	1.58400E+03
14	1.58400E+03	3.72600E+01
15	3.72600E+01	1.00000E-01
16	1.00000E-01	1.00000E-05

REM/HR/(N/SEC-CM**2)
(GROUP AVERAGE)

1.779579E-04
1.480736E-04
1.273286E-04
1.289578E-04
1.175837E-04
8.307393E-05
4.780253E-05
3.073550E-05
1.741842E-05
8.706003E-06
4.805043E-06
3.608882E-06
3.675812E-06
3.845325E-06
4.405964E-06
3.675043E-06

Gamma RFCC output:

MULTIGROUP REP. OF THE GAMMA FLUX
TO DOSE RATE CONVERSION FACTOR

GROUP	UPPER E BOUND (EV)	LOWER E BOUND (EV)
1	1.40000E+07	4.00000E+06
2	4.00000E+06	2.00000E+06
3	2.00000E+06	1.00000E+06
4	1.00000E+06	4.00000E+05
5	4.00000E+05	2.00000E+05
6	2.00000E+05	1.00000E+05
7	1.00000E+05	6.00000E+04
8	6.00000E+04	1.00000E+04

REM/HR/(PHOTON/SEC-CM**2)
(GROUP AVERAGE)

8.783468E-06
4.167297E-06
2.620405E-06
1.510685E-06
7.532709E-07
3.860888E-07
2.692778E-07
4.511449E-07

RFCC MANUAL; 20 FEBRUARY 1987.

PROGRAM RFC

TAPE MANAGEMENT INFORMATION

NT5=TAPE5,INPUT

NT6=TAPE6,OUTPUT

NT7=TAPE7,PUNCH

NT10=TAPE10,INPUT MACKLIB IN BCD FORMAT

NT15=TAPE15,INPUT/OUTPUT MACKLIB IN
BINARY FORMAT

INPUT DATA

FORMAT-FREE INPUT

IRFC=0, CROSS SECTION MIXING MODE ONLY
=1, MULTIGROUP RESPONSE FUNCTION
GENERATION MODE ONLY
=2, BOTH MODES TO BE USED

PROVIDE ICASE,IMG,NG,AND ER (AND POSSIBLY EBB)
ONLY IF IRFC EQUALS

ICASE= RESPONSE FUNCTION CASE NUMBER

IMG= ID OF RESPONSE FUNCTION THAT IS TO BE PUT
IN MULTIGROUP FORM
=1, WATT FISSION SPECTRUM (INTEGRAL RESPONSE)
=2, 1/E NEUTRON SPECTRUM (INTEGRAL RESPONSE)
[GROUP ENERGIES: .00001 EV - 20 MEV]
=3, THERMAL MAXWELLIAN SPECTRUM (INTEGRAL RESPONSE)
=4, MAXWELLIAN FISSION SPECTRUM (INTEGRAL RESPONSE)
=5, LOS ALAMOS FISSION SPECTRUM, 1982
(INTEGRAL RESPONSE)
=6, VITAMIN C NEUTRON SPECTRUM (INTEGRAL RESPONSE)
[GROUP ENERGIES: .00001 EV - 20 MEV]
=7, CSRL NEUTRON SPECTRUM (INTEGRAL RESPONSE)
[GROUP ENERGIES: .00001 EV - 20 MEV]
=8, NEUTRON QUALITY FACTOR (AVERAGE RESPONSE)
[GROUP ENERGIES SHOULD BE LESS THAN OR
EQUAL TO 20 MEV]
=9, NEUTRON FLUX-TO-DOSE EQUIVALENCE RATE
CONVERSION FACTOR (AVERAGE RESPONSE)
[GROUP ENERGIES SHOULD BE LESS THAN
OR EQUAL TO 20 MEV]

=10, GAMMA RAY FLUX-TO-DOSE RATE CONVERSION FACTOR
(AVERAGE RESPONSE)
[GROUP ENERGIES: .03 MEV - 15 MEV]
=11, ELECTRON FLUX-TO-DOSE RATE CONVERSION FACTOR
(AVERAGE RESPONSE)
[GROUP ENERGIES: .1 MEV - 10000 MEV]
=12, BLACK BODY SPECTRUM (INTEGRAL RESPONSE)
=13, ENERGY RELEASED BLACK BODY SPECTRUM
(INTEGRAL RESPONSE)
=14, SILICON DISPLACEMENT DAMAGE (AVERAGE RESPONSE)
[NEUTRON GROUP ENERGIES: 1.7 KEV - 17 MEV]
=15, SILICON IONIZATION ENERGY DEPOSITION
(AVERAGE RESPONSE) [NEUTRON GROUP ENERGIES:
1.7 KEV - 17 MEV]
=16, CALCIUM FLUORIDE DISPLACEMENT DAMAGE
(AVERAGE RESPONSE)
[NEUTRON GROUP ENERGIES: 1.7 KEV - 17 MEV]
=17, CALCIUM FLUORIDE IONIZATION ENERGY DEPOSITION
(AVERAGE RESPONSE)
[NEUTRON GROUP ENERGIES: 1.7 KEV - 17 MEV]
=18, ANSI STANDARD SILICON DISPLACEMENT DAMAGE
(AVERAGE RESPONSE)
[NEUTRON GROUP ENERGIES: 0 - 18.25 MEV]
=19, PHOTON ENERGY DEPOSITION IN SILICON
(AVERAGE RESPONSE)
[GROUP ENERGIES: 1 KEV - 100 MEV]
=20, PHOTON ENERGY DEPOSITION IN GOLD
(AVERAGE RESPONSE)
[GROUP ENERGIES: 1 KEV - 100 MEV]
=21, DELAY NEUTRON SPECTRUM (EBAR=0.40)

NG= NUMBER OF ENERGY GROUPS IN THE MULTIGROUP
FORMULATION

ER(NG+1)= ENERGY BOUNDS FOR THE NG ENERGY GROUPS,
STARTING WITH THE MAXIMUM ENERGY

EBB= BLACK BODY ENERGY (INPUT ONLY IF IMG= 12 OR 13)

CONTINUE WITH AS MANY SETS OF ICASE,IMG,NG, AND ER
(AND EBB) AS DES AT THE END OF THIS PART OF THE DATA
SET, INSERT 0 0 0 (ICASE=IMG=NG THIS WILL BRING THE
RESPONSE FUNCTION GENERATION MODE TO AN END.

PROVIDE THE FOLLOWING CROSS SECTION MIXING MODE DATA
ONLY IF IRFC EQUALS 0 OR 2. AFTER THE TITLE CARD,
THE PROGRAM USES FIDAS-TYPE INP

TITLE CARD(10A8)

BLOCK ONE

1$ ARRAY(11)

LTBL=TABLE LENGTH OF INPUT MACK LIBRARY

NOG=NUMBER OF GROUPS ON INPUT MACK LIBRARY

NCVT=0, NO LIBRARY FORMAT CONVERSION REQUIRED
=1, CONVERT LIBRARY FORMAT TO BINARY

LBF=0, INPUT LIBRARY FORMAT IS ANISN BINARY TAPE
=1, INPUT LIBRARY FORMAT IS CARD IMAGE

NEDIT=0, NO EDIT OF INPUT LIBRARY DATA
=N, EDIT N INPUT MATERIALS

NMTN=NUMBER OF RESPONSE FUNCTIONS TO EDIT FOR
EACH MATERIAL

NMIX=0, NO MIXING REQUIRED
=N, MIX N MATERIALS

MTBL=LENGTH OF MIXING TABLE

NRESP=NUMBER OF RESPONSE FUNCTIONS TO MIX

NCOL=0, NO COLLAPSING OF MIXED RESPONSES REQUIRED
=N, COLLAPSE MIXED RESPONSES TO N GROUPS

NBCD=MAXIMUM NUMBER OF NUCLIDES TO BE READ FROM BCD TAPE

T

BLOCK TWO

2$ ARRAY(NEDIT)

MATERIAL IDENTIFIERS FOR MATERIALS TO BE EDITED

3$ ARRAY(NMTN)

LIBRARY TABLE POSITIONS FOR EDITED RESPONSES

T

```
BLOCK THREE
  4$ ARRAY(NRESP)
    TABLE POSITIONS OF RESPONSES TO MIX
  5$ ARRAY(MTBL)
    MATERIAL NUMBERS FOR MIXING TABLE
  6$ ARRAY(MTBL)
    NUCLIDE IDENTIFIERS FOR MIXING TABLE
  7* ARRAY(MTBL)
    NUMBER DENSITIES FOR MIXING TABLE
T
BLOCK FOUR
  8$ ARRAY(NOG)
    FINE GROUP TO FEW GROUP INSTRUCTIONS
  9** ARRAY(NOG)
    FINE GROUP SPECTRUM
T
```

```
Sample FEMP1D input file with RFCC input.
1$$ 2   3    0   5
    4  16    8   3
    3   4    0  21
    0   0   21   1
   64   4    0   0
    2 500   10   0
    0   0    0  -2
    1   1    2

2** 1.0E-5   1.009   3.3787E+22 T

10$$ 4R1 13R2 2R3 2R4

11$$ 41093   40000   3006   3007
     7014    92235   92238  74182   74183   74184   74186
             41093   40000   3006   3007    4009    6012
     41093   40000
     3006    3007


12** 1.1425E-2 1.1541E-4 6.8148E-4 8.4050E-3
     1.5015E-2 1.3461E-2 1.5539E-3 6.4963E-4 3.5321E-4
               6.9613E-4 7.0644E-4 1.1407E-2 1.1523E-4
               5.9377E-4 7.3232E-3
               7.5108E-3 3.7554E-3
     5.5046E-2 5.5602E-4
     3.4748E-3 4.2856E-2 T

30** 0.0000    1.0000    2.0000    3.0000    4.0000
                5.0000    6.0000    7.0000    8.0000
                9.0000
     10.0000   11.0000   12.0000   13.0000   14.0000   15.0000
               16.0000
               17.0000   18.0000   19.0000   20.0000   21.0000
               22.0000
               23.0000   24.0000   25.0000   26.0000   27.0000
               28.0000
               29.0000   30.0000   31.0000   32.0000   33.0000
               34.0000
               35.0000   36.0000   37.0000   38.0000   39.0000
               40.0000
               41.0000
   42.0000
   42.2500     43.2500   44.1500   45.2500   46.2500   47.2500
               48.2500
               49.2500   50.2500   51.2500   52.2500   53.2500
               54.2500
               55.2500   56.2500   57.2500   58.2500   59.2500
               60.2500
               61.2500
   62.2500
```

```
31$$ 1 2 3 4

32$$ 10R1 32R2 1R3 20R4

33** 31.0 31.0 F0.0

34**  62.25

35**  1.779579-4 1.430736-4 1.273286-4 1.289578-4
      1.175837-4 8.307393-5 4.780253-5 3.073550-5
      1.741842-5 8.706003-6 4.805043-6 3.608882-6
      3.875812-6 3.845325-6 4.405964-6 3.675043-6
      24R0.0
      8.783468-6 4.167297-6 2.620405-6 1.510685-6
      7.532709-7 3.860888-7 2.692778-7 4.511449-7 T
```

DISTRIBUTION LIST

AFWL/AWYS
ATTN: MAJ DAVID BOYLE
KIRTLAND AFB, NM 87117-6008

OAK RIDGE NATIONAL LABORATORY
ATTN: DR DAVID BARINE
P.O. BOX X
OAK RIDGE, TN 37830

AFWL/AWYS
ATTN: LT MICHAEL JACOX
KIRTLAND AFB, NM 87117-6008

AFWL/AWYS
ATTN: DR MICHAEL SCHULLER
KIRTLAND AFB, NM 87117-6008

AFWL/AWYS
ATTN: LT DAVID EK
KIRTLAND AFB, NM 87117-6008

UNIVERSITY OF NEW MEXICO
ATTN: DR NORMAN RODRICK
CHEMICAL AND NUCLEAR ENGINEERING DEPT
ALBUQUERQUE, NM 87131

UNIVERSITY OF NEW MEXICO
ATTN: DR MOHAMED EL-GENK
CHEMICAL AND NUCLEAR ENGINEERING DEPT
ALBUQUERQUE, NM 87131

MISSISSIPPI STATE UNIVERSITY
ATTN: DR CHARLES SPARROW
P.O. BOX 1983
MISSISSIPPI STATE, MS 39762

SANDIA NATIONAL LABORATORY
ATTN: DR PATRICK J. McDANIEL
DIVISION 6512
P.O. BOX 5800
ALBUQUERQUE, NM 87115

AUL/LSE
MAXWELL AFB, AL 36112

DTIC /FDAC
CAMERON STATION
ALEXANDRIA, VA 22304-6145

AFWL/SUL
KIRTLAND AFB, NM 87117-6008

AFWL/HO
KIRTLAND AFB, NM 87117-6008

AFSC/DLW
ANDREWS AFB, DC 20334

AFCSA/SAMI
WASHINGTON, DC 20330-5425

KAMAN TEMPO
ATTN: MR F. WIMENITZ, DASIAC/DETIR
2560 HUNTINGTON AVE, SUITE 500
ALEXANDRIA, VA 22303

KAMAN TEMPO
ATTN: D. REITZ, DASIAC/DETIR
816 STATE STREET P.O. DRAWER QQ
SANTA BARBARA, CA 93102

OFFICIAL RECORD COPY
(AFWL/AWYS/LT LEE)
KIRTLAND AFB, NM 87117-6008